Evaluating Uncertainty In Model Representations Of Land-Atmosphere Carbon Exchange And Atmosphere-Watershed Interactions Toward Informed Climate Change Impact Planning

by

Samantha Basile

A dissertation submitted in partial fulfillment
of the requirements for the degree of
Doctor of Philosophy
(Climate and Space Sciences and Engineering)
in the University of Michigan
2019

Doctoral Committee:

Assistant Professor Gretchen Keppel-Aleks, Co-Chair
Professor Allison Steiner, Co-Chair
Professor Maria Carmen-Lemos
Assistant Professor Christine Kirchhoff
Professor Richard Rood

Samantha Basile

sjbasile@umich.edu

ORCID iD: 0000-0003-2953-9221

Dedication

For those who connect science and society through openness, equity, and representation.

Acknowledgements

Thank you to Mom and Dad for always encouraging me to read, ask questions, and build on the many learning opportunities you provided. Thank you to my sister, Cassandra for your enduring friendship, patience, and humor. To my whole family, thank you for your encouragement and love. Throughout my undergraduate and graduate experiences, I have benefited from the incredible support of scientists, graduate students, and community members in Albany, NY and Ann Arbor, MI. I sincerely say thank you for your kindness, your encouragement, and your time. Thank you to the many women in STEM who continue to break barriers inside and outside of academia. I'm constantly inspired by your kindness and indebted to your sacrifices. I'm immensely grateful for the guidance of Dr. Gretchen Keppel-Aleks over the last five years. She has helped me think deeply and carefully about each project topic and challenged me to refocus after each setback. I'm also incredibly grateful for the mentorship of Dr. Allison Steiner throughout graduate school. Her reassurance and creativity helped me to understand my strengths as a scientist. I appreciate the incredible amount of support from my many mentors and friends on my journey for mental health wellness. I wish peace to Dr. Natalia Andronova whose support for students was as unwavering as her passion for science. Many, many thanks to Dr. Richard Rood and those at the Great Lakes Sciences and Assessments Program for fostering my motivation to work in climate science communication and policy. Thank you to all of the co-authors who made invaluable contributions to this dissertation work.

Table of Contents

List of Tables

List of Figures

List of Appendices

Abstract

Investigating uncertainty within Earth's complex climate system, as well as within tools used to represent system interactions, can contribute to multidisciplinary projects such as model benchmarking and scenario planning. In this dissertation, three case studies are presented that focus on climate system connections to land management and water quality. First, global soil heterotrophic respiration (HR) is a component land flux that drives net carbon exchange between the atmosphere and terrestrial ecosystems. Due to observational limitations, it is difficult to quantify HR or to evaluate it in global-scale model simulations, leading to error ranges with comparable magnitude to recent fossil fuel burning. We analyze three soil model configurations that simulate HR fluxes within a biogeochemical testbed and subsequently quantify the effects of variation in carbon fluxes on atmospheric CO_2 distributions using a three-dimensional atmospheric tracer transport model. We show that atmospheric CO_2 can provide a useful constraint on large-scale patterns of soil heterotrophic respiration. Second, Lake Erie has experienced a resurgence of harmful algal blooms (HABs) that is attributed to agricultural practices and fertilizer run-off exacerbated by spring rain events. We examine extreme precipitation events for the Great Lakes Basin and the Western Lake Erie Basin subregion for historical and mid-21st century periods by quantifying changes in precipitation seasonality and daily intensity. We utilize three model ensembles that cover a range of spatial scales and future emissions scenarios to evaluate the roles of model method and grid resolution within the projection output. Third, climate change influences regional drivers of HABs, emphasizing the need for usable information in planning and policy. HAB modeling and mitigation actions have

focused on the agricultural sector to reduce land run-off and nutrient loading in Western Lake Erie. Other regional stakeholders, such as drinking water managers, beach managers, marina operators, and recreational land owners, respond and adapt to algal blooms once they form, representing different data needs from those in the mitigation space. We define sources of uncertainty in climate, watershed, and HAB modeling and present four pathways for conceptualizing uncertainty across a modeling chain. We further discuss how scenario planning can incorporate model uncertainty information and stakeholder knowledge for HAB decision-making.

Chapter 1 Introduction

1.1 Human and climate system interactions

The global climate system consists of multiple complex components, including atmospheric composition, ecosystems on land, and water flow patterns, which interact over a range of spatial and temporal scales (IPCC, 2014). Through these interactions there is exchange of many quantities including radiation (energy), water, and carbon. Wind, precipitation and ocean circulation patterns redistribute energy, forming distinct climate zones that govern ecosystem structure and function (Swann et al., 2012). Shifts in energy manifest in local temperature change and subsequently water phase changes, which affect seasonal phenomena such as regional monsoons (Trenberth, 2000). Precipitation and temperature also introduce variability in carbon and nutrient cycling across local and global scales (Friedlingstein, 2014). Humans add more complexity to the system by altering these component interactions through activities such as deforestation, agriculture, water use, and fossil fuel burning and extraction. These layers of climate-human system complexity contain inherent uncertainty. For example, global observations for temperature change over 60 years show confidence in the amount of observed warming with a relatively small error range compared to the overall magnitude (Figure 1; IPCC 2013). There is a clear warming contribution from greenhouse gas emissions attributed to human (anthropogenic) activity, despite uncertainty in the overall magnitude that arises from detangling the response of temperature to individual forcings (see greenhouse gases and other anthropogenic

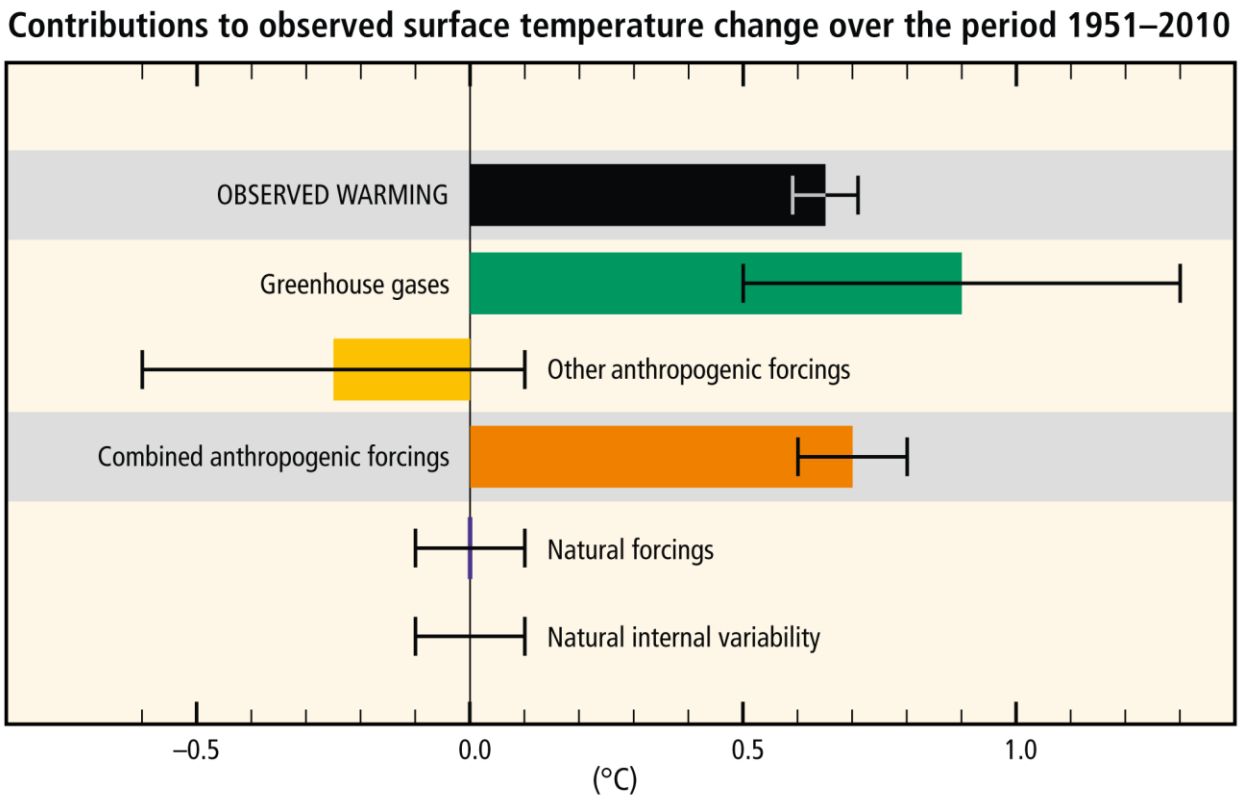

Figure 1.1: Contributions to global surface temperature change from 1951 to 2010 (IPCC, 2013). Uncertainty on the magnitude of observed warming is small relative to the magnitude, but uncertainty on the attribution of warming is larger.

forcing in Figure 1.1; IPCC 2013). Natural forcing of global surface temperature has a smaller overall magnitude compared to that of combined human activity, but retains a similar error range –meaning natural systems could amplify or mitigate human-climate feedbacks (Figure 1.1, IPCC, 2013). Further, these component forcings do not work in isolation. Human activity interacts with several natural components of the climate system, which has implications for how uncertainty is characterized.

Overlap in human and natural systems can be illustrated by considering land management strategies (Figure 1.2a; IPCC, 2019). Different types of land management and utilization practices, from unmanaged lands to agriculture and forestry, affect the carbon cycle and hydrologic cycle as well as chemical reactions and changes to radiative balance in the atmosphere (Figure 1.2a; IPCC, 2019). Additionally, deviations from the climate state average, or variability, tests the vulnerability of both human and natural systems. For example, above average annual temperatures affect agricultural yields, soil health, and ecosystem turnover (Koven et al., 2017; Lobell and Field, 2007). Intense rainfall and flooding impacts everything from fertilizer application to drinking water to coastal erosion (Lall et al., 2018).

The impact of human activity can also be tracked within estimation of Earth's carbon budget, specifically through deforestation and in the burning of fossil fuels (Figure 1.2b; Le Quéré et al., 2018). Fossil fuel burning releases formerly stored carbon dioxide (CO_2) into the atmosphere, which has been documented to alter the radiation imbalance at the top of Earth's atmosphere (IPCC, 2014). The greenhouse gas forcing accounted for in Figure 1.1 arises because atmospheric CO_2 absorbs infrared radiation (energy) from Earth's surface and re-emits some of this energy back to the surface (Zhong and Haigh, 2013). Ultimately Earth's surface temperature must increase to account for this extra energy and achieve radiative balance at the top of the atmosphere. These interactions result in more energy (heat) remaining in Earth's climate system leading to feedbacks that manifests in changes to climate phenomena, including seasonal precipitation, growing season length and lake temperatures. Additionally, land cover change modifies surface energy balance through reflectivity of radiation, evaporation of water from soils, and transpiration of water from plants (Seneviratne et al., 2010). Thus human activity such

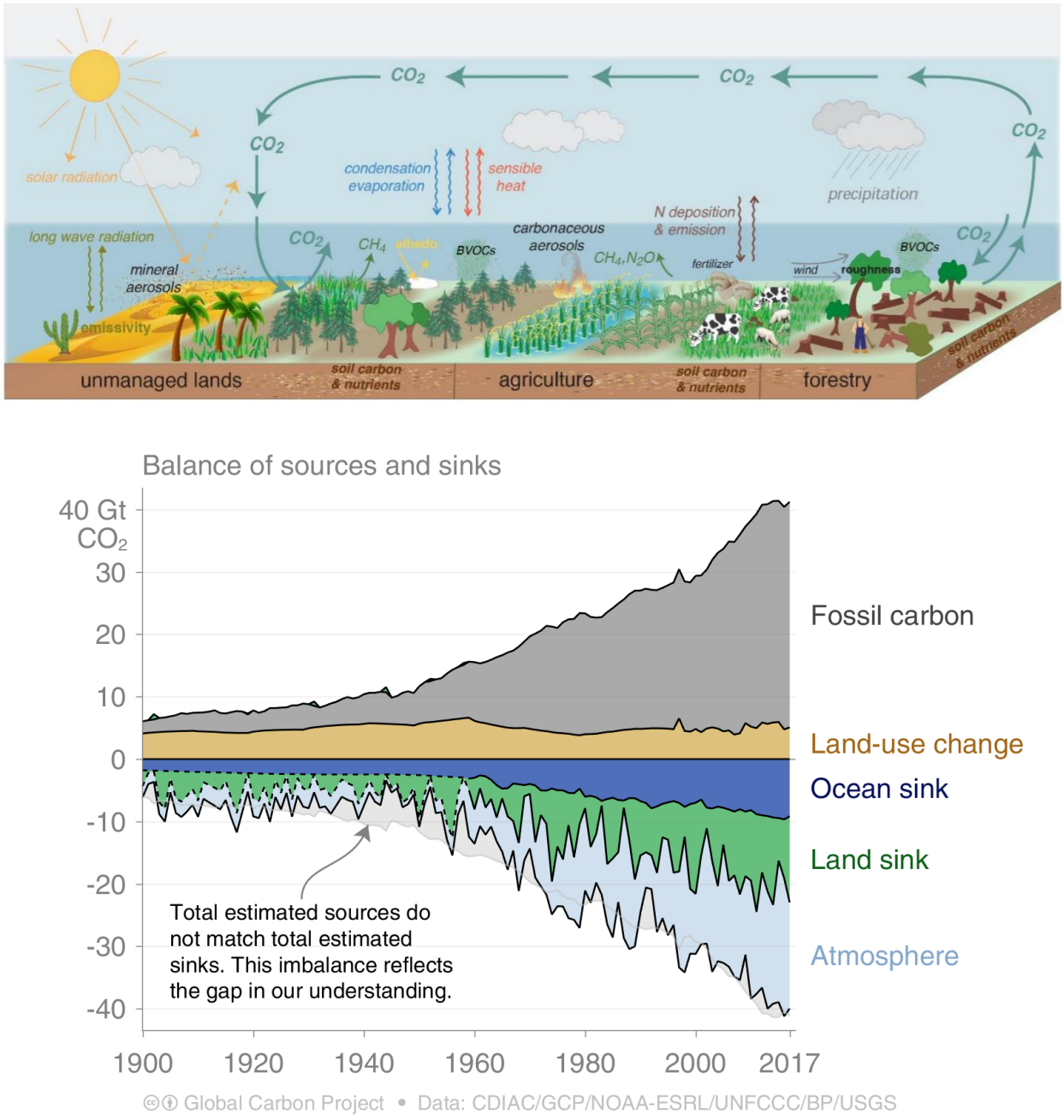

Figure 1.2: (a) Land management strategies and the interactions with the climate system (IPCC, 2019). (b) Sources and sinks within the carbon budget (LeQuéré et al., 2018).

as deforestation, agriculture, and urban development also affects the transfer of energy (heat) into the atmosphere (Figure 1.2a).

The terrestrial biosphere, or the land areas containing living organisms, contributes important carbon-climate feedbacks on a timescale relevant to policy making (between 1-100 years). Since the mid-20th century, land-based ecosystems have taken up about 25% of human CO_2 emissions, reducing the total amount of this potent greenhouse gas in the atmosphere and dampening the overall severity of climate change (Figure 1.2b; Le Quéré et al., 2018). Variations in the land sink are therefore directly reflected in the atmosphere and uncertainty in land sink estimates contributes to the total budget imbalance (Figure 1.2b).

Processes making up the terrestrial land sink vary geographically and over seasonal and annual timescales. The net flux between terrestrial ecosystems and the atmosphere is a combination of both plant and soil level processes which depend on factors such as atmospheric CO_2 accumulation, temperature and growing season length, available organic matter, seasonal rainfall and evapotranspiration (Wang et al, 2016; Zhang et al, 2016). Photosynthesis describes the processes by which CO_2 molecules diffuse through leaf openings and are chemically converted to sugars using energy from sunlight (Farquhar et al., 2001; Hind and Olson, 1968). Water is also necessary for energy transfer within the light-based chemical reactions of photosynthesis. However, CO_2 is taken up through openings on the leaf surface, which allows water to escape from the plant. In addition to light and water limitations, photosynthesis is regulated by enzyme activity which occurs at an optimal temperature. Thus stress from climate extremes such as drought and heat waves can inhibit photosynthesis. Sugars created through photosynthesis are stored within plants and can be used for growing leaves, stalks, and trunks. When sugars are

accessed for plant growth, they are converted back to CO_2, and this loss of carbon biomass is termed autotrophic respiration ($R_{autotrophic}$; Chapin et al., 2011). Similarly autotrophic respiration also occurs below the surface in root systems ($R_{autotrophic}$ (belowground); Chapin et al., 2011). Additionally within soils, dead biomass is metabolized by microbes releasing CO_2 to the atmosphere, termed heterotrophic respiration (HR; Wieder et al., 2018). Microbial decomposition of soil organic matter process depends on local climate, soil type, and microbial community structure (Wieder et al., 2015).

$$Photosynthesis: CO_2 + H_2O \xrightarrow{hv} CH_2O + O_2$$

$$NPP = Gross\ Primary\ Productivity\ (photosynthesis) - R_{autotrophic}$$

$$HR = R_{soil} - R_{autotrophic}(belowground)$$

$$Net\ Ecosystem\ Production\ (net\ carbon\ exchange) = HR - NPP$$

Drawdown of atmospheric CO_2 through photosynthesis occurs dominates during a regional growing season (Figure 1.3a). As photosynthesis declines, the impact of respiration becomes more pronounced as microbes in soils breakdown organic matter including leaf litterfall (Figure 1.3b). In available global estimates, total soil respiration can reach fluxes up to 9 times as large as current annual fossil fuel burning (~90 PgC yr^{-1}), but is nearly completely offset by photosynthesis in the present climate state (Zhao et al., 2017; Lajtha et al., 2018). The error range for global heterotrophic respiration is close to 10 PgC yr^{-1} (Hashimoto et al., 2015; Zhao et al., 2017), which is the same order of magnitude as recent annual fossil fuel estimates (9 PgC yr^{-1}; Bruhwiler et al., 2018), highlighting the need to better constrain component respiration

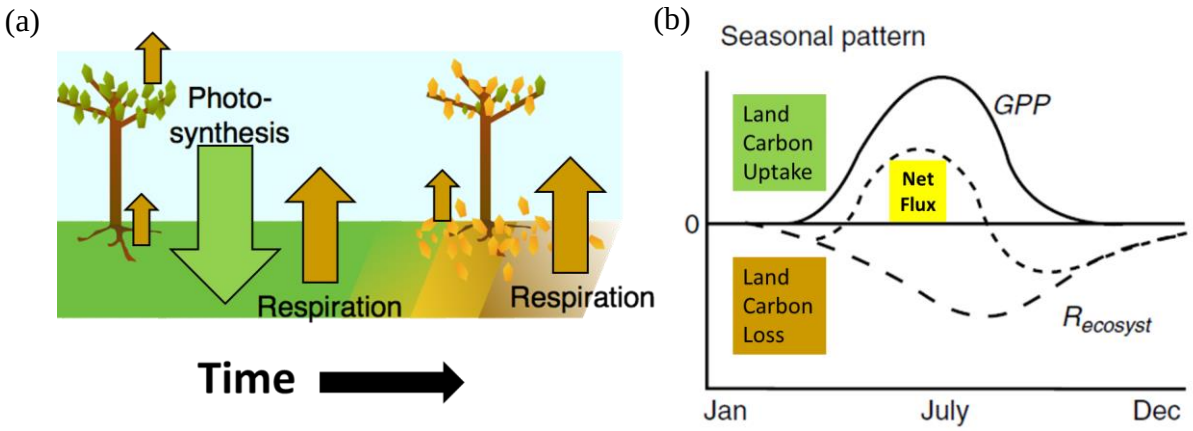

Figure 1.3: (a) Quantities that make up a net flux of carbon between land and the atmosphere. (b) Modified from Chapin et al., 2011. Gross primary productivity (GPP) represents a measurable estimate of photosynthesis in plant growth. Ecosystem respiration ($R_{ecosystem}$) represents soil and plant processes that release CO_2. These fluxes evolve over the annual cycle and contribute to net carbon exchange between land and the atmosphere.

estimates. Soil heterotrophic respiration is extremely heterogeneous in space and time, and is therefore difficult to measure directly or to upscale local measurements to global scale. Often total carbon fluxes are inferred at an ecosystem level by measurements of turbulent eddies (mixing) in the atmosphere (Baldocchi et al., 2008). Field measurements are used in combination with eddy flux measurements to estimate the amount of soil heterotrophic respiration (Zhao et al., 2017).

1.2 Climate change and ecosystem services

Ecosystem services, such as CO_2 uptake, forestry, agriculture, and water supply have inherent vulnerability to changing climate conditions and human activity (van der Geest et al., 2019). Reforestation within the Northern Hemisphere has contributed to the increasing trend of land CO_2 uptake over the 20th century (Bruhwiler et al., 2018). Currently, North American land is

estimated to account for about 10% (0.31 PgC yr^{-1}) of the land sink (3.0 ± 0.8 Pg C yr^{-1}; Bruhwiler et al., 2018). Tropical rainforests alone may be responsible for up to 50% of the global land sink (Schimel, 2014) whereas semi-arid regions are a main contributor to interannual variability in the global land sink (Adams and Piovesan, 2005; Ahlström et al., 2015; Huxman et al., 2004; Poulter et al., 2014; Zhang et al, 2016). However deforestation in both extratropical and tropical rainforests during the late 20^{th} and early 21^{st} centuries may be counteracting land carbon gains (Hristov et al., 2018). Agricultural practices around the globe can link to deforestation, such as peatland burning, or additional release of greenhouse gases such as methane from cattle farming (Bruhwiler et al., 2018; IPCC, 2019). In the United States overall agricultural land area has declined slightly, but cropland alone accounts for over 40% of total agricultural land use (Hristov et al., 2018). With a growing global population, demand for agricultural land may outweigh continued reforestation or natural land management. Further, land management practices feedback on climate driven changes to the global land sink. Several earth system model projections that either prescribed (used as forcing) or calculated land use emissions show land as a net carbon source to the atmosphere by the end of the 21st century (Friedlingstein, 2014).

Agricultural management practices can also have cascading impacts to lake water quality through seasonal runoff (Michalak et al, 2013). Algal blooms, or densely packed regions of algae growth, reoccur annually in coastal waters as well as inland lakes (Hudnell and Dortch, 2008). Historically, algal blooms in freshwater lakes and rivers have been tied to lake pollution that raised levels of nutrients like phosphorus and nitrogen (Anderson et al., 2002; Watson et al. 2016). Harmful algal blooms deplete lake oxygen and can include toxin-producing bacteria

which affects both in-lake on onshore biodiversity (Paerl et al., 2001; Watson et al., 2016). In the Midwest region of the United States, phosphorus and nitrogen fertilizers are applied to agricultural land at the start of the growing season. Extreme spring precipitation within the Great Lakes Basin then contributes to surface run-off of these fertilizers and increases lake nutrient loading, which fuels late-summer harmful algal blooms (Basile et al., 2017; Michalak et al., 2013; Paerl and Huisman, 2008). In the last 20 years, Lake Erie has experienced a resurgence in record breaking HAB events (Rinta-Kanto et al., 2005; Steffen et al., 2014). Great Lakes ecosystems services cover several functions including provisioning (commercial fishing, drinking water, water for the energy sector) and cultural categories (recreation, nature and viewscape enjoyment, historical interests, spiritual fulfilment; Allan et al., 2017). Depending on bloom location and toxicity, service risks include drinking water contamination, reduced fishing yield, and decreased use of recreational land and water (beaches, campgrounds, and marinas; Jetoo et al., 2015; Palm-Forster et al., 2016; Wolf et al., 2017).

1.3 Communication of climate information

Throughout human history, societies around the globe have made decisions influenced by climate conditions. Thus, resilient development involves planning for both changing climate mean states and variability. Informed policy and ecosystem planning necessitates actionable information from the scientific community. However, layers of complexity across scales can be difficult to capture through climate modeling techniques that require some form of simplification of the climate system. Communication of climate impacts involves explanation of model and expert sources of uncertainty (Patt, 2007). However, uncertainty means different things to

different stakeholders with differing perspectives, even for the same environmental issue. Over the last 39 years, climate information has largely been communicated through synthesis reports from international to local scales. In 1980 the U.S. Department of Energy became a lead sponsor for a yearlong study surrounding climate change and its potential impacts, led by physical and social scientists. The study was proposed as a thought experiment on climate change by Climate Program members of the International Federation of Institutes for Advanced Study (IFIAS) at the University of Bonn in 1974, and later in a 1978 workshop co-sponsored by the World Meteorological Programme and the United Nations Environment Program. Study findings were released in a report called *Climate Change and Society*, which offered an evaluation of strategies to mitigate or avert potential long-term climate change effects, while at the same time making social systems more immediately resilient or "climate proof" (Kellogg and Schware, 1981).

> *Many of the long term strategies designed to deal with a climate warming would also make agricultural and other social systems more nearly "climate proof" now. They can guard against the adverse effects of the normal short term climate fluctuations, giving added insurance in the event of a long term climate change. If the public perceives these benefits clearly, then implementing the strategies may be more politically acceptable.*
> *Kellogg and Schware (1981)*

Later that decade in 1988, the Intergovernmental Panel on Climate Change (IPCC) was established to synthesize the state of climate change research and since has released five reports. In the last two decades, the IPCC has expanded the scope of its assessments, specifically to address interactions of human and environmental systems leading to the establishment of its Working Group on Impacts, Adaptation, and Vulnerability (IPCC, 1997).

In the 30 years since its formation, the IPCC has only increased its confidence that post-industrial era climate change is attributed to human emissions of greenhouse gases (IPCC). Evidence of the human impact on the environment is provided by observations of radiative imbalance at the top of the atmosphere as well as model simulations of natural climate variability that fail to show the global warming trend of the last 200 years. Most recently, in 2018, the IPCC fulfilled a mandate from the 2015 Paris Climate Accords (termed the Paris Agreement) by releasing a special report on the implications of global mean temperature increases of 1.5°C and 2°C. The report provided a scientific basis for the rapid reduction of fossil fuel emissions by 2030 to avert dangerous climate change effects including heat and precipitation extremes, sea level rise, increased health risks, threatened water and food supply, and irreversible ecosystem degradation (IPCC, 2018).

1.4 Quantification of climate model uncertainty

Application of climate information requires framing of uncertainty for different disciplines and stakeholders (Gettelman and Rood, 2016). Characterizing sources of uncertainty can contextualize model output for the decision-making problem, or issue at hand. Using global climate model output from the Intergovernmental Panel on Climate Change (IPCC) third assessment report Hawkins and Sutton (2009) categorized sources of uncertainty as arising from forcing scenario, model structure, and internal variability. Within the IPCC's fifth assessment report, the forcing scenario uncertainty results from possible amounts of 21st century radiation measured at the top of the atmosphere, ranging from 2.6 to 8.5 W/m^2 beyond the preindustrial radiative balance (Hawkins and Sutton, 2009). Climate model structure adds uncertainty in how

model components respond to the choice of radiative forcing scenario. Climate models also contain their own climate equilibrium state (based on the model structure and input starting state) which contributes uncertainty in the simulated variability, or fluctuations from the mean climate state (e.g. timing and strength of atmospheric-ocean interactions such as El Niño). Additionally, variable probabilities can be used to gauge confidence in the magnitude and sign of future change. The IPCC has developed a method of characterizing uncertainty through confidence descriptions based on both evidence and expert judgement (IPCC, 2014).

Framing of uncertainty can take shape at different scales and with different goals. Many underlying relationships of climate phenomena can be represented in equations derived from the laws of physics. Equations for the state of matter and fluid flows, among others, are used in the foundation of climate models. However climate simulations are subject to uncertainty since these equations have to be discretized to a limited number of model gridpoints. Smaller scale processes are not accounted for at the grid level of many established climate models and are represented using parameterizations –that is, functional or observed relationships, which are simplifications of reality. Beyond dynamical equations and physical parameterizations, model structure can contain uncertainty from missing processes and scale mismatches for interacting processes. Initialization of model climate states, computational resources to run complex modeling experiments, and representations of sub-grid processes push up against limits of model development. Regional scale climate models have been developed with finer grid resolution aimed at better process representation, however these models also require information from global models along domain boundaries.

The method used to characterize uncertainty based on model structure is tied to the scale of physical processes examined and may require multiple types of simulations. The scientific community has tested the role of human activity in climate change through large scale model intercomparison projects centered on ensembles of physically-based model projections that produce a range of future climate change realizations. Model benchmarking is expanding how uncertainty is addressed in model intercomparison projects. For example, the International Land Model Benchmarking Project (ILAMB) accounts for regional accuracy in land variables by tracking model behavior through performance-based metrics. This focus on a mechanistic representation of climate system processes is distinct from recent reliance on emergent constraints to test model fidelity, or historical variable relationships that may or may not hold under future climate change.

1.5 Application of climate information

Despite decades of scientific reports, climate action has been slow to materialize despite over 20 years in international negotiation. The Kyoto Protocol was established in 1997 to cap global carbon dioxide emissions, entering into force in 2005 with the first commitment period of 2008 to 2012 (United Nations Climate Change, https://unfccc.int/kyoto_protocol). However United States did not end up ratifying the Protocol, eventually opting out (Siddiqi, 2011). Additionally, China and India, two large developing countries, were exempt from the emissions reductions (Siddiqi, 2011). In 2011, Canada formally withdrew from the Kyoto Protocol, days after international negotiations agreed to move forward with plans for a second commitment period (United Nations News, https://news.un.org/en/story/2011/12/398142). In 2015, the Paris

Agreement was constructed using climate change mitigation and adaptation actions offered directly by participating countries (United Nations Climate Change, https://unfccc.int/process-and-meetings/the-paris-agreement/the-paris-agreement). Examination of these commitments shows there is still an emissions gap between the Paris Agreement and emissions level needed to avoid dangerous climate change (IPCC, 2018).

Barriers to the application of climate information arise from the fit of climate information, interactions of knowledge producers and users and interplay of existing and new knowledge (Lemos et al., 2012). Climate scientists often focus on large scale phenomena, and most climate models are run at global scales. In contrast, stakeholders, including local governments, business owners, resource managers, and landowners, work within regional boundaries on timescales of 50 years or less. In 1990, U.S. federal law mandated a National Climate Assessment (NCA) carried out by the U.S. Global Change Research Program (USGCRP). Between 1997 and 2018 four NCA reports were released. As of 2014 the USGCRP has focused on sustaining its assessments regionally, and has released special reports on risks to human well-being and the U.S. economy. Over the last decade, subnational reports have been released by interdisciplinary partnerships which have included state offices, government research laboratories, universities, cities, utility companies, and community stakeholders (National Academies of Sciences, Engineering, and Medicine, 2019; Kirchhoff et al., 2019). Among these subnational reports, scientific basis and stakeholder engagement are common, however there is divergence on the inclusion of policy discussion and follow up action (National Academies of Sciences, Engineering, and Medicine 2019; Kirchhoff et al., 2019).

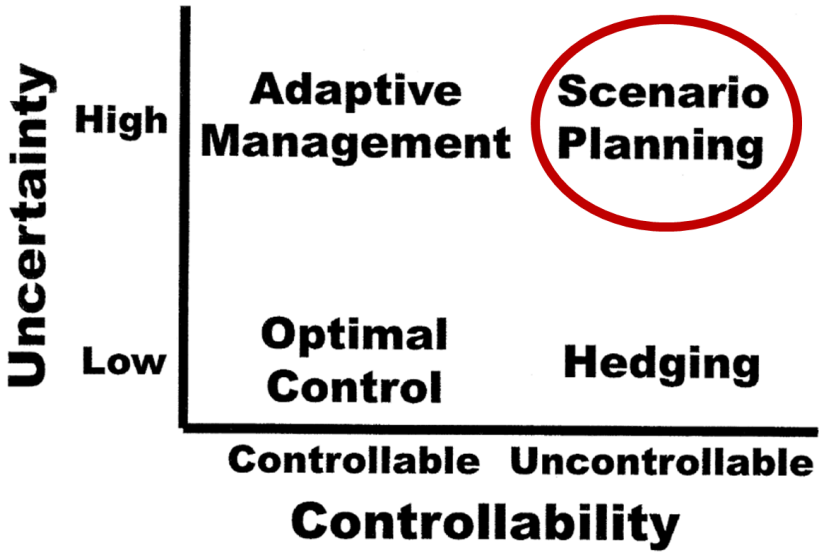

Figure 1.4: Matrix of decision making tools for system uncertainty versus system controllability Figured modified from Peterson et al., 2003. Scenario planning has been used as a tool for climate change impact planning.

A further barrier to actionable climate data and projections is that local stakeholders look for tailored climate data, however the applicability of model output is limited to the specifications of the simulations. Climate modelers and scientists may also lack the sectoral knowledge of practitioners, managers or officials needed to develop usable model output. Improved climate communication starts with producing legitimate, credible and salient information (Cash et al., 2003), and includes managing boundaries between knowledge and action (Lemos et al., 2012). Co-production, or two-way communication between knowledge producers and users that target iteration on science questions, methods or applications, has emerged as a practical way to address the lack of usability of climate information (Kirchhoff et al. 2013; Lemos and Morehouse, 2005; Lemos et al. 2019). Co-production on climate science knowledge encompasses multiple modes of interaction (contractual, consultative, collaborative, and

collegial), and can take shape through several research approaches depending on available resources such as time, funding and training (Meadow et al., 2015). The climate system contains a high degree of uncertainty due to complex interactions, and operates on long timescales making real-time experiments difficult to impossible, thus scenario planning is one tool often used in forming climate impact strategies (Figure 1.4). Scenario planning, or problem-solving through development of possible futures, follows an iterative process involving problem identification (orientation), system assessment (exploration), scenario creation (synthesis), and scenario testing (action and monitoring; Peterson et al., 2003; Weeks et al., 2011).

1.6 Scope of dissertation work

This dissertation focuses on aspects of climate change with potential to impact human health and ecosystem services, but which also contain substantial uncertainty in measured and or modeled values. Carbon cycle prediction requires simplifying the complex structures of soil biology, Great Lakes precipitation is represented through sub-model grid processes in a non-uniform area, and harmful algal bloom modeling currently relies on historical datasets, without capacity to directly incorporate climate change information. The work presented here will discuss three case studies of how uncertainty is treated in model parameterization and model coupling for land management and ecosystem planning. Three science questions are addressed as:

I. Can atmospheric CO_2 observations be used to analyze regional carbon flux signatures based on different soil model representations of microbial activity?

The first chapter investigates the imprint of soil heterotrophic respiration on atmospheric CO_2 using three soil models with implicit and explicit microbial representations. Uncertainty in soil carbon fluxes is investigated through feedback to the global atmospheric CO_2 growth rate and regional CO_2 variability. The potential use of atmospheric CO_2 to constrain soil carbon respiration is evaluated for soil model benchmarking.

II: How can changing precipitation patterns from a range of climate model simulations be interpreted for timescales relevant to ecosystem service planning?

The second chapter quantifies changes to Great Lakes and Western Lake Erie precipitation by the mid-21st century using an ensemble of global and regional climate models. Uncertainty in projections is quantified through probability in precipitation seasonality and daily intensity. The effects of model resolution and lake representation are discussed in context of reducing regional precipitation bias.

III: How can uncertainty be tracked in coupled climate, watershed, and harmful algal bloom modeling to inform ecosystem service adaptation decisions?

The third chapter poses four modeling pathways to conceptualize uncertainty surrounding future harmful algal bloom impacts to Western Lake Erie. Modeling pathways capture the compounding of simplifying impact of model structure and bias correction. Interdisciplinary project designs are presented to address the different data needs of adaptation versus mitigation decision-making.

References

Adams, J. M. and Piovesan, G.: Long series relationships between global interannual CO_2 increment and climate : Evidence for stability and change in role of the tropical and boreal-temperate zones, Chemosphere, 59, 1595–1612, doi:10.1016/j.chemosphere.2005.03.064, 2005.

Ahlström, A., Raupach, M., Schurgers, G., Smith, B., Arneth, A., Jung, M., Reichstein, M., Canadell, J., Friedlingstein, P., Jain, A., Kato, E., Poulter, B., Sitch, S., Stocker, B., Viovy, N., Wang, Y. P., Wiltshire, A., Zaehle, S. and Zeng, N.: The dominant role of semi-arid ecosystems in the trend and variability of the land CO_2 sink, Science (80-.)., 348(6237), 895–899, doi:10.1002/2015JA021022, 2015.

Allan, J. D., Manning, N. F., Smith, S. D. P., Dickinson, C. E., Joseph, C. A. and Pearsall, D. R.: Ecosystem services of Lake Erie: Spatial distribution and concordance of multiple services, J. Great Lakes Res., 43(4), 678–688, doi:10.1016/j.jglr.2017.06.001, 2017.

Anderson, D. M., Gilbert, P. M. and Burkholder, J. M.: Harmful Algal Blooms and Eutrophication: Nutrient Sources, Composition, and Consequences, Esutaries, 25(4b), 704–726, doi:10.1039/b709565c, 2002.

Baldocchi, D.: 'Breathing'of the terrestrial biosphere: lessons learned from a global network of carbon dioxide flux measurement systems. Aust. J. Bot., 56(1), 1–26, doi:10.1071/BT07151, 2008.

Basile, S. J., Rauscher, S. A. and Steiner, A. L.: Projected precipitation changes within the Great Lakes and Western Lake Erie Basin: a multi-model analysis of intensity and seasonality, Int. J. Climatol., 37(14), 4864–4879, doi:10.1002/joc.5128, 2017.

Bruhwiler, L., Michalak, A. M., Birdsey, R., Huntzinger, D. N., Fisher, J. B., Miller, J. and Houghton, R. A.: Overview of the Global Carbon Cycle, Second State Carbon Cycle Rep., 1–33, 2018.

Canada's withdrawal from Kyoto Protocol regrettable – UN climate official: https://news.un.org/en/story/2011/12/398142, last access 22 September 2019.

Cash, D.W., Clark, W.C., Alcock, F., Dickson, N.M., Eckley, N., Guston, D.H., Jäger, J. and Mitchell, R.B.: Knowledge systems for sustainable development., P. Natl. Acad. Sci. USA, 100(14), 8086–8091, doi:/10.1073/pnas.1231332100, 2003.

Chapin III, F.S., Matson, P.A. and Vitousek, P.: Principles of terrestrial ecosystem ecology. Springer Science & Business Media, New York, NY, doi:10.1007/978-1-4419-9504-9, 2011.

Farquhar, G. D., Caemmerer, S. Von and Berry, J. A.: Models of Photosynthesis Models of Photosynthesis, Plant Physiol., 125(February), 42–45, doi:10.1104/pp.125.1.42, 2001.

Friedlingstein, Pierre, Meinshausen, Malte, Arora, Vivek K., Jones, Chris D., Anav, Alessandro, Liddicoat, Spencer K., Knutti, R.: Uncertainties in CMIP5 Climate Projections due to Carbon Cycle Feedbacks, , 511–526, doi:10.1175/JCLI-D-12-00579.1, 2014.

van der Geest, K., de Sherbinin, A., Kienberger, S., Zommers, Z., Sitati, A., Roberts, E. and James, R.: Loss and Damage from Climate Change, Loss Damage from Clim. Chang., 1–557, doi:10.1007/978-3-319-72026-5_20, 2019.

Gettelman, A. and Rood, R. B.: Demystifying Climate Models, Earth Syst. Data Model., 2(2011), 282, doi:10.1007/978-3-662-48959-8, 2016.

Hashimoto, S., Carvalhais, N., Ito, A., Migliavacca, M., Nishina, K. and Reichstein, M.: Global spatiotemporal distribution of soil respiration modeled using a global database, Biogeosciences, 12(13), 4121–4132, doi:10.5194/bg-12-4121-2015, 2015.

Hawkins, E. and Sutton, R.: The potential to narrow uncertainty in regional climate predictions, Bull. Am. Meteorol. Soc., 90(8), 1095–1107, doi:10.1175/2009BAMS2607.1, 2009.

Hind, G. and Olson, J. M.: Electron transport, Annu. Rev. Plant Physiol., 1968.

Hristov, A. N., Johnson, J. M. F., Rice, C. W., Brown, M. E., Conant, R. T., Del Grosso, S. J., Gurwick, N. P., Rotz, C. A., Sainju, U. M., Skinner, R. H., West, T. O., Runkle, B. R. K., Janzen, H., Reed, S., Cavallaro, N., Shrestha, G. and Birdsey, R.: Chapter 5: Agriculture. Second State of the Carbon Cycle Report, 229–263, doi:10.7930/SOCCR2.2018.Ch5, 2018.

Hudnell, H.K., Dortch, Q. and Zenick, H.: An overview of the interagency, international symposium on cyanobacterial harmful algal blooms (ISOC-HAB): advancing the scientific understanding of freshwater harmful algal blooms., Cyanobacterial Harmful Algal Blooms: State of the Science and Research Needs, 1–16 pp, Springer, New York, NY, 2008.

Huxman, T.E., Snyder, K.A., Tissue, D., Leffler, A.J., Ogle, K., Pockman, W.T., Sandquist, D.R., Potts, D.L. and Schwinning, S.: Precipitation pulses and carbon fluxes in semiarid and arid ecosystems. Oecologia, 141(2), 254–268. doi:10.1007/s00442-004-1682-4, 2004.

IPCC: The Regional Impacts of Climate Change: An assessment of vulnerability, Summary for Policymakers [R.T.Watson, M.C.Zinyowera, R.H.Moss (Eds)], Cambridge University Press, UK. 517 pp., 1997.

IPCC: Climate Change 2013: The Physical Science Basis. Contribution of Working Group I to the Fifth Assessment Report of the Intergovernmental Panel on Climate Change [Stocker, T.F., D. Qin, G.-K. Plattner, M. Tignor, S.K. Allen, J. Boschung, A. Nauels, Y. Xia, V. Bex and P.M. Midgley (eds.)]. Cambridge University Press, Cambridge, United Kingdom and New York, NY, USA, 1535 pp., 2013.

IPCC: Climate Change 2014: Synthesis Report. Contribution of Working Groups I, II and III to the Fifth Assessment Report of the Intergovernmental Panel on Climate Change [Core Writing Team, R.K. Pachauri and L.A. Meyer (eds.)]. IPCC, Geneva, Switzerland, 151 pp., 2014.

IPCC: Summary for Policymakers. In: Global Warming of 1.5°C. An IPCC Special Report on the impacts of global warming of 1.5°C above pre-industrial levels and related global greenhouse gas emission pathways, in the context of strengthening the global response to the threat of climate change, sustainable development, and efforts to eradicate poverty [Masson-Delmotte, V., P. Zhai, H.-O. Pörtner, D. Roberts, J. Skea, P.R. Shukla, A. Pirani, W. Moufouma-Okia, C. Péan, R. Pidcock, S. Connors, J.B.R. Matthews, Y. Chen, X. Zhou, M.I. Gomis, E. Lonnoy, T. Maycock, M. Tignor, and T. Waterfield (eds.)]., World Meteorological Organization, Geneva, Switzerland, 32 pp., 2018.

IPCC: Climate Change and Land: An IPCC Special Report on climate change, desertification, land degradation, sustainable land management, food security, and greenhouse gas fluxes in terrestrial ecosystems: Chapter 2: Land-Climate Interactions [Bernier, P., J.C. Espinoza, S. Semenov (eds.)]., In Press, 2019.

Jetoo, S., Grover, V. I. and Krantzberg, G.: The toledo drinking water advisory: Suggested application of the water safety planning approach, Sustain., 7(8), 9787–9808, doi:10.3390/su7089787, 2015.

Kellogg, W.W. and Schware, R.: Climate Change and Society, Westview Press, Boulder, Colorado, United States, 1981.

Kirchhoff, C.J., Lemos, M.C. and Dessai, S.: Actionable knowledge for environmental decision making: broadening the usability of climate science. Annual review of environment and resources, 38, doi:10.1146/annurev-environ-022112-112828, 2013.

Kirchhoff, C.J., Barsugli, J.J., Galford, G.L., Karmalkar, A.V., Lombardo, K., Stephenson, S., Barlow, M., Seth, A., Wang, G., and Frank, A.: Climate assessments for local action., Bull. Amer. Meteor. Soc., doi:10.1175/BAMS-D-18-0138.1, 2019.

Koven, C.D., Hugelius, G., Lawrence, D.M. and Wieder, W.R.: Higher climatological temperature sensitivity of soil carbon in cold than warm climates, Nature Climate Change, 7(11), 817, 2017.

Lajtha, K., Bailey, V. L., McFarlane, K., Paustian, K., Bachelet, D., Abramoff, R., Angers, D., Billings, S. A., Cerkowniak, D., Dialynas, Y. G., Finzi, A., French, N. H. F., Frey, S., Gurwick, N. P., Harden, J., Johnson, J. M. F., Johnson, K., Lehmann, J., Liu, S., McConkey, B., Mishra, U., Ollinger, S., Paré, D., Paz Pellat, F., deB. Richter, D., Schaeffer, S. M., Schimel, J., Shaw, C., Tang, J., Todd-Brown, K., Trettin, C., Waldrop, M., Whitman, T. and Wickland, K.: Chapter 12: Soils, Second State Carbon Cycle Rep. A Sustain. Assess. Rep., 469–506, available from: https://carbon2018.globalchange.gov/downloads/SOCCR2_Ch12_Soils.pdf, 2018.

Lall, U., T. Johnson, P. Colohan, A. Aghakouchak, C. Brown, G. McCabe, R. Pulwarty, and A. Sankarasubramanian: Water. in: Impacts, Risks, and Adaptation in the United States: Fourth National Climate Assessment, Volume II [Reidmiller, D.R., C.W. Avery, D.R. Easterling, K.E. Kunkel, K.L.M. Lewis, T.K. Maycock, and B.C. Stewart (eds.)]., U.S. Global Change Research Program, Washington, DC, USA, 145–173, doi: 10.7930/NCA4.2018.CH3, 2018.

Lemos, M. C. and Morehouse, B. J.: The co-production of science and policy in integrated climate assessments, Glob. Environ. Chang., 15(1), 57–68, doi:10.1016/j.gloenvcha.2004.09.004, 2005.

Lemos, M. C., Kirchhoff, C. J. and Ramprasad, V.: Narrowing the climate information usability gap, Nat. Clim. Chang., 2(11), 789–794, doi:10.1038/nclimate1614, 2012.

Lemos, M.C., Wolske, K.S., Rasmussen, L.V., Arnott, J.C., Kalcic, M. and Kirchhoff, C.J.: The Closer, the Better? Untangling Scientist–Practitioner Engagement, Interaction, and Knowledge Use. Weather Clim. Soc., 11(3), 535-548, doi:10.1175/WCAS-D-18-0075.1, 2019.

Le Quéré, C., Andrew, R. M., Friedlingstein, P., Sitch, S., Pongratz, J., Manning, A. C., Korsbakken, J. I., Peters, G. P., Canadell, J. G., Jackson, R. B., Boden, T. A., Tans, P. P., Andrews, O. D., Arora, V. K., Bakker, D. C. E., Barbero, L., Becker, M., Betts, R. A., Bopp, L., Chevallier, F., Chini, L. P., Ciais, P., Cosca, C. E., Cross, J., Currie, K., Gasser, T., Harris, I., Hauck, J., Haverd, V., Houghton, R. A., Hunt, C. W., Hurtt, G., Ilyina, T., Jain, A. K., Kato, E., Kautz, M., Keeling, R. F., Klein Goldewijk, K., Körtzinger, A., Landschützer, P., Lefèvre, N., Lenton, A., Lienert, S., Lima, I., Lombardozzi, D., Metzl, N., Millero, F., Monteiro, P. M. S., Munro, D. R., Nabel, J. E. M. S., Nakaoka, S., Nojiri, Y., Padín, X. A., Peregon, A., Pfeil, B., Pierrot, D., Poulter, B., Rehder, G., Reimer, J., Rödenbeck, C., Schwinger, J., Séférian, R., Skjelvan, I., Stocker, B. D., Tian, H., Tilbrook, B., van der Laan-Luijkx, I. T., van der Werf, G. R., van Heuven, S., Viovy, N., Vuichard, N., Walker, A. P., Watson, A. J., Wiltshire, A. J., Zaehle, S. and Zhu, D.: Global Carbon Budget 2017, Earth Syst. Sci. Data Discuss., 1–79, doi:10.5194/essd-2017-123, 2017.

Lobell, D.B. and Field, C.B.: Global scale climate–crop yield relationships and the impacts of recent warming. Environmental research letters, 2(1), 014002, doi:10.1088/1748-9326/2/1/014002, 2007.

Meadow, A.M., Ferguson, D.B., Guido, Z., Horangic, A., Owen, G. and Wall, T.: Moving toward the deliberate coproduction of climate science knowledge. Weather Clim. Soc., 7(2), 179-191, doi:10.1175/WCAS-D-14-00050.1, 2015.

Michalak, A. M., Anderson, E. J., Beletsky, D., Boland, S., Bosch, N. S., Bridgeman, T. B., Chaffin, J. D., Cho, K., Confesor, R., Daloglu, I., Depinto, J. V, Evans, M. A., Fahnenstiel, G. L., He, L., Ho, J. C., Jenkins, L., Johengen, T. H., Kuo, K. C., Laporte, E., Liu, X., McWilliams, M. R., Moore, M. R., Posselt, D. J., Richards, R. P., Scavia, D., Steiner, A. L., Verhamme, E., Wright, D. M. and Zagorski, M. a: Record-setting algal bloom in Lake Erie caused by agricultural and meteorological trends consistent with expected future conditions., Proc. Natl. Acad. Sci. U. S. A., 110(16), 6448–6452, doi:10.1073/pnas.1216006110, 2013.

National Academies of Sciences, Engineering, and Medicine: Finding Commonalities and Differences with Other Subnational Assessments (Part 2), in: Making Climate Assessments Work: Learning from California and Other Subnational Climate Assessments: Proceedings of a Workshop, The National Academies Press., Washington, DC, doi:10.17226/25324, 2019.

Paerl, H. W. and Huisman, J.: Blooms like it hot, Science, 320(5872), 57–58, doi:10.1126/science.1155398, 2008.

Paerl, H. W., Fulton, R. S., Moisander, P. H. and Dyble, J.: Harmful freshwater algal blooms, with an emphasis on cyanobacteria., ScientificWorldJournal., 1, 76–113, doi:10.1100/tsw.2001.16, 2001.

Palm-Forster, L. H., Lupi, F. and Chen, M.: Valuing lake erie beaches using value and function transfers, Agric. Resour. Econ. Rev., 45(2), 270–292, doi:10.1017/age.2016.15, 2016.

Patt, A.: Assessing model-based and conflict-based uncertainty, Glob. Environ. Chang., 17(1), 37–46, doi:10.1016/j.gloenvcha.2006.10.002, 2007.

Peterson, G.D., Cumming, G.S. and Carpenter, S.R.: Scenario planning: a tool for conservation in an uncertain world. Conserv. Biol., 17(2), 358-366, doi:10.1046/j.1523-1739.2003.01491.x, 2003.

Poulter, B., Frank, D., Ciais, P., Myneni, R.B., Andela, N., Bi, J., Broquet, G., Canadell, J.G., Chevallier, F., Liu, Y.Y. and Running, S.W.: Contribution of semi-arid ecosystems to interannual variability of the global carbon cycle., Nature, 509(7502), 600–603, doi:10.1038/nature13376, 2014.

Rinta-Kanto, J. M., Ouellette, A. J. A., Boyer, G. L., Twiss, M. R., Bridgeman, T. B. and Wilhelm, S. W.: Quantification of toxic Microcystis spp. during the 2003 and 2004 blooms in western Lake Erie using quantitative real-time PCR, Environ. Sci. Technol., 39(11), 4198–4205, doi:10.1021/es048249u, 2005.

Schimel, D., Stephens, B. B. and Fisher, J. B.: Effect of increasing CO_2 on the terrestrial carbon cycle, P. Natl. Acad. Sci. USA, doi:10.1073/pnas.1407302112, 2014.

Seneviratne, S.I., Corti, T., Davin, E.L., Hirschi, M., Jaeger, E.B., Lehner, I., Orlowsky, B. and Teuling, A.J: Investigating soil moisture–climate interactions in a changing climate: A review. Earth-Science Reviews, 99(3-4), 125–161 pp, 2010.

Siddiqi, T.: China and India: More cooperation than competition in energy and climate change. J. Int. Aff., 64(2), 73-90, available at: https://www.jstor.org/stable/24385535, 2011.

Steffen, M. M., Belisle, B. S., Watson, S. B., Boyer, G. L. and Wilhelm, S. W.: Status, causes and controls of cyanobacterial blooms in Lake Erie, J. Great Lakes Res., 40(2), 215–225, doi:10.1016/j.jglr.2013.12.012, 2014.

Swann, A.L., Fung, I.Y. and Chiang, J.C.: Mid-latitude afforestation shifts general circulation and tropical precipitation. P. Natl. Acad. Sci. USA., 109(3), 712–716, doi:10.1073/pnas.1116706108, 2012.

The Paris Agreement: https://unfccc.int/process-and-meetings/the-paris-agreement/the-paris-agreement, last access 22 September 2019.

Trenberth, K. E., Stepaniak, D. P. and Caron, J. M.: The global monsoon as seen through the divergent atmospheric circulation, J. Clim., 13(22), 3969–3993, doi:10.1175/1520-0442(2000)013<3969:TGMAST>2.0.CO;2, 2000.

Wang, Y. P., Law, R. M. and Pak, B.: A global model of carbon, nitrogen and phosphorus cycles for the terrestrial biosphere, Biogeosciences, 7(7), 2261–2282, doi:10.5194/bg-7-2261-2010, 2010.

Watson, S. B., Miller, C., Arhonditsis, G., Boyer, G. L., Carmichael, W., Charlton, M. N., Confesor, R., Depew, D. C., Höök, T. O., Ludsin, S. A., Matisoff, G., McElmurry, S. P., Murray, M. W., Peter Richards, R., Rao, Y. R., Steffen, M. M. and Wilhelm, S. W.: The re-eutrophication of Lake Erie: Harmful algal blooms and hypoxia, Harmful Algae, 56, 44–66, doi:10.1016/j.hal.2016.04.010, 2016.

Weeks, D., Malone, P. and Welling, L.: Climate change scenario planning: a tool for managing parks into uncertain futures. Park Science, 28(1), 26-33, 2011.

What is the Kyoto Protocol?: https://unfccc.int/kyoto_protocol, last access 22 September 2019.

Wieder, W. R., Grandy, A. S., Kallenbach, C. M., Taylor, P. G. and Bonan, G. B.: Representing life in the Earth system with soil microbial functional traits in the MIMICS model, Geosci. Model Dev., 8(6), 1789–1808, doi:10.5194/gmd-8-1789-2015, 2015.

Wieder, W. R., Hartman, M. D., Sulman, B. N., Wang, Y. P., Koven, C. D. and Bonan, G. B.: Carbon cycle confidence and uncertainty: Exploring variation among soil biogeochemical models, Glob. Chang. Biol., 24(4), 1563–1579, doi:10.1111/gcb.13979, 2018.

Wolf, D., Georgic, W. and Klaiber, H. A.: Reeling in the damages: Harmful algal blooms' impact on Lake Erie's recreational fishing industry, J. Environ. Manage., 199, 148–157, doi:10.1016/j.jenvman.2017.05.031, 2017.

Zhang, Y., Xiao, X., Guanter, L., Zhou, S., Ciais, P., Joiner, J., Sitch, S., Wu, X., Nabel, J., Dong, J., Kato, E., Jain, A. K., Wiltshire, A. and Stocker, B. D.: Precipitation and carbon-water coupling jointly control the interannual variability of global land gross primary production, Sci. Rep., 6(November), 39748, doi:10.1038/srep39748, 2016.

Zhao, Z., Peng, C., Yang, Q., Meng, F. R., Song, X., Chen, S., Epule, T. E., Li, P. and Zhu, Q.: Model prediction of biome-specific global soil respiration from 1960 to 2012, Earth's Futur., 5(7), 715–729, doi:10.1002/2016EF000480, 2017.

Zhong, W. and Haigh, J.D.: The greenhouse effect and carbon dioxide. Weather, 68(4), 100–105, doi:10.1002/wea.2072, 2013.

Chapter 2 Leveraging the signature of heterotrophic respiration on atmospheric CO_2 for model benchmarking.

N.B: This chapter was submitted for publication in 2019 as

Basile, S. J., Lin, X., Wieder, W.R., Hartman, M.D., and Keppel-Aleks, G.: Leveraging the signature of heterotrophic respiration on atmospheric CO_2 for model benchmarking, Biogeosciences, In Review.

2.1 Introduction

Atmospheric CO_2 observations reflect net exchange of carbon between the land and oceans with the atmosphere. Observations of atmospheric CO_2 concentration have been collected *in situ* since the late 1950s (Keeling et al., 2011), and global satellite observations have become available within the last decade (Crisp et al., 2017; Yokota et al., 2009). The high precision and accuracy of *in situ* observations and the fact that these measurements integrate information about ecosystem carbon fluxes over a large concentration footprint make atmospheric CO_2 a strong constraint on model predictions of net carbon exchange (Keppel-Aleks et al., 2013). For example, at seasonal timescales, atmospheric CO_2 can be used to evaluate the growing-season net flux, especially in the Northern Hemisphere (Yang et al., 2007). At interannual timescales, variations in the atmospheric CO_2 growth rate are primarily driven by changes in terrestrial carbon fluxes in response to climate variability (Cox et al., 2013; Humphrey et al., 2018; Keppel-Aleks et al., 2014). Recent studies have hypothesized that soil carbon processes represent one of the key processes in driving these interannual variations (Cox et al., 2013; Wunch et al, 2013). Moreover, soil carbon processes represent one of the largest uncertainties in predicting future carbon-climate feedbacks, in part because non-permafrost soils contain an estimated 1500 to

2400 PgC (Bruhwiler et al., 2018), at least a factor of three larger than the pre-industrial atmospheric carbon reservoir.

Soil heterotrophic respiration (HR), the combination of litter decay and microbial breakdown of organic matter, is the main pathway for CO_2 release from soil carbon pools to the atmosphere. Currently, insights on HR rates and controls are mostly derived from local-scale observations. For example, soil chamber observations can be used to measure soil respiration (which includes root and heterotrophic respiration fluxes) at spatial scales on the order of 100 cm^2 (Davidson et al., 2002; Pumpanen et al., 2004; Ryan and Law, 2005). Ecosystem respiration (combined autotrophic and heterotrophic respiration fluxes) can also be backed out from eddy covariance net ecosystem exchange observations at spatial scales around 1 km^2, but with substantial uncertainty (Baldocchi 2008; Barba et al., 2018; Lavigne et al., 1997). Because fine-scale variations in environmental drivers such as soil type and soil moisture affect rates of HR, it is difficult to scale local respiration observations to zonal or global scales. Even with use of advanced techniques such as artificial neural networks, lack of information for remote or under-sampled zones contributes uncertainty to bottom-up HR estimates (Bond-Lamberty et al., 2018; Zhao et al, 2017).

Local-scale observations reveal that HR is sensitive to numerous climate drivers, including temperature, moisture, and freeze-thaw state (Baldocchi 2008; Barba et al., 2018; Lavigne et al., 1997). Because of these links to climate, predicting the evolution of HR and soil carbon stocks within coupled Earth system models is necessary for climate predictions. Within prognostic models, heterotrophic respiration has been represented as a first-order decay process based on

precipitation, temperature, and a linear relationship with available substrate (Jenkinson et al., 1990; Parton, 1993, Randerson et al., 1996). However, such representations may neglect key processes for the formation of soil and persistence of soil organic carbon (SOC) stocks (Lehmann and Kleber 2015; Rasmussen et al. 2018; Schmidt et al. 2011). More recently, models have begun to explicitly represent microbial processes into global-scale simulations of the formation and turnover of litter and SOC (Sulman et al., 2014; Wieder et al., 2013) as well as to evaluate microbial trait-based signatures on SOC dynamics (Wieder et al., 2015). These advances in the representation of SOC formation and turnover increase capacities to test emerging ideas about soil C persistence and vulnerabilities, but also increase the uncertainties in how to implement and parameterize these theories in models (Bradford et al. 2016; Sulman et al. 2018; Wieder et al. 2018).

Given these uncertainties, developing methods to benchmark model representations of HR fluxes is an important research goal (Bond-Lamberty et al. 2018b) as model predictions for soil carbon change over the 21st century are highly uncertain (Schuur et al., 2018; Todd-Brown et al., 2014). A common method for model evaluation is to directly compare spatial or temporal variations in model properties (e.g., leaf area index) or processes (e.g., gross primary productivity) against observations (Randerson 2009; Turner et al., 2006). Such comparisons assess model fidelity under present day climate, but may not ensure future predictivity of the model. The use of functional response metrics, which evaluate the relationship between a model process and an underlying driver, may ensure that the model captures the sensitivities required to predict future evolution (Collier 2018, Keppel-Aleks et al., 2018). A third benchmarking approach is to use hypothesis-driven approaches or experimental manipulations to evaluate processes (Medlyn et

al., 2015). It is likely that these methods will have maximum utility when combined within a benchmarking framework (e.g., Collier, 2018; Hoffman et al., 2016) since they evaluate different aspects of model predictive capability.

Here, we hypothesize that atmospheric CO_2 data can be used to evaluate simulations of soil heterotrophic respiration and differentiate between the chemical and microbial parameterizations used in state-of-the-art models. Previous work has shown that atmospheric CO_2 observations are inherently sensitive to HR across a range of timescales. For example, at seasonal timescales, improving the parameterization for litterfall in the CASA model improved its phasing of the simulated atmospheric CO_2 annual cycle (Randerson et al., 1996). At interannual timescales, variations in the Northern Hemisphere CO_2 seasonal minimum are hypothesized to arise from variations in respiration (Wunch et al., 2013) and variations in the growth rate have been linked to tropical respiration and its temperature sensitivity (Anderegg et al., 2015). In this analysis, we simulate atmospheric CO_2 distributions using three different soil model representations that are part of a soil biogeochemical testbed (Wieder et al., 2018). The three sets of HR fluxes, were shown in Wieder et al., (2018) to have distinct patterns at seasonal timescales, are used as boundary conditions for a 3-dimensional atmospheric transport model. We evaluate temporal variability in the resulting CO_2 simulations against observations, quantify the functional relationships between CO_2 variability and temperature variability, and quantify the regional influences of land carbon fluxes on global CO_2 variability. The methods and results are presented in Section 2 and 3, and discussion of the implications for benchmarking and our understanding of drivers of atmospheric CO_2 variability are presented in Section 3.4.

2.2 Data and Methods

2.2.1 Observations and timeseries analysis

For this analysis we use reference CO_2 measurements from 34 marine boundary layer sites (MBL, Table S1) within the NOAA Earth System Research Laboratory sampling network (ESRL, Figure 2.1; Dlugokencky et al., 2016). These sites were chosen to minimize the influence of local anthropogenic emissions and had at least 50% data coverage over the 29-year period between 1982 and 2010. We detrend all timeseries data using a third-order polynomial fit to remove the impact of annually increasing atmospheric concentration in our seasonal and interannual calculations (SFigure 2.1). Using the detrended CO_2 data, we calculate a period median annual cycle by averaging all observations for a given calendar month. To calculate CO_2 interannual variability (CO_2 IAV), the median annual cycle is subtracted from the detrended timeseries (SFigure 2.1, Figure 2.4). We diagnose the magnitude of CO_2 IAV using one standard deviation, unless otherwise noted. Model simulated CO_2 seasonality and interannual variability is calculated using the same methods.

Following the approach in Keppel-Aleks et al., 2018, we aggregate site specific CO_2 by averaging measurement timeseries across six latitude zones (Figure 2.1, solid lines): Northern Hemisphere high latitudes (61 to 90°N), midlatitudes (24 to 60°N), tropics (1 to 23°N), Southern Hemisphere tropics (0 to 23°S), and extratropics (24 to 60°S and 61 S to 90 S). The global mean CO_2 timeseries is constructed as an area-weighted average of these six atmospheric zones.

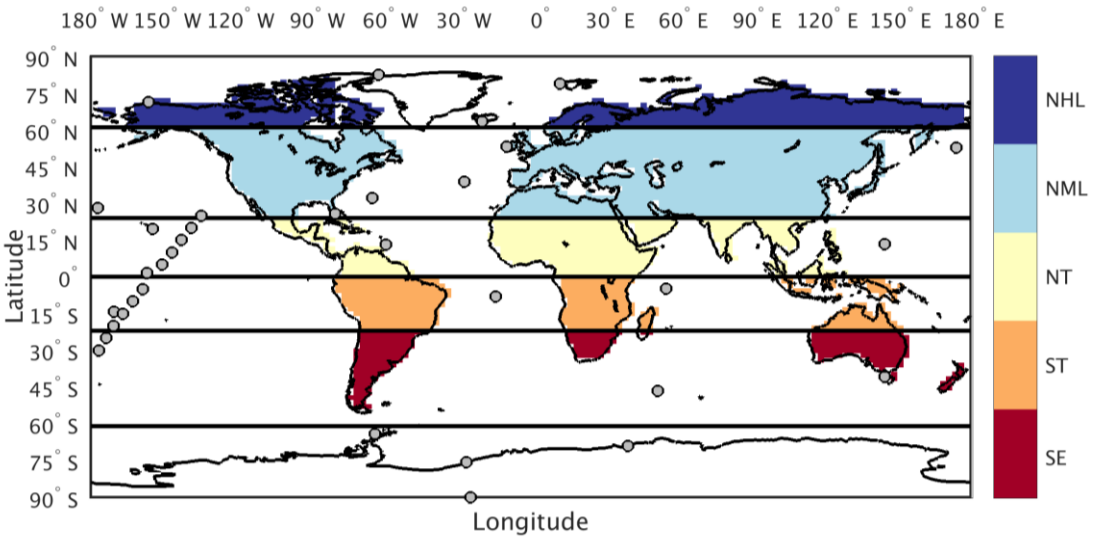

Figure 2.1: Tagged flux regions and marine boundary layer CO_2 observing sites used in our analysis. The 5 tagged flux regions are shown in color fill: Northern High Latitude (NHL), Northern Mid-Latitude (NML), Northern Tropics (NT), Southern Tropics (ST) and Southern Extratropics (SE). For sampling simulated CO_2 consistent with the tagged flux regions, we aggregate marine boundary layer sites (filled circles) into 6 latitude bands defined by the black lines.

2.2.2 Soil testbed representations of heterotrophic respiration

We used a soil biogeochemical testbed (Wieder et al., 2018), which generates daily estimates of soil carbon stocks and fluxes at global scale without the computational burden of running a full land model. The testbed is a chain of model simulations where soil models with different structures can be run under the same forcing data, including the same net primary productivity (NPP) fluxes, soil temperature, and soil moisture. Each testbed soil model in this analysis produces unique gridded heterotrophic respiration (HR) values based on its own underlying mechanism and soil C stocks. Currently, we are running with a carbon-only configuration of the testbed. From the testbed output we calculate the net ecosystem productivity (NEP) as the difference between HR and NPP, specifically HR-NPP, to account for the opposite sign convention between the component fluxes.

For the simulations described in this paper, the chain starts with the Community Land Model 4.5 (CLM4.5; Oleson et al., 2013), run with satellite phenology with CRU-NCEP climate reanalysis as forcing data (Jones et al., 2013; Kalnay et al., 1996; Le Quéré et al., 2018). In this simplified formulation of CLM, a single plant functional type is assumed in each 2° by 2° gridcell. Daily values for gross primary productivity (GPP), soil moisture, soil temperature, and air temperature from CLM4.5 are passed to the Carnegie-Ames Stanford Approach terrestrial model (CASA-CNP; Potter et al. 1993; Randerson et al., 1996; Randerson et al., 1997; Wang et al., 2010). The CASA-CNP plant model uses the data from CLM4.5 to calculate NPP and carbon allocation to roots, wood, and leaves. This module also determines the timing of litterfall. Finally, metabolic litter, structural litter, and decomposing coarse woody debris (CWD) are then passed to the soil biogeochemical models.

The three soil models make distinct assumptions about microbial processes. More details regarding these formulations and their implementation in the testbed are found in Wieder et al. (2018), but we provide brief descriptions here. The CASA-CNP soil model computes first-order, linear decay rates modified by soil temperature and moisture, implicitly representing microbial activity and soil carbon turnover through a cascade of organic matter pools (CASA: Randerson et al., 1997; CASA-CNP: CASA carbon cycling with additional nitrogen, and phosphorus cycling, Wang et al. 2010). These include metabolic and structural litter, as well as a fast, slow, and passive soil carbon pools. The Microbial-Mineralization Carbon Stabilization model (MIMICS; Wieder et al., 2014; Wieder et al., 2015) explicitly represents microbial activity with a temperature-sensitive reverse Michaelis-Menten kinetics (Buchkowski et al., 2017; Moorhead

and Weintraub, 2018) but has no soil moisture controls. The decomposition pathway is set up with two litter pools (identical to those simulated by CASA-CNP), three soil organic matter pools (available, chemically and physically protected), and two microbial biomass pools for copiotrophic (fast) and oligotrophic (slow) microbial functional groups. The Carbon, Organisms, Rhizosphere, and Protection in the Soil Environment model (CORPSE) is also microbially explicit and uses reverse Michaelis-Menten kinetics, but it assumes different microbial and soil carbon pools. Surface litter and soil C pools are considered separately, but only soil C has a parallel set of physically protected pools that are isolated from microbial decomposition. CORPSE includes a temperature dependent Maximum Reaction Velocity ($V_{max)}$ parameter, but also includes a term for the soil moisture controls on decomposition rates that uses volumetric liquid soil water content. For all three models, soil texture inputs were also derived from the CLM surface data set (Oleson et al., 2013). We acknowledge that one potential limitation of the approach is a lack of vertical resolution in terms of temperature or frozen fraction of soil moisture (Koven et al. 2013).

While this modeling approach contains necessary simplifications, it provides the ability to query the role of structure in driving differences in fluxes. Model output includes daily net primary production (NPP) from CASA-CNP and HR simulated by CASA-CNP, CORPSE and MIMICS. Daily fluxes between 1982 and 2010 are averaged to monthly values and masked into land regions that align with the CO_2 sampling zones (section 2.2.1, Figure 2.1, color fill): Northern Hemisphere high latitudes (NHL; 61 to 90°N), midlatitudes (NML; 24 to 60°N), tropics (NT; 1 to 23°N), Southern Hemisphere tropics (ST; 0 to 23°S), and extratropics (SE; 24 to 90°S) – here the two Southern Hemisphere extratropical regions were combined into one flux area since

Antarctic carbon fluxes are negligible. Land-area integrated flux timeseries are then used for seasonal and interannual calculations (method described in section 2.2.1). However, the raw daily fluxes between 1980 and 2010 are used as boundary conditions to an atmospheric transport model, again separated by latitude zones listed above, to simulate the imprint of these different soil model configurations on monthly atmospheric CO_2.

2.2.3 GEOS-Chem atmospheric transport modeling of CO_2

We simulate the imprint of the testbed fluxes on atmospheric CO_2 using GEOS-Chem, a 3-D atmospheric transport model. We run the GEOS-Chem v12.0.0 CO_2 simulation between 1980 and 2010 at a resolution of 2.0° in latitude by 2.5° in longitude with 47 vertical levels. The model is driven by hourly meteorological fields from the Modern-Era Retrospective analysis for Research and Application version 2 (MERRA2) reanalysis data (Gelaro et al., 2017; https://gmao.gsfc.nasa.gov/reanalysis/MERRA-2/), with the dynamic timestep set to be 600 seconds. The model is initialized with a globally-uniform atmospheric CO_2 mole fraction equal to 350 ppm. Results of the first two years (1980 and 1981) are reserved for model spin-up, and we analyze the monthly average outputs for the period 1982–2010. To minimize influence of land-atmosphere boundary layer dynamics and the influence of anthropogenic emissions, we sample the resulting GEOS-Chem simulations at the 3rd vertical level for grid cell points with latitude and longitude values closest to 34 marine boundary layer (MBL) sites within the NOAA ESRL network. We calculated the latitude zone averaging, median annual cycle and interannual variability calculations using the methods described for observed CO_2 (see section 2.2.1). Aggregating CO_2 from individual sites is consistent with our hypothesis that atmospheric CO_2 may provide constraints on large-scale, rather than local, patterns of heterotrophic respiration. As

such, averaging simulated and observed CO_2 across latitude zones smooths local information while retaining information about regional scale fluxes.

We isolate the imprint of NPP and three representations of HR on the spatial and temporal evolution of atmospheric CO_2 by using daily testbed results as boundary conditions (section 2.2.2). We also separately tag CO_2 originating from the five flux zones delineated in the previous section (Figure 2.1). Overall, we track 20 CO_2 tracers in total (4 sets of fluxes and 5 flux regions) within the GEOS-Chem model. Throughout the manuscript, we refer to CO_2 originating from these NPP and HR component fluxes as CO_2^{NPP} and CO_2^{HR}, respectively. For the atmospheric CO_2 simulations, we used the sign convention that a positive flux indicates a flux into the atmosphere. Therefore, CO_2^{NEP}, indicating CO_2 from net ecosystem production (NEP), is calculated from the addition of CO_2^{NPP} and CO_2^{HR}. The same notation will be used to denote the testbed ensemble sources. For example, CO_2^{HR} simulated from CORPSE fluxes is defined as $CO_2^{CORPSE\ HR}$, similarly for $CO_2^{CORPSE\ NEP}$. We note that the net CO_2 response from the model (i.e., CO_2^{NEP}) is approximately equivalent to observations in terms of seasonal and interannual variations, although we neglect ocean fluxes and emissions from fossil fuels, land use and land cover change, and fire. Previous studies have demonstrated that NEP drives most of the atmospheric CO_2 seasonality (> 90%; Nevison et al., 2008; Randerson et al., 1997) and interannual variability (e.g., Rayner et al. 2008; Battel et al. 2000).

2.2.4 Global temperature sensitivity and separation of regional influences

For insight on a functional climate response, we investigate the global temperature sensitivity of the atmospheric CO_2 growth rate and the testbed ensemble fluxes. Variability in the CO_2 growth

rate anomaly was calculated as the difference between timestep *n* and *n*-1 for the monthly and annual interannual variability (IAV) timeseries. Testbed flux timeseries were averaged to monthly resolution and interpolated (averaged between months) to match the monthly initiation of each corresponding CO_2 growth rate anomaly timeseries. Following Arora et al. (2013), we calculate temperature sensitivity (γ) using an ordinary linear regression for the timeseries of temperature interannual variability (T IAV) with 1) atmospheric CO_2 growth rate anomalies, and 2) land flux IAV (see section 2.2.2). For atmospheric CO_2 growth rate anomalies, each timeseries was converted from ppm y^{-1} to PgC y^{-1} based on the global mass of atmospheric dry air. Thus, all global sensitivity values are reported in units of PgC y^{-1} K^{-1}. A reference global temperature sensitivity value for the CO_2 growth rate was calculated for 1982 to 2010 using ESRL CO_2 observations and the Climatic Research Unit's gridded temperature product (CRU TS4; Jones et al., 2012). The CRU TS4 historical product was used because it consists of directly interpolated station data.

We also assess the influence of individual regions on the global mean signal for both component land fluxes (NPP, HR) and simulated atmospheric CO_2 (CO_2^{NPP}, CO_2^{HR}, CO_2^{NEP}). To quantify each region's contribution to global variability we calculate the ratio of regional IAV magnitude to global IAV magnitude, which we define as relative standard deviation (σ_{REL}). For each flux and CO_2 region (NHL, NML, NT, ST, SE), this ratio is calculated from the standard deviation of each monthly IAV timeseries. However, for the regional values of simulated CO_2 IAV, we identify the global mean response to a single region's fluxes. That is, the CO_2 IAV averaged across all six CO_2 regions but sourced only from testbed fluxes in the NHL, or NML, etc., without influence from the other flux regions. We then take the standard deviation of this

regionally-selected global mean IAV for the ratio to total global CO_2 IAV magnitude (derived from all global fluxes). To measure the strength of each region's impact on global values, we use the same regional-global partitioning to calculate correlation coefficients (r) for the timeseries of component flux IAV and CO_2 IAV. Thus, if an individual region were responsible for all observed global flux or CO_2 variability, it would have both σ_{REL} and r values equal to 1 in this comparison. The value for σ_{REL} decreases with the magnitude of regional variability, and r decreases if the variability is not coherent with the global signal, even if the magnitude of variability is high.

2.3 Results

2.3.1 Seasonal imprint of heterotrophic respiration

The three soil carbon models in the testbed impart different fingerprints on atmospheric CO_2 variability. Both CO_2^{NPP} and CO_2^{HR} show largest seasonality in the NHL, with seasonal amplitudes decaying toward the tropics and Southern Hemisphere. In the NHL, the peak-to-trough amplitude of CO_2^{NPP} is 39±2 ppm, with a seasonal maximum in April and a seasonal minimum in August (Figure 2.2a). The seasonal cycles for CO_2^{HR} simulated from all testbed models are out of phase with that of CO_2^{NPP}, and there are large amplitude differences in CO_2^{HR} among the model ensemble members. Specifically, the NHL amplitude of $CO_2^{CORPSE\ HR}$ is 28±3 ppm, while the amplitudes for $CO_2^{MIMICS\ HR}$ and $CO_2^{CASA\text{-}CNP\ HR}$ are only 17±1 ppm, accounting for about 40-70% of the amplitude from CO_2^{NPP} (Table 2.1). However, in all latitude bands, the largest CO_2^{HR} amplitude comes from the microbially explicit models – CORPSE for the Northern Hemisphere and MIMICS for the Southern Hemisphere (Table 2.1). The amplitudes of CO_2^{NPP} and CO_2^{HR} decrease further south, but the amplitude ratio of CO_2^{HR} to CO_2^{NPP} in NML

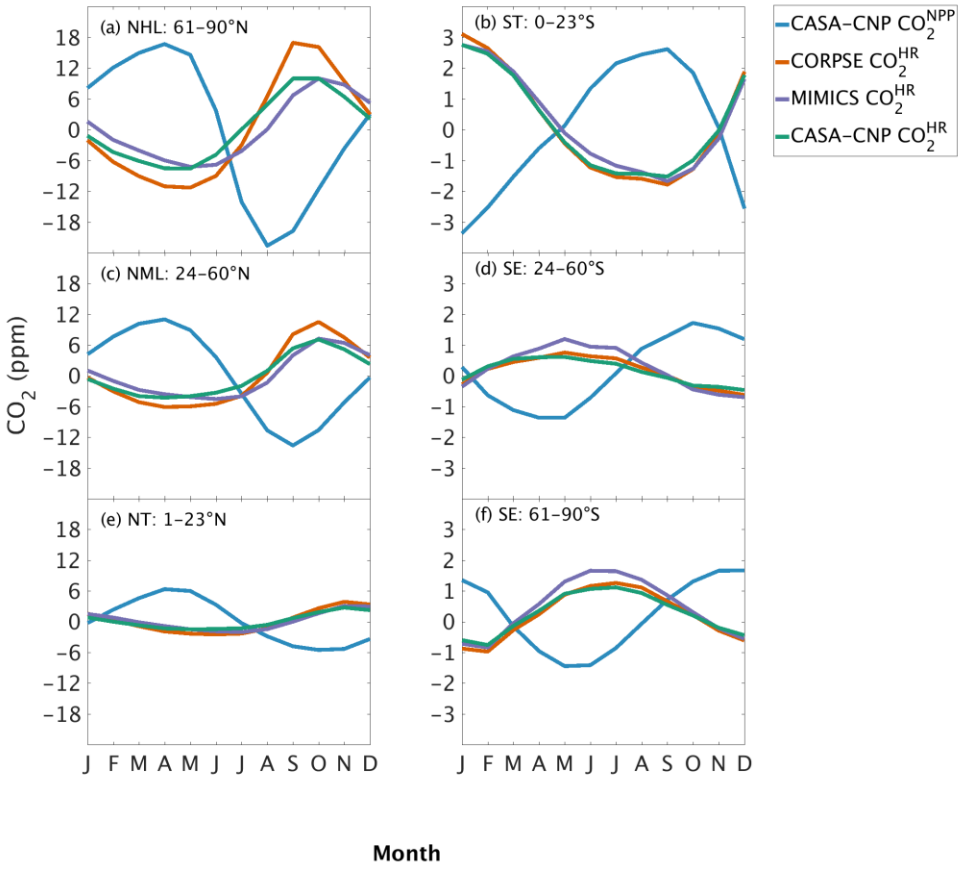

Figure 2.2: Climatological annual cycle (median) of atmospheric CO_2 simulated from individual flux components (CO_2^{NPP}, CO_2^{HR}) between 1982 and 2010 for atmospheric sampling bands in the Northern Hemisphere (a-c) and Southern Hemisphere (d-f). Note the change in y-axis scale between the two hemispheres.

and NT remains about 0.4-0.7 (Figure 2.2b-c; Table 2.1). In the Southern Hemisphere tropics, the amplitude of CO_2^{NPP} was smaller than that the Northern Hemisphere, however amplitude of CO_2^{HR} was similar to the NT values (Table 2.1). In the Southern Hemisphere extratropics, the amplitudes for all components were less 3 ppm (Table 2.1).

Table 2.1: Atmospheric CO_2 mean annual cycle amplitude (in ppm) simulated from heterotrophic respiration (HR), net primary productivity (NPP), and net ecosystem productivity (NEP). The median annual cycle amplitudes for observed CO_2 (CO_2^{OBS}) averaged over latitude bands are also reported.

	NHL 61°-90°N	**NML** 24°-60°N	**NT** 0°-23°N	**ST** 1°-23°S	**SE** 24°-60°S	**SE** 61°-90°S
$CO_2^{CASA\text{-}CNP\ HR}$	17.6	11.4	4.3	4.3	1.1	1.9
$CO_2^{CORPSE\ HR}$	28.2	16.6	6.4	4.9	1.4	2.2
$CO_2^{MIMICS\ HR}$	17.2	11.8	5.1	4.4	1.9	2.5
$CO_2^{CASA\text{-}CNP\ NPP}$	39.3	24.6	11.9	6.0	3.1	3.1
$CO_2^{CASA\text{-}CNP\ NEP}$	26.2	16.3	9.3	1.6	2.2	2.2
$CO_2^{CORPSE\ NEP}$	23.4	14.8	8.7	1.3	2.2	2.4
$CO_2^{MIMICS\ NEP}$	32.8	19.0	10.4	1.7	1.9	2.1
CO_2^{OBS}	15.3	10.6	6.1	0.9	0.8	1.4

The phasing of CO_2^{HR} is an important driver of the overall comparison between CO_2^{NEP} and observed CO_2 seasonality (Figure 2.3). When the contributions of NPP and HR seasonality are considered together (i.e., CO_2^{HR} + CO_2^{NPP}), the simulated amplitude of CO_2^{NEP} is larger than the observed CO_2 across all latitude bands (Figure 2.3). The largest mismatch is in the NHL zone, where the observed mean annual cycle is 15±0.9 ppm, while the peak-to-trough CO_2^{NEP} ranges from 23±1.3 ppm for CORPSE to 33±1.4 ppm for MIMICS (Figure 2.3a). The smaller CO_2^{NEP} amplitude simulated by CORPSE is due to the large CO_2^{HR} seasonality that counteracts the seasonality in NPP (Figure 2.2a-b). Furthermore, $CO_2^{MIMICS\ HR}$ and $CO_2^{CASA\text{-}CNP\ HR}$ have similar amplitudes in the NHL (Figure 2.2a; Table 2.1), but the CO_2^{NEP} amplitude from these two

models differs (33±1.2 ppm versus 26±1 ppm, respectively; Figure 2.3a; Table 2.1). This occurs because $CO_2^{MIMICS\ HR}$ peaks one-month later than $CO_2^{CASA\text{-}CNP\ HR}$, and has a zero-crossing that is more closely aligned with the trough of CO_2^{NPP} (Figure 2.2a), leading to the larger amplitude in $CO_2^{MIMICS\ NEP}$ (Figure 2.3a; Table 2.1). Although the amplitude mismatch decreases towards the south (Figure 2.3b-f), the overall bias in the Northern Hemisphere suggests that either the seasonality of NPP is too large, or that all testbed models underestimate the seasonality of HR. Within the ST region, ensemble CO_2^{HR} minima are opposite to that in CO_2^{NPP}, leading to a small annual cycle in simulations whereas the double peak in the ESRL observations may reflect fluxes not accounted for in our framework (Figures 2.2d, 2.3d).

2.3.2 Interannual imprint of heterotrophic respiration

The testbed ensemble reasonably simulates the magnitude and timing of interannual variability (IAV) compared with CO_2 observations (Figure 2.4). Across the six latitude bands analyzed, simulated CO_2^{NEP} IAV generally falls within one standard deviation of the median variation from observations for most of the study period (Figure 2.4). Taking a closer look at the CO_2 from the component fluxes (NPP and HR), across all six latitude bands, the CO_2^{NPP} IAV standard deviation is between 0.9 and 1.1 ppm for component fluxes (Figure 2.5a). $CO_2^{CASA\text{-}CNP\ HR}$ IAV shows similar standard deviation as CO_2^{NPP} IAV, whereas the standard deviations of $CO_2^{CORPSE\ HR}$ and $CO_2^{MIMICS\ HR}$ range from 0.7-1.4 ppm and 0.5-1.1 ppm, respectively (Figure 2.5a).

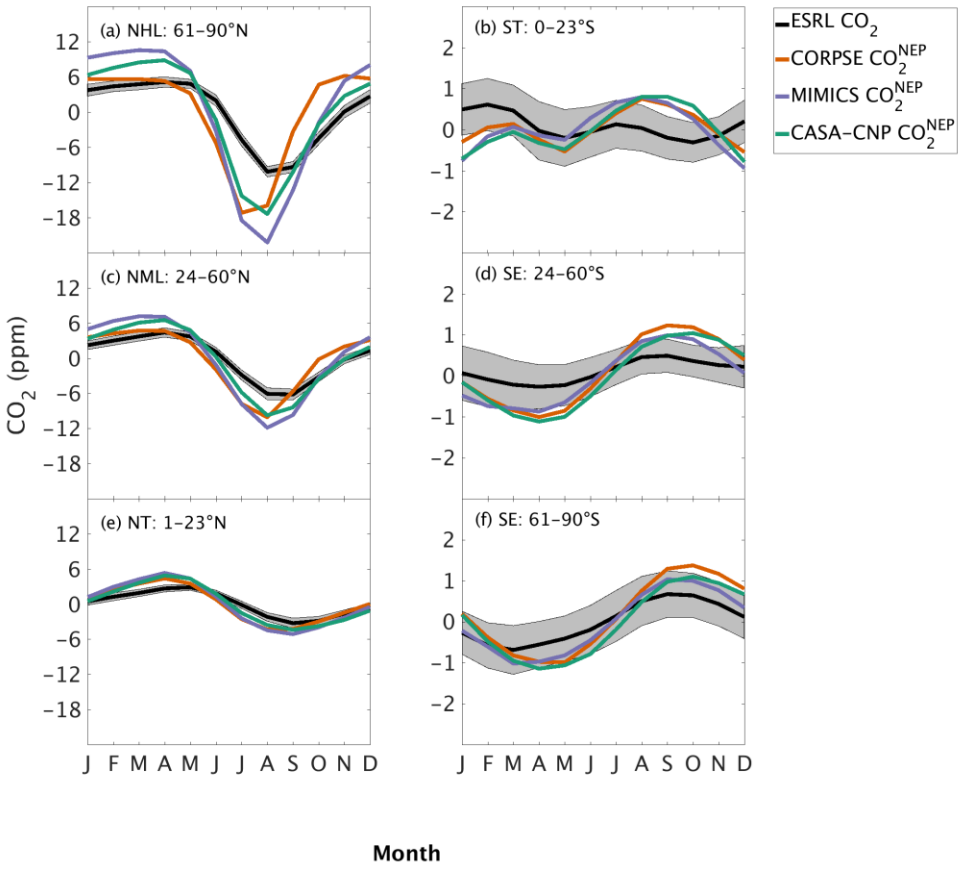

Figure 2.3: Climatological annual cycle (median) of CO_2 for observations (black) and global net ecosystem productivity flux (CO_2^{NEP}, colors) between 1982 and 2010 for six atmospheric sampling bands in the Northern Hemisphere (a-c) and Southern Hemisphere (d-f). Note the change in y-axis scale between the two hemispheres. Shading on the observed line represents one standard deviation due to interannual variability in the seasonal cycle.

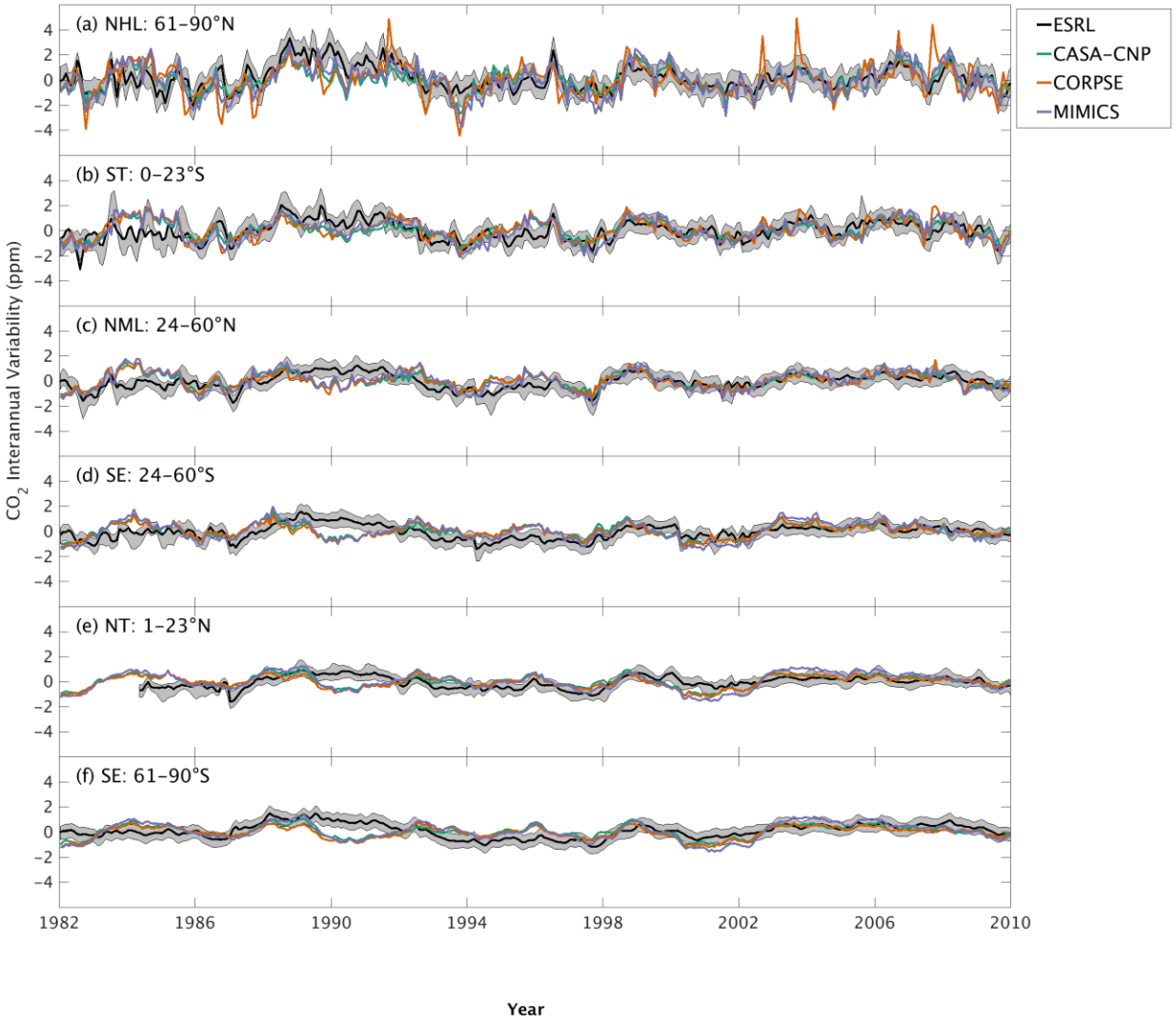

Figure 2.4: Interannual variability of CO_2 from global net ecosystem productivity (CO_2^{NEP} IAV) for testbed models (colors) and marine boundary layer observations from the NOAA ESRL network (black). Gray shading outlines one standard deviation of observed CO_2 interannual variability. High-latitude, mid-latitude and tropical land belts are shown for the Northern Hemisphere (a-c) and Southern Hemisphere (d-f).

Combining the CO_2 responses from component fluxes to CO_2^{NEP} reveals a latitudinal gradient in IAV standard deviation similar to that of ESRL observations, with largest standard deviation found in the northern extratropics (Figure 2.5b). Among the three testbed models, the standard deviation of $CO_2^{CASA\ NEP}$ agrees best with observations across all latitude bands ($CO_2^{CASA\ NEP}$:

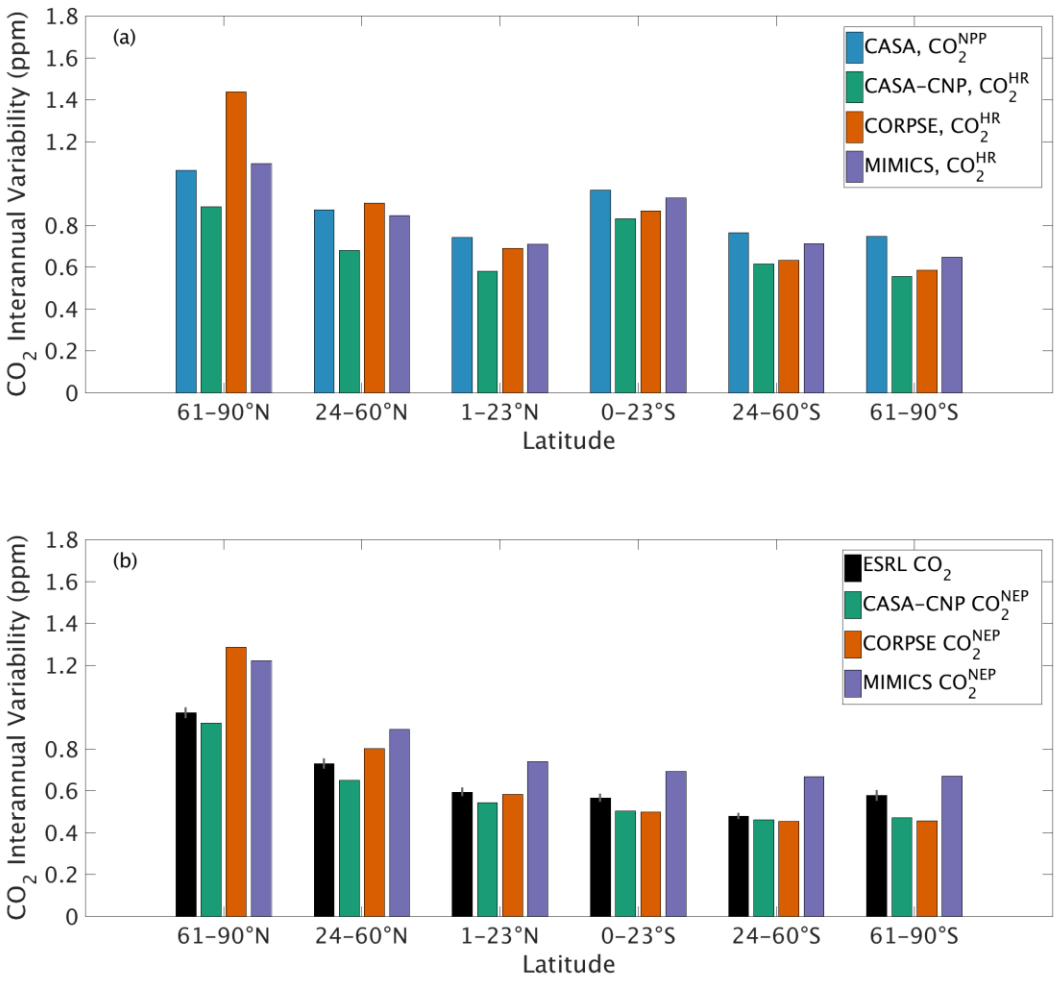

Figure 2.5: Magnitude of CO_2 interannual variability resulting from (a) individual flux components (CO_2^{NPP} IAV, CO_2^{HR} IAV) and (b) global net ecosystem productivity (CO_2^{NEP} IAV). Observed CO_2 IAV from NOAA ESRL network are shown with black bars whereas colors represent simulated data. Errorbars shown on the observed IAV represent two standard deviations, calculated as the median magnitude after removing a 12 month sliding window from the IAV timeseries.

0.5-0.9 ppm; ESRL: 0.6-1.0 ppm; Figure 2.5b). $CO_2^{CORPSE\ NEP}$ overestimates IAV by up to 30% in NHL and NML, but agrees better with observations in the tropics and Southern Hemisphere. $CO_2^{MIMICS\ NEP}$ overestimates IAV standard deviations across all latitude bands (Figure 2.5b). Interestingly, in the NHL, the overestimation is 20% even though $CO_2^{MIMICS\ HR}$ shows similar

IAVs as CO_2^{NPP} (both 1.1 ppm; Figure 2.5). This suggests that the phasing of $CO_2^{MIMICS\ HR}$ IAV relative to CO_2^{NPP} contributes to $CO_2^{MIMICS\ NEP}$ bias.

Both global NPP and HR fluxes are sensitive to temperature variations at interannual timescales, with increased build-up of CO_2 in the atmosphere at higher temperatures. Since these temperature sensitivities cannot be directly constrained from observations, we calculate temperature sensitivities for the CO_2 resulting from these component fluxes as well as from NEP. For CASA-CNP, the temperature sensitivity (γ) for globally integrated NPP and HR fluxes is 2.5 PgC yr^{-1} K^{-1} and 1.7 PgC yr^{-1} K^{-1}; respectively (Figure 2.6a). The temperature sensitivity of HR was higher for the microbially explicit models: 2.1 PgC yr^{-1} K^{-1} for CORPSE and 4.2 PgC yr^{-1} K^{-1} for MIMICS (Figure 2.6a). For any given testbed flux (NPP, HR, or NEP), the temperature sensitivity of the resulting global mean CO_2 growth rate anomaly is higher than that of the underlying flux IAV. For example, the temperature sensitivity of the globally integrated NPP flux IAV (γNPP) is 2.5 PgC yr^{-1} K^{-1} whereas γCO_2^{NPP} is 3.2 PgC yr^{-1} K^{-1}. The apparent amplification of the temperature sensitivity was even larger for HR. For example, the temperature sensitivity of MIMICS HR IAV (γHR^{MIMICS}) was 4.2 PgC yr^{-1} K^{-1}, whereas $\gamma CO_2^{MIMICS\ HR}$ was 7.7 PgC yr^{-1} K^{-1} (Figure 2.6a). The resulting testbed CO_2^{NEP} overestimates the temperature sensitivity of the observed atmospheric CO_2 growth rate anomaly (6.1±2.5 PgC yr^{-1} K^{-1}; Figure 2.6b). CASA-CNP and CORPSE have temperature sensitivities within the range of the observed sensitivity, but $\gamma CO_2^{MIMICS\ NEP}$ is 80% larger than observed value (10.9 PgC yr^{-1} K^{-1}; Figure 2.6b). We note that the γHR and γCO_2^{HR} is an emergent property that reflects both direct and indirect temperature influences, including the impact of temperature variability on NPP and litterfall (Table S2.3).

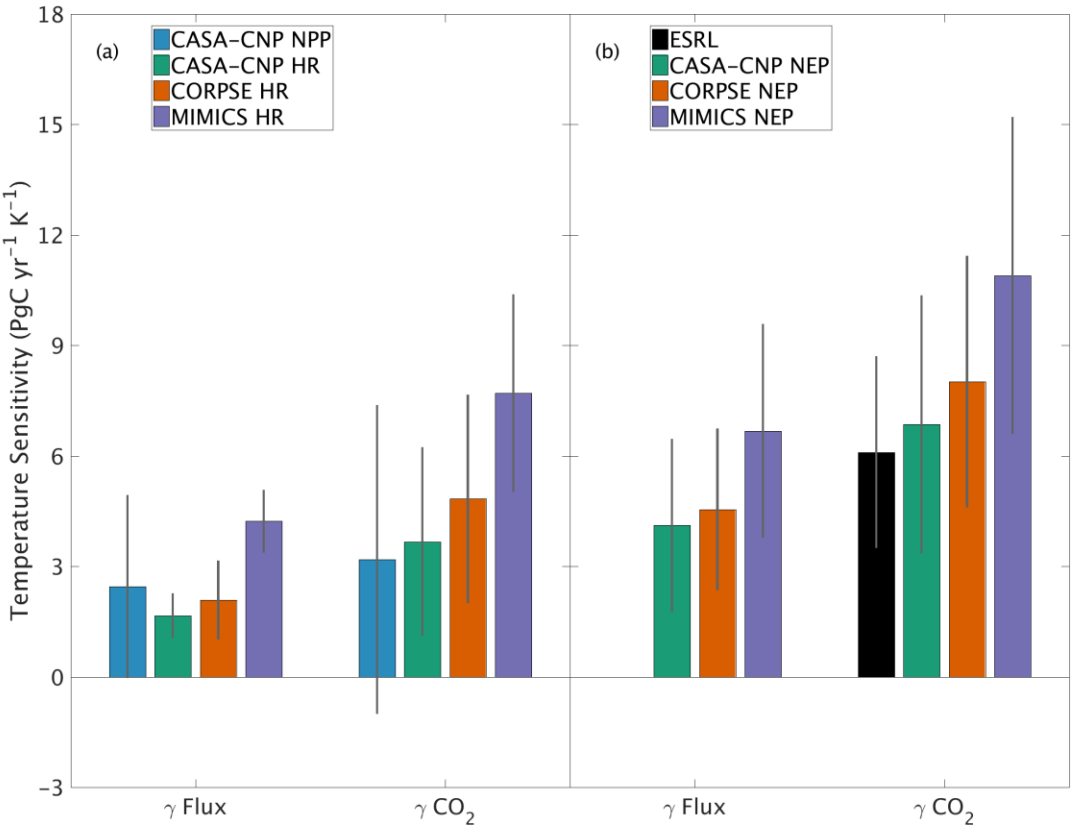

Figure 2.6: Temperature sensitivity (γ) calculated for interannual variability (IAV) of CASA-CNP air temperature and (a) flux IAV and corresponding CO_2 growth rate anomalies, (b) NEP IAV and CO_2^{NEP} growth rate anomalies. Reference sensitivity value (black) was calculated using NOAA ESRL CO_2 and CRU TS4 air temperature. Sensitivity values were calculated as the ordinary linear regression coefficient between IAV timeseries for 1982 to 2010. Errorbars represent the 95% confidence interval for coefficient values.

2.3.3 Geographic origins of CO_2 IAV

The interannual variability (IAV) in global NPP and HR originate from different geographic regions. The IAV in global NPP fluxes are dominated by variations within the NT and ST

regions, with relative standard deviation σ_{REL} ~ 0.5 and correlation coefficient r ~ 0.6 (Figure 2.7a-b). The NML region also has a similar contribution to the NT in magnitude, but with a lower timing coherence (r = 0.44; Figure 2.7a-b). In contrast to the dominance of the tropics in IAV of global NPP, the NML region contributes most to IAV in global HR, with $\sigma_{REL} \geq 0.6$ and r ~ 0.8 for all three testbed models (Figure 2.7c-d). The NHL region is also important in driving global HR flux variability based on CORPSE model results (σ_{REL} = 0.59 and r = 0.82; Figure 2.7c-d). Despite high NPP variability in the tropics, the magnitude of tropical HR variability is only about 10-30% of global HR variability, and the timing coherence with the global signal is generally low (r < 0.45; Figure 2.7a-b). MIMICS HR IAV is the exception for the ST measuring close to 40% of global HR IAV magnitude and relatively high correlation (r = 0.58; Figure 2.7a-b). Together, the tropics and NML contribute roughly equally to the magnitude of global NEP variability (σ_{REL} between 0.44-0.55; Figure 2.7e). Although the NML and NT show relatively high timing coherence (0.41-0.55), the ST shows the strongest timing coherence with global NEP IAV (r > 0.7; Figure 2.7f).

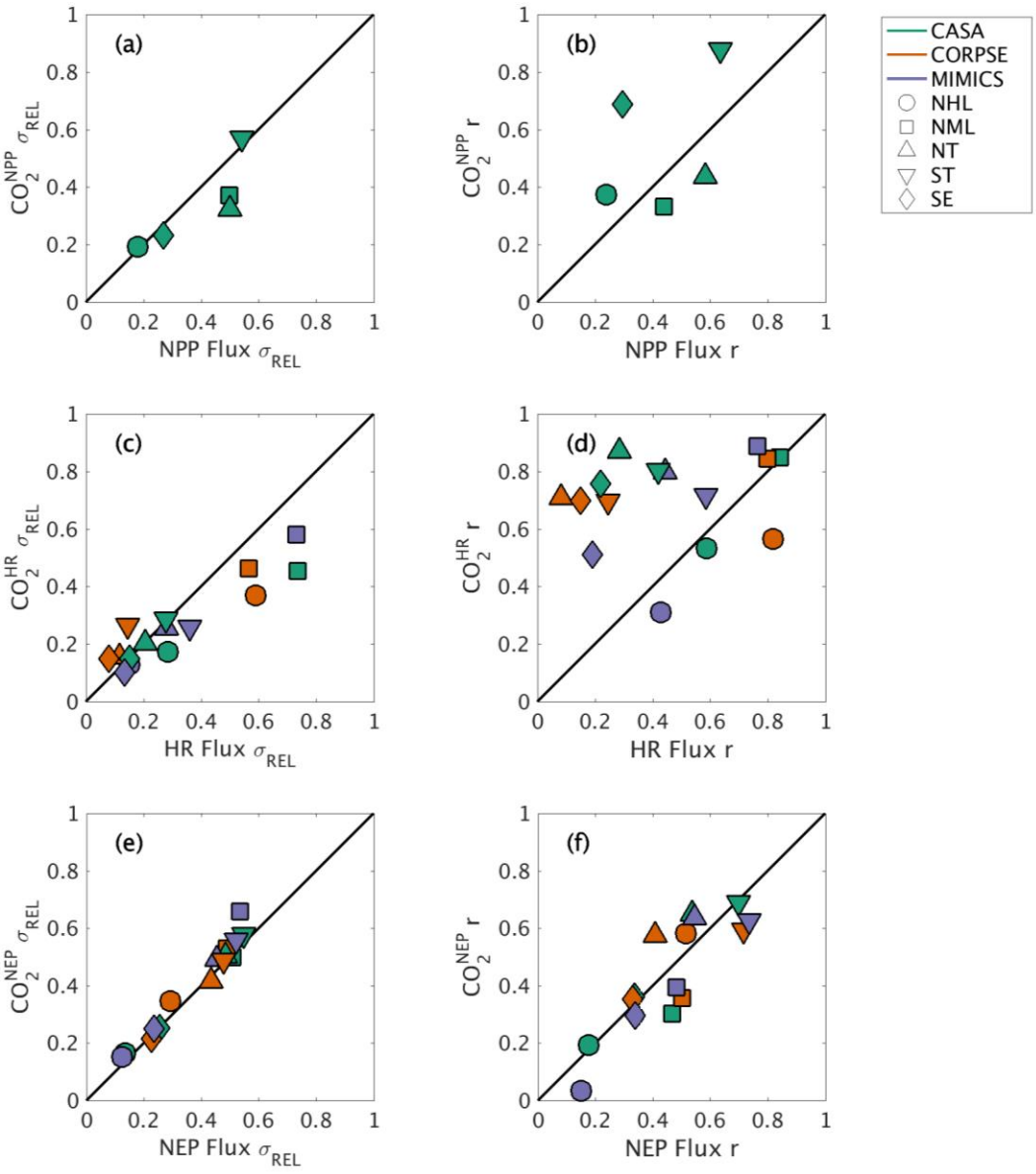

Figure 2.7: Comparison of regional and global interannual variability (IAV) from land fluxes and resulting atmospheric CO_2 between 1982 and 2010. (a, c, e) Normalized ratio taken between regional IAV and global IAV magnitude. (b, d, f) Linear correlation between regional IAV and global IAV. The scatterplot shows a direct comparison of ratio and correlation values for land flux values (x-axes) and corresponding CO_2 (y-axes). Shapes denote the source regions for both land fluxes and CO_2 response.

Atmospheric transport modifies patterns of IAV in fluxes, emphasizing tropical flux patterns and de-emphasizing northern hemisphere flux patterns. For example, the role of ST in driving global

CO_2^{NPP} variability is amplified compared to the underlying fluxes, as the timing coherence with the global signal increases from $r = 0.64$ for flux IAV to $r = 0.88$ for CO_2^{NPP} IAV for this region (Figure 2.7b). Conversely, the role of NML is dampened, with timing coherence decreasing to $r = 0.33$ for CO_2^{NPP} IAV versus $r = 0.44$ for NPP IAV (Figure 2.7b). Similarly, timing coherence for tropical CO_2^{HR} IAV is substantially higher than that for HR fluxes in ST and NT (>0.7), although the atmospheric transport impact differs across the three testbed models (Figure 2.7d). In contrast to closely aligned NML correlation values for CO_2^{HR} and HR ($r \sim 0.8$-0.9), NML CO_2^{HR} IAV shows σ_{REL} between 0.45 and 0.58, a decrease from the HR IAV contribution (NML HR IAV σ_{REL} range: 0.57 to 0.74; Figure 2.7c). For CO_2^{NEP} IAV, the regional contribution is more consistent with similar σ_{REL} and r to flux IAV (Figure 2.7e-f).

2.4 Discussion

Modeled differences in heterotrophic respiration impart discernible signatures on atmospheric CO_2. We analyzed the atmospheric CO_2 response to soil heterotrophic respiration (HR) using a soil testbed ensemble with three plausible representations of HR (CASA-CNP, CORPSE, MIMICS) and a 3-D atmospheric transport model. Results show that HR phasing is important for ecosystem carbon flux (NEP) at both seasonal and interannual timescales. Regional patterns of HR variability provide non-negligible contributions to global CO_2 variability. Here we discuss these findings in more detail as well as implications for the use of CO_2 observations for flux evaluation and model benchmarking.

2.4.1 Impacts of heterotrophic respiration on seasonality

Our evaluation of CO_2 simulated using testbed fluxes revealed that all testbed models overestimated the mean annual cycle amplitude of atmospheric CO_2 observations. In the Northern Hemisphere, the bias was largest for MIMICS, as the $CO_2^{\text{MIMICS NEP}}$ amplitude was overestimated by up to 100% (Figure 2.3). The mismatch was smallest in $CO_2^{\text{CORPSE NEP}}$, which was within 70% of the observed annual cycle amplitude where CORPSE simulates the largest seasonal HR fluxes (Figure 2.3a-c, Table 2.1). We note that the mismatch across all three testbed formulations could be due to overestimation of the NPP flux used by all three testbed models, or underestimation of HR seasonality. However, an advantage of the testbed approach is that, because all of the models are driven by the same NPP and climate variables, the differences in the HR flux amplitudes arise from structural differences in the testbed. In the Southern Hemisphere, in contrast to the large differences found in the Northern Hemisphere, the simulated CO_2 annual cycle amplitudes were similar across all three models, with small absolute mismatches (about 1 ppm) compared to observations.

One challenge in using atmospheric CO_2 to evaluate HR representation in soil models is the influence of productivity (NPP) on both HR fluxes and atmospheric CO_2 variations. The seasonal diagnostics we present are very sensitive to the phasing of HR fluxes relative to NPP. For example, in NHL a one-month lag in the seasonal maximum of CO_2^{HR} between MIMICS and CASA-CNP (Figure 2.2) leads to a 7 ppm difference in the overall amplitude of CO_2^{NEP}— this despite identical amplitudes of CO_2^{HR} for the two models (Figure 2.3). Although the substantial impacts of subtle phase differences complicate benchmarking, the sensitivity reveals interesting and important differences related to model structural choices (i.e. first order versus microbially

explicit). Wieder et al., (2018) noted that the microbially explicit models in the testbed had seasonal HR fluxes that peaked in the fall, about a month later than the HR fluxes simulated by CASA-CNP. The timing of CASA-CNP fluxes largely depend on soil temperature (highest HR flux when temperature is highest), whereas MIMICS and CORPSE have maximum HR fluxes set by trade-offs between the timing of maximal temperature and maximal microbial biomass, which is more tightly linked with litterfall (Figure 7 from Wieder et al., 2018). Thus, phasing of HR is a sensitive diagnostic for benchmarking, especially if additional constraints on the magnitude and phasing of NPP are available.

In this study, determining the unique contribution from HR was possible since NPP was common among the three soil models used in the testbed, but the contribution of NPP will need to be resolved for model evaluation in other contexts. Long-term records of vegetation productivity at regional and global scales have been observed via satellite vegetation indices (Hicke et al., 2002; Meroni et al., 2009; Running et al., 2004), and more recently chlorophyll fluorescence (Frankenberg et al., 2011; Guan et al., 2016; Kohler et al., 2018; Li et al., 2018). Our study underscores the importance of developing methods to use these datasets together with atmospheric CO_2 to inform the dynamics of carbon cycling and its component fluxes.

2.4.2 Impacts of heterotrophic respiration on interannual variability

Similar to the analyses on seasonal cycles, the testbed ensemble simulations showed a higher CO_2 IAV associated with explicit microbial representation (Figure 2.5). This is especially true for CO_2^{CORPSE} in the NHL and NML (Figure 2.5a). Interestingly, in the tropics and SE, $CO_2^{MIMICS\ HR}$ IAV is only slightly higher than that of $CO_2^{CASA\text{-}CNP\ HR}$ or $CO_2^{CORPSE\ HR}$, but IAV

of $CO_2^{MIMICS\ NEP}$ was 20-30% higher than that of other models. Further, in these regions MIMICS HR IAV also shows an inverse, but highly correlated relationship with NPP IAV (R^2 > 0.60, Table S2.3). This suggests that the large IAV of $CO_2^{MIMICS\ NEP}$ may result from differences in phasing between NPP and MIMICS HR fluxes, similar to phasing between MIMICS NPP and HR affecting the shape of the CO_2^{NEP} annual cycle in NHL. In the NHL, all testbed models show HR IAV is correlated with both NPP IAV and temperature IAV (R^2 of 0.32 to 0.77; Table S2.3). Additionally, NPP IAV is sensitive to temperature variability ($\gamma = 0.15$, $R^2 = 0.43$; Table S2.3). Thus better diagnostics for atmospheric CO_2 IAV owing to HR requires additional constraints on NPP fluxes, especially at high latitudes.

The high IAV in $CO_2^{MIMICS\ NEP}$ is consistent with this model having the highest global temperature sensitivity overestimating observed value by 80% (Figure 2.6b). CORPSE, the other microbially explicit model, had a 30% higher temperature sensitivity in CO_2^{NEP} than observed globally (Figure 2.6b). This large bias in temperature sensitivity demonstrates the structural uncertainty associated with current HR parameterization, and highlights the need for continued investigation of model microbial representation to improve the functional relationship with temperature in soil models.

2.4.3 Implications for model benchmarking using atmospheric CO_2

Our results provide useful insights for model benchmarking using atmospheric CO_2. On a global scale, interannual variability (IAV) of simulated atmospheric CO_2 was shown to be affected by the variability in component fluxes (NPP, HR) from different land regions (Figures 2.5-2.7). The tropics dominate IAV in global NPP, while northern extratropics dominate the IAV in global HR

(Figure 2.7a-d). Taken together, NEP variability reflects roughly equal contributions from northern hemisphere temperate ecosystems (NML) and tropical ecosystems (NT and ST; Figure 2.7e-f). These results suggest that the interannual variability of atmospheric CO_2 results from two different processes (respiration and productivity) across multiple ecoclimate regions, whereas previous studies have mostly identified tropical (e.g. Cox et al., 2013; Wang et al., 2013) or subtropical, semi-arid regions (e.g. Ahlstorm et al., 2015; Poulter et al., 2014) as dominant controls on the global CO_2 IAV.

Our analysis underscores that patterns of variability in atmospheric CO_2 are tied not only to variabilities in the underlying fluxes, but also to atmospheric transport. For example, we showed that the temperature sensitivity of CO_2 growth rate anomalies was larger than the sensitivity estimated from the fluxes themselves (Figure 2.6). The enhanced temperature sensitivity for CO_2^{HR} was larger than for that of CO_2^{NPP}, which suggests that the geographic origin of the fluxes relative to dominant patterns of transport affects the result (Figure 2.6a). This transport enhancement of the apparent temperature sensitivity of CO_2 growth rate anomalies is consistent with results from Keppel-Aleks et al. (2018). While these results may be tied to the choice of GEOS-Chem to simulate atmospheric transport, they do underscore that (1) atmospheric CO_2 must be simulated from land fluxes to be use as a benchmark and (2) atmospheric observations should not be assumed to be a direct proxy for fluxes themselves.

We employed several benchmarking approaches, including timeseries comparison and functional response to temperature, to evaluate if CO_2 patterns reflect underlying representations of soil heterotrophic respiration. We found that soil heterotrophic respiration leaves non-negligible

imprints on atmospheric CO_2, leaving open the possibility of more explicitly accounting for respiration variability using atmospheric CO_2 observations. Given that HR links to NPP, soil C pools, and temperature, we recommend synergistically using datasets that reflect these variables (instead of identifying metrics in isolation). This could provide better model process evaluation if implemented in a larger benchmarking framework, such as the International Land Model Benchmarking Project (ILAMB; Collier, 2018; Hoffman et al., 2016). Model development will be crucial in the next decade of carbon cycle research, but so will tools to test mechanistic understanding and elucidate a coherent picture of the land-atmosphere carbon response to a changing climate.

2.5 Conclusions

Soil heterotrophic respiration remains a source of uncertainty in tracking carbon flows between terrestrial ecosystems and the atmosphere. Ground observations are limited by geographic region and empirical calculations of carbon fluxes. Model representations of microbial communities simplify complex biological systems and require evaluation for added predictive capability in carbon exchange. The Soil Biogeochemical Testbed offers a foundation for efficient comparison of different soil model structures. Here we utilized the Testbed in combination with ESRL observations of atmospheric CO_2 to gain insight on structural uncertainty as it relates to soil heterotrophic respiration and its imprint on atmospheric CO_2 variability. We found that structural differences, such as explicit microbial pools, are distinguishable in HR output and cascade to resulting CO_2 patterns, providing a fingerprint by which this flux can be benchmarked at regional scales using atmospheric observations. Additionally, comparison of trends at interannual timescales revealed regional HR influences on global CO_2 and traceable imprints of HR parameterization. These results suggest that CO_2 observations combined with observational

constraints on productivity could be leveraged for insight on soil heterotrophic respiration in a model benchmarking setting, expanding the potential to advance mechanistic understanding of this important component of the carbon cycle.

References

Ahlström, A., Raupach, M., Schurgers, G., Smith, B., Arneth, A., Jung, M., Reichstein, M., Canadell, J., Friedlingstein, P., Jain, A., Kato, E., Poulter, B., Sitch, S., Stocker, B., Viovy, N., Wang, Y. P., Wiltshire, A., Zaehle, S. and Zeng, N.: The dominant role of semi-arid ecosystems in the trend and variability of the land CO_2 sink, Science (80-.)., 348(6237), 895–899, doi:10.1002/2015JA021022, 2015.

Arora, V. K., Boer, G. J., Friedlingstein, P., Eby, M., Jones, C. D., Christian, J. R., Bonan, G., Bopp, L., Brovkin, V., Cadule, P., Hajima, T., Ilyina, T., Lindsay, K., Tjiputra, J. F. and Wu, T.: Carbon-concentration and carbon-climate feedbacks in CMIP5 earth system models, J. Clim., 26(15), 5289–5314, doi:10.1175/JCLI-D-12-00494.1, 2013.

Baldocchi, D.: TURNER REVIEW No. 15. "Breathing" of the terrestrial biosphere: Lessons learned from a global network of carbon dioxide flux measurement systems, Aust. J. Bot., 56(1), 1–26, doi:10.1071/BT07151, 2008.

Barba, J., Cueva, A., Bahn, M., Barron-Gafford, G. A., Bond-Lamberty, B., Hanson, P. J., Jaimes, A., Kulmala, L., Pumpanen, J., Scott, R. L., Wohlfahrt, G. and Vargas, R.: Comparing ecosystem and soil respiration: Review and key challenges of tower-based and soil measurements, Agric. For. Meteorol., 249(August 2017), 434–443, doi:10.1016/j.agrformet.2017.10.028, 2018.

Basile, S., Lin, X., Keppel-Aleks, G.: Simulated CO_2 dataset using the atmospheric transport model GEOSChem v12.0.0: Response to regional land carbon fluxes, https://doi.org/10.7302/xjzc-xy05, 2019.

Bond-Lamberty, B.: New Techniques and Data for Understanding the Global Soil Respiration Flux, Earth's Futur., 6(9), 1176–1180, doi:10.1029/2018EF000866, 2018.

Bond-Lamberty, B. and Thomson, A.: A global database of soil respiration data, Biogeosciences, 7(6), 1915–1926, doi:10.5194/bg-7-1915-2010, 2010.

Bond-Lamberty, B., Bailey, V. L., Chen, M., Gough, C. M. and Vargas, R.: Globally rising soil heterotrophic respiration over recent decades, Nature, 560(7716), 80–83, doi:10.1038/s41586-018-0358-x, 2018.

Bradford, M. A., Wieder, W. R., Bonan, G. B., Fierer, N., Raymond, P. A. and Crowther, T. W.: Managing uncertainty in soil carbon feedbacks to climate change, Nat. Clim. Chang., 6(8), 751–758, doi:10.1038/nclimate3071, 2016.

Bruhwiler, L., Michalak, A. M., Birdsey, R., Huntzinger, D. N., Fisher, J. B., Miller, J. and Houghton, R. A.: Overview of the Global Carbon Cycle, Second State Carbon Cycle Rep., 1–33, doi:10.7930/SOCCR2.2018.Ch1, 2018.

Buchkowski, R. W., Bradford, M. A., Grandy, A. S., Schmitz, O. J. and Wieder, W. R.: Applying population and community ecology theory to advance understanding of belowground biogeochemistry, Ecol. Lett., 20(2), 231–245, doi:10.1111/ele.12712, 2017.

Collier, N., Hoffman, F. M., Lawrence, D. M., Keppel-Aleks, G., Koven, C. D., Riley, W. J., Mu, M. and Randerson, J. T.: The International Land Model Benchmarking (ILAMB) System: Design, Theory, and Implementation, J. Adv. Model. Earth Syst., 10(11), 2731–2754, doi:10.1029/2018MS001354, 2018.

Collins, W., Deaven, D., Gandin, L., Iredell, M., Jenne, R. and Joseph, D.: The NCEP NCAR 40-Year Reanalysis Project, Bull. Am. Meteorol. Soc., 77(3), 437–472, doi:10.1175/JCLI-D-16-0758.1, 1996.

Cox, P. M., Pearson, D., Booth, B. B., Friedlingstein, P., Huntingford, C., Jones, C. D. and Luke, C. M.: Sensitivity of tropical carbon to climate change constrained by carbon dioxide variability., Nature, 494(7437), 341–4, doi:10.1038/nature11882, 2013.

Crisp, D., Pollock, H., Rosenberg, R., Chapsky, L., Lee, R., Oyafuso, F., Frankenberg, C., Dell, C., Bruegge, C., Doran, G., Eldering, A., Fisher, B., Fu, D., Gunson, M., Mandrake, L., Osterman, G., Schwandner, F., Sun, K., Taylor, T., Wennberg, P. and Wunch, D.: The on-orbit performance of the Orbiting Carbon Observatory-2 (OCO-2) instrument and its radiometrically calibrated products, Atmos. Meas. Tech., 10(1), 59–81, doi:10.5194/amt-10-59-2017, 2017.

Davidson, E. A., Savage, K., Verchot, L. V. and Navarro, R.: Minimizing artifacts and biases in chamber-based measurements of soil respiration, Agric. For. Meteorol., 113(1–4), 21–37, doi:10.1016/S0168-1923(02)00100-4, 2002.

Dlugokencky, E. J., Lang P. M., Mund J. W., Crotwell A. M., Crotwell M. J., and Thoning K. W.: Atmospheric carbon dioxide dry air mole fractions from the NOAA ESRL carbon cycle cooperative global air sampling network, 1968–2015, version 2016-08-30. NOAA, accessed 4 January 2017, ftp://aftp.cmdl.noaa.gov/data/trace_gases/co2/flask/surface/, 2016.

Frankenberg, C., Fisher, J. B., Worden, J., Badgley, G., Saatchi, S. S., Lee, J. E., Toon, G. C., Butz, A., Jung, M., Kuze, A. and Yokota, T.: New global observations of the terrestrial carbon cycle from GOSAT : Patterns of plant fluorescence with gross primary productivity, , 38, 1–6, doi:10.1029/2011GL048738, 2011.

Gelaro, R., McCarty, W., Suárez, M. J., Todling, R., Molod, A., Takacs, L., Randles, C. A., Darmenov, A., Bosilovich, M. G., Reichle, R., Wargan, K., Coy, L., Cullather, R., Draper, C., Akella, S., Buchard, V., Conaty, A., da Silva, A. M., Gu, W., Kim, G. K., Koster, R., Lucchesi, R., Merkova, D., Nielsen, J. E., Partyka, G., Pawson, S., Putman, W., Rienecker, M., Schubert, S. D., Sienkiewicz, M. and Zhao, B.: The modern-era retrospective analysis for research and

applications, version 2 (MERRA-2), J. Clim., 30(14), 5419–5454, doi:10.1175/JCLI-D-16-0758.1, 2017.

Guan, K., Berry, J. A., Zhang, Y., Joiner, J., Guanter, L., Badgley, G. and Lobell, D. B.: Improving the monitoring of crop productivity using spaceborne solar-induced fluorescence, Glob. Chang. Biol., 22(2), 716–726, doi:10.1111/gcb.13136, 2016.

Hicke, J. A., Asner, G. P., Randerson, J. T., Tucker, C., Los, S., Birdsey, R., Jenkins, J. C. and Field, C.: Trends in North American net primary productivity derived from satellite observations, 1982-1998, Global Biogeochem. Cycles, 16(2), 2-1-2–14, doi:10.1029/2001gb001550, 2002.

Hoffman, F. M., Koven, C. D., Keppel-Aleks, G., Lawrence, D. M., Riley, W. J., Randerson, J. T., Ahlström, A., Abramowitz, G., Baldocchi, D. D., Best, M. J., Bond-Lamberty, B., De Kauwe, M. G., Denning, A. S., Desai, A. R., Eyring, V., Fisher, J. B., Fisher, R. A., Gleckler, P. J., Huang, M., Hugelius, G., Jain, A. K., Kiang, N. Y., Kim, H., Koster, R. D., Kumar, S. V., Li, H., Luo, Y., Mao, J., McDowell, N. G., Mishra, U., Moorcroft, P. R., Pau, G. S. H., Ricciuto, D. M., Schaefer, K., Schwalm, C. R., Serbin, S. P., Shevliakova, E., Slater, A. G., Tang, J., Williams, M., Xia, J., Xu, C., Joseph, R. and Koch, D.: 2016 International Land Model Benchmarking (ILAMB) Workshop Report, , doi:10.2172/1330803, 2017.

Humphrey, V., Zscheischler, J., Ciais, P., Gudmundsson, L., Sitch, S. and Seneviratne, S. I.: Sensitivity of atmospheric CO_2 growth rate to observed changes in terrestrial water storage, Nature, 560(7720), 628–631, doi:10.1038/s41586-018-0424-4, 2018.

Jenkinson, A. D. S., Andrew, S. P. S., Lynch, J. M., Goss, M. J., Tinker, P. B. and Jenkinson, D. S.: The turnover of organic carbon and nitrogen in soil, Philos. Trans. R. Soc. London. Ser. B Biol. Sci., 329(1255), 361–368, doi:10.1098/rstb.1990.0177, 1990.

Jiang, L., Ji, D., Luo, Y., Liang, J., Xia, J., Li, Z., Wang, Y.-P., Rinke, A., Zhang, G., Ahlström, A., Koven, C., Chen, G., McGuire, A. D., Ciais, P., Peng, S., Hayes, D. J., Shi, Z., Krinner, G., Dong, J., Moore, J. C., Yan, L., Cheng, W. and Xiao, X.: Non-uniform seasonal warming regulates vegetation greening and atmospheric CO 2 amplification over northern lands , Environ. Res. Lett., 13(12), 124008, doi:10.1088/1748-9326/aae9ad, 2018.

Jones, P., and Harris, I.: CRU TS3. 21: Climatic Research Unit (CRU) Time-Series (TS) version 3.21 of high resolution gridded data of month-by-month variation in climate (Jan. 1901–Dec. 2012). NCAS British Atmospheric Data Centre, http://badc.nerc.ac.uk/view/badc.nerc.ac.uk__ATOM__ACTIVITY_0c08abfc-f2d5-11e2-a948-00163e251233, doi:10.5285/D0E1585D-3417-485F-87AE-4FCECF10A992, 2013.

Jones, P. D., Lister, D. H., Osborn, T. J., Harpham, C., Salmon, M. and Morice, C. P.: Hemispheric and large-scale land-surface air temperature variations: An extensive revision and an update to 2010, J. Geophys. Res. Atmos., 117(5), doi:10.1029/2011JD017139, 2012.

Keeling, C. D., Piper, S. C., Whorf, T. P. and Keeling, R. F.: Evolution of natural and anthropogenic fluxes of atmospheric CO 2 from 1957 to 2003, Tellus, Ser. B Chem. Phys. Meteorol., 63(1), 1–22, doi:10.1111/j.1600-0889.2010.00507.x, 2011.

Keppel-Aleks, G., Randerson, J. T., Lindsay, K., Stephens, B. B., Keith Moore, J., Doney, S. C., Thornton, P. E., Mahowald, N. M., Hoffman, F. M., Sweeney, C., Tans, P. P., Wennberg, P. O. and Wofsy, S. C.: Atmospheric carbon dioxide variability in the community earth system model: Evaluation and transient dynamics during the twentieth and twenty-first centuries, J. Clim., 26(13), 4447–4475, doi:10.1175/JCLI-D-12-00589.1, 2013.

Keppel-Aleks, G., Wolf, A. S., Mu, M., Doney, S. C., Morton, D. C., Kasibhatla, P. S., Miller, J. B., Dlugokencky, E. J. and Randerson, J. T.: Small phytoplankton drive high summertime carbon and nutrient export in the Gulf of California and Eastern Tropical North Pacifi, Global Biogeochem. Cycles, 29, 1295–1310, doi:10.1002/2014GB004890.Received, 2014.

Keppel-Aleks, G., Basile, S. J. and Hoffman, F. M.: A functional response metric for the temperature sensitivity of tropical ecosystems, Earth Interact., 22(7), doi:10.1175/EI-D-17-0017.1, 2018.

Konings, A. G., Bloom, A. A., Liu, J., Parazoo, N. C., Schimel, D. S. and Bowman, K. W.: Global, Satellite-Driven Estimates of Heterotrophic Respiration, Biogeosciences Discuss., 2100(November), 1–26, doi:10.5194/bg-2018-466, 2018.

Koven, C. D., Riley, W. J., Subin, Z. M., Tang, J. Y., Torn, M. S., Collins, W. D., Bonan, G. B., Lawrence, D. M. and Swenson, S. C.: The effect of vertically resolved soil biogeochemistry and alternate soil C and N models on C dynamics of CLM4, Biogeosciences, 10(11), 7109–7131, doi:10.5194/bg-10-7109-2013, 2013.

Lavigne, M. B., Ryan, M. G., Anderson, D. E., Baldocchi, D. D., Crill, P. M., Fitzjarrald, D. R., Goulden, M. L., Gower, S. T., Massheder, J. M., McCaughey, J. H., Rayment, M. and Striegl, R. G.: Comparing nocturnal eddy covariance measurements to estimates of ecosystem respiration made by scaling chamber measurements at six coniferous boreal sites, J. Geophys. Res. Atmos., 102(D24), 28977–28985, doi:10.1029/97jd01173, 1997.

Lehmann, J. and Kleber, M.: The contentious nature of soil organic matter, Nature, 528(7580), 60–68, doi:10.1038/nature16069, 2015.

Medlyn, B. E., Zaehle, S., De Kauwe, M. G., Walker, A. P., Dietze, M. C., Hanson, P. J., Hickler, T., Jain, A. K., Luo, Y., Parton, W., Prentice, I. C., Thornton, P. E., Wang, S., Wang, Y. P., Weng, E., Iversen, C. M., Mccarthy, H. R., Warren, J. M., Oren, R. and Norby, R. J.: Using ecosystem experiments to improve vegetation models, Nat. Clim. Chang., 5(6), 528–534, doi:10.1038/nclimate2621, 2015.

Meroni, M., Rossini, M., Guanter, L., Alonso, L., Rascher, U., Colombo, R. and Moreno, J.: Remote sensing of solar-induced chlorophyll fluorescence: Review of methods and applications, Remote Sens. Environ., 113(10), 2037–2051, doi:10.1016/j.rse.2009.05.003, 2009.

Moorhead, D. L. and Weintraub, M. N.: The evolution and application of the reverse Michaelis-Menten equation, Soil Biol. Biochem., 125(May), 261–262, doi:10.1016/j.soilbio.2018.07.021, 2018.

Myneni, R. B., Canadell, J. G., White, M. A., Nemani, R. R., Sitch, S., Ciais, P., Wang, W., Hashimoto, H., Milesi, C. and Piao, S.: Variations in atmospheric CO_2 growth rates coupled with tropical temperature, Proc. Natl. Acad. Sci., 110(32), 13061–13066, doi:10.1073/pnas.1219683110, 2013.

Nevison, C. D., Mahowald, N. M., Doney, S. C., Lima, I. D., van der Werf, G. R., Randerson, J. T., Baker, D. F., Kasibhatla, P. and McKinley, G. A.: Contribution of ocean, fossil fuel, land biosphere, and biomass burning carbon fluxes to seasonal and interannual variability in atmospheric CO_2, J. Geophys. Res. Biogeosciences, 113(1), 1–21, doi:10.1029/2007JG000408, 2008.

Oleson, K. W., Lawrence, D. M., Bonan, G. B., Drewniak, B., Huang, M., Charles, D., Levis, S., Li, F., Riley, W. J., Zachary, M., Swenson, S. C., Thornton, P. E., Bozbiyik, A., Fisher, R., Heald, C. L., Kluzek, E., Lamarque, F., Lawrence, P. J., Leung, L. R., Muszala, S., Ricciuto, D. M. and Sacks, W.: Technical description of version 4.5 of the Community Land Model (CLM), NCAR Technical Note NCAR/TN-503+STR, Natl. Cent. Atmos. Res. Boulder, CO, (July), 420pp, doi:10.5065/D6RR1W7M, 2013.

Parton, W. J.: The CENTURY Model, in: Evaluation of Soil Organic Matter Models, edited by: Powlson, D. S., Smith, P. and Smith, J. U., Springer-Verlag, Berlin, Heidelberg, Germany, 283–291, 1996.

Potter, C. S., Randerson, J. T., Field, C. B., Matson, P. A., Vitousek, P. M., Mooney, H. A., and Klooster, S. A.: Terrestrial ecosystem production: A process model based on global satellite and surface data, Global Biogeochem. Cycles, 7(4), 811–841, doi:10.1029/93GB02725, 1993.

Poulter, B., Frank, D., Ciais, P., Myneni, R.B., Andela, N., Bi, J., Broquet, G., Canadell, J.G., Chevallier, F., Liu, Y.Y., Running, S.W., Stich, S. and van der Werf, G.R.: Contribution of semi-arid ecosystems to interannual variability of the global carbon cycle, Nature, 509(7502), 600–603, doi:10.1038/nature13376, 2014.

Pumpanen, J., Kolari, P., Ilvesniemi, H., Minkkinen, K., Vesala, T., Niinistö, S., Lohila, A., Larmola, T., Morero, M., Pihlatie, M., Janssens, I., Yuste, J. C., Grünzweig, J. M., Reth, S., Subke, J. A., Savage, K., Kutsch, W., Østreng, G., Ziegler, W., Anthoni, P., Lindroth, A. and Hari, P.: Comparison of different chamber techniques for measuring soil CO 2 efflux, Agric. For. Meteorol., 123(3–4), 159–176, doi:10.1016/j.agrformet.2003.12.001, 2004.

Le Quéré, C., Andrew, R. M., Friedlingstein, P., Sitch, S., Pongratz, J., Manning, A. C., Korsbakken, J. I., Peters, G. P., Canadell, J. G., Jackson, R. B., Boden, T. A., Tans, P. P., Andrews, O. D., Arora, V. K., Bakker, D. C. E., Barbero, L., Becker, M., Betts, R. A., Bopp, L., Chevallier, F., Chini, L. P., Ciais, P., Cosca, C. E., Cross, J., Currie, K., Gasser, T., Harris, I., Hauck, J., Haverd, V., Houghton, R. A., Hunt, C. W., Hurtt, G., Ilyina, T., Jain, A. K., Kato, E.,

Kautz, M., Keeling, R. F., Klein Goldewijk, K., Körtzinger, A., Landschützer, P., Lefèvre, N., Lenton, A., Lienert, S., Lima, I., Lombardozzi, D., Metzl, N., Millero, F., Monteiro, P. M. S., Munro, D. R., Nabel, J. E. M. S., Nakaoka, S., Nojiri, Y., Padín, X. A., Peregon, A., Pfeil, B., Pierrot, D., Poulter, B., Rehder, G., Reimer, J., Rödenbeck, C., Schwinger, J., Séférian, R., Skjelvan, I., Stocker, B. D., Tian, H., Tilbrook, B., van der Laan-Luijkx, I. T., van der Werf, G. R., van Heuven, S., Viovy, N., Vuichard, N., Walker, A. P., Watson, A. J., Wiltshire, A. J., Zaehle, S. and Zhu, D.: Global Carbon Budget 2017, Earth Syst. Sci. Data Discuss., 1–79, doi:10.5194/essd-2017-123, 2018.

Randerson, J. T., Hoffman, F. M., Thornton, P. E., Mahowald, N. M., Lindsay, K., Lee, Y. H., Nevison, C. D., Doney, S. C., Bonan, G., Stöckli, R., Covey, C., Running, S. W. and Fung, I. Y.: Systematic assessment of terrestrial biogeochemistry in coupled climate-carbon models, Glob. Chang. Biol., 15(10), 2462–2484, doi:10.1111/j.1365-2486.2009.01912.x, 2009.

Randerson, J. T., Thompson, M. V., Conway, T. J., Fung, I. Y. and Field, C. B.: The contribution of sources and sinks to trends in the seasonal cycle of atmospheric carbon dioxide, Global Biogeochem. Cycles, 11(4), 535–560, doi:10.1029/97GB02268, 1997.

Randerson, J. T., Thompson, M. V., Malmstrom, C. M.: Substrate Limitations for Heterotrophs: Implications for models that estimate the seasonal cycle of atmospheric CO_2, Global Biogeochem. Cycles, 10(4), 585–602, doi:10.1029/96GB01981, 1996.

Rasmussen, C., Heckman, K., Wieder, W. R., Keiluweit, M., Lawrence, C. R., Berhe, A. A., Blankinship, J. C., Crow, S. E., Druhan, J. L., Hicks Pries, C. E., Marin-Spiotta, E., Plante, A. F., Schädel, C., Schimel, J. P., Sierra, C. A., Thompson, A. and Wagai, R.: Beyond clay: towards an improved set of variables for predicting soil organic matter content, Biogeochemistry, 137(3), 297–306, doi:10.1007/s10533-018-0424-3, 2018.

Rayner, P. J., Law, R. M., Allison, C. E., Francey, R. J., Trudinger, C. M. and Pickett-Heaps, C.: Interannual variability of the global carbon cycle (1992-2005) inferred by inversion of atmospheric CO 2 and δ 13 CO 2 measurements, Global Biogeochem. Cycles, 22(3), 1–12, doi:10.1029/2007GB003068, 2008.

Rienecker, M. M., Suarez, M. J., Gelaro, R., Todling, R., Bacmeister, J., Liu, E., Bosilovich, M. G., Schubert, S. D., Takacs, L., Kim, G. K., Bloom, S., Chen, J., Collins, D., Conaty, A., Da Silva, A., Gu, W., Joiner, J., Koster, R. D., Lucchesi, R., Molod, A., Owens, T., Pawson, S., Pegion, P., Redder, C. R., Reichle, R., Robertson, F. R., Ruddick, A. G., Sienkiewicz, M. and Woollen, J.: MERRA: NASA's modern-era retrospective analysis for research and applications, J. Clim., 24(14), 3624–3648, doi:10.1175/JCLI-D-11-00015.1, 2011.

Running, S. W., Nemani, R. R., Heinsch, F. A., Zhao, M., Reeves, M. and Hashimoto, H.: A Continuous Satellite-Derived Measure of Global Terrestrial Primary Production, Bioscience, 54(6), 547, doi:10.1641/0006-3568(2004)054[0547:ACSMOG]2.0.CO;2, 2004.

Ryan, M. G. and Law, B. E.: Interpreting, measuring, and modeling soil respiration, Biogeochemistry, 73(1), 3–27, doi:10.1007/s10533-004-5167-7, 2005.

Schmidt, M. W. I., Torn, M. S., Abiven, S., Dittmar, T., Guggenberger, G., Janssens, I. A., Kleber, M., Kögel-Knabner, I., Lehmann, J., Manning, D. A. C., Nannipieri, P., Rasse, D. P., Weiner, S. and Trumbore, S. E.: Persistence of soil organic matter as an ecosystem property., Nature, 478(7367), 49–56, doi:10.1038/nature10386, 2011.

Sulman, B. N., Phillips, R. P., Oishi, A. C., Shevliakova, E. and Pacala, S. W.: Microbe-driven turnover offsets mineral-mediated storage of soil carbon under elevated CO 2, Nat. Clim. Chang., 4(12), 1099–1102, doi:10.1038/nclimate2436, 2014.

Sulman, B. N., Moore, J. A. M., Abramoff, R., Averill, C., Kivlin, S., Georgiou, K., Sridhar, B., Hartman, M. D., Wang, G., Wieder, W. R., Bradford, M. A., Luo, Y., Mayes, M. A., Morrison, E., Riley, W. J., Salazar, A., Schimel, J. P., Tang, J. and Classen, A. T.: Multiple models and experiments underscore large uncertainty in soil carbon dynamics, Biogeochemistry, 141(2), 109–123, doi:10.1007/s10533-018-0509-z, 2018.

Todd-Brown, K. E. O., Randerson, J. T., Hopkins, F., Arora, V., Hajima, T., Jones, C., Shevliakova, E., Tjiputra, J., Volodin, E., Wu, T., Zhang, Q. and Allison, S. D.: Changes in soil organic carbon storage predicted by Earth system models during the 21st century, Biogeosciences, 11(8), 2341–2356, doi:10.5194/bg-11-2341-2014, 2014.

Turner, D. P., Ritts, W. D., Cohen, W. B., Gower, S. T., Running, S. W., Zhao, M., Costa, M. H., Kirschbaum, A. A., Ham, J. M., Saleska, S. R. and Ahl, D. E.: Evaluation of MODIS NPP and GPP products across multiple biomes, Remote Sens. Environ., 102(3–4), 282–292, doi:10.1016/j.rse.2006.02.017, 2006.

Wang, Y. P., Law, R. M. and Pak, B.: A global model of carbon, nitrogen and phosphorus cycles for the terrestrial biosphere, Biogeosciences, 7(7), 2261–2282, doi:10.5194/bg-7-2261-2010, 2010.

Wieder, W. R., Bonan, G. B. and Allison, S. D.: Global soil carbon projections are improved by modelling microbial processes, Nat. Clim. Chang., 3(10), 909–912, doi:10.1038/nclimate1951, 2013.

Wieder, W. R., Grandy, A. S., Kallenbach, C. M. and Bonan, G. B.: Integrating microbial physiology and physio-chemical principles in soils with the MIcrobial-MIneral Carbon Stabilization (MIMICS) model, Biogeosciences, 11(14), 3899–3917, doi:10.5194/bg-11-3899-2014, 2014.

Wieder, W. R., Grandy, A. S., Kallenbach, C. M., Taylor, P. G. and Bonan, G. B.: Representing life in the Earth system with soil microbial functional traits in the MIMICS model, Geosci. Model Dev., 8(6), 1789–1808, doi:10.5194/gmd-8-1789-2015, 2015.

Wieder, W. R., Hartman, M. D., Sulman, B. N., Wang, Y. P., Koven, C. D. and Bonan, G. B.: Carbon cycle confidence and uncertainty: Exploring variation among soil biogeochemical models, Glob. Chang. Biol., 24(4), 1563–1579, doi:10.1111/gcb.13979, 2018.

Wunch, D., Wennberg, P. O., Messerschmidt, J., Parazoo, N. C., Toon, G. C., Deutscher, N. M., Keppel-Aleks, G., Roehl, C. M., Randerson, J. T., Warneke, T. and Notholt, J.: The covariation of Northern Hemisphere summertime CO_2 with surface temperature in boreal regions, Atmos. Chem. Phys., 13(18), 9447–9459, doi:10.5194/acp-13-9447-2013, 2013.

Yokota, T., Yoshida, Y., Eguchi, N., Ota, Y., Tanaka, T., Watanabe, H. and Maksyutov, S.: Global Concentrations of CO_2 and CH_4 Retrieved from GOSAT: First Preliminary Results, Sola, 5, 160–163, doi:10.2151/sola.2009-041, 2009.

Zhao, Z., Peng, C., Yang, Q., Meng, F. R., Song, X., Chen, S., Epule, T. E., Li, P. and Zhu, Q.: Model prediction of biome-specific global soil respiration from 1960 to 2012, Earth's Futur., 5(7), 715–729, doi:10.1002/2016EF000480, 2017.

Chapter 3 Projected precipitation changes within the Great Lakes and Western Lake Erie Basin: a multi-model analysis of intensity and seasonality

N.B.: This chapter was published in 2017 as

Basile, S. J., Rauscher, S. A. and Steiner, A. L.: Projected precipitation changes within the Great Lakes and Western Lake Erie Basin: a multi-model analysis of intensity and seasonality, Int. J. Climatol., 37(14), 4864–4879, doi:10.1002/joc.5128, 2017.

3.1 Introduction

The Laurentian Great Lakes have the largest freshwater lake surface area in the world and support a diverse network of agriculture, transportation, and tourism. Precipitation is a key element of the water cycle in the Great Lakes Basin (GLB; Gronewold *et al.*, 2013; Gronewold and Stow, 2014), and the impacts of shifts in seasonal and daily precipitation have been documented across the region (Cherkauer and Sinha,2010; Michalak et al., 2013; Mishra and Cherkauer, 2011). The release of greenhouse gases which feedback to a rise in global temperatures are associated with changes in precipitation, and are likely to induce more frequent heavy rain and flooding events (Karl et al., 2009; Melillo et al., 2014). The most recent National Climate Assessment identifies an increasing regional trend in total precipitation over the Midwestern United States since 1991 (Melillo et al., 2014). Further, for the Midwest and Northeast regions that encompass the Great Lakes, the amount of precipitation falling in very heavy events (the heaviest 1% of all daily events) has increased by 37 and 71%, respectively over the same period (Melillo et al., 2014). Here, we investigate climate model simulations of

precipitation seasonality and intensity in the GLB and how they are projected to change with future climate.

Climate model simulation of precipitation depends on a suite of atmospheric and terrain-induced physical processes. Both the models' spatial resolution and the inclusion of complex terrain and coastlines such as the Great Lakes have a large impact on simulated precipitation. Many of the global climate models in the third Climate Model Intercomparison Project (CMIP3; Meehl et al., 2007) and the fifth iteration (CMIP5; Taylor et al., 2012) have coarse spatial resolution such that they do not explicitly represent the Great Lakes. To increase the resolution in complex topographic regions such as the Great Lakes, two common downscaling techniques are employed: dynamical downscaling and statistical downscaling (Wilby et al., 1998). Dynamical downscaling is a technique that uses high-resolution regional models driven by global climate model boundary conditions. For example, the North American Regional Climate Change Assessment Program (NARCCAP) ensemble of regional climate model (RCM) simulations was driven with initial and lateral boundary conditions obtained from global climate model output from the CMIP3 archive (Mearns et al., 2013). In contrast, statistical downscaling relies on observed relationships between large-scale variables and local variables over a historical period, and applies these relationships to increase the spatial resolution of existing global climate model output. While less computationally intensive than dynamical downscaling, a major drawback of statistical downscaling is the stationarity assumption, which requires that the statistical relationships remain the same in the observed period and in the future.

Previous climate and climate impact studies centered around or in the Great Lakes region have used either ensembles of global climate model data or downscaled data to understand how future precipitation may change in the Great Lakes region. Using a suite of global models from CMIP3, a statistical downscaling study suggests that winter and spring precipitation may increase between 20 and 30% by the end of century (2070–2099) (Hayhoe et al., 2010). Patz et al. (2008) calculated a 10–40% increase in the magnitude of extreme precipitation events in southern Wisconsin also based on CMIP3 model projections. A study using the NARCCAP ensemble to investigate changes across the agriculturally dominated Canadian prairie regions found up to a 15% increase in spring and summer precipitation as well as change in return periods for rain-dominated precipitation extremes (Khaliq et al., 2015). Vavrus and Behnke (2014) compared precipitation from global models with statistical and dynamically downscaled model output, and found a projected increase of annual precipitation <10% with more seasonal precipitation in all seasons except summer, increases in the intensity of daily extreme precipitation events (<30% increase in accumulation), and an even larger change in the return periods of extreme events (up to −50%).

Dynamically downscaled experiments have improved our understanding of the role of lake–atmosphere interactions in the present and under future climate conditions. Bryan et al. (2015) used dynamical downscaling with RegCM4 for the Great Lakes region to examine land–lake–atmosphere feedbacks in a high-resolution ensemble under present day conditions, and found that the simulation of lake temperature can introduce biases in simulated precipitation. Similar results were found when dynamically downscaling with the Weather Research and Forecast (WRF) model (Mallard et al., 2014). For future climate, Notaro et al. (2015) used dynamically

downscaled simulations to show that cold-season precipitation is projected to increase due to reductions in lake ice cover, yet the frequency of the lake effect snowstorms is expected to decrease. Gula and Peltier (2012) found that a regional model (WRF) and its global driving model [the Community Climate System Model (CCSM)] produced different spatial patterns of projected precipitation over the Great Lakes region. The global model (CCSM) projected an increase 15–25% in annual precipitation by mid-century (2050–2060), whereas the dynamically downscaled WRF simulations showed a precipitation reduction in the southern Great Lakes region and an increase in the northern Great Lakes. This difference was attributed to atmosphere–lake feedbacks. d'Orgeville et al. (2014) also used WRF with different physics parameterizations, and found that precipitation extremes are expected to increase in the Great Lakes region. Together, these studies highlight that there may be added value in using high-resolution simulations that accurately resolve the lake and its physical properties, and that global models are not likely to capture these regional nuances.

In this study, we conduct a multi-scale regional analysis of Great Lakes precipitation to identify the role of climate model method and grid resolution on precipitation projections. We examine the GLB as a whole, which is noted to be difficult to simulate due to the treatment of the lakes (Mearns et al., 2013). We also evaluate the specific subregion of the Western Lake Erie Basin (WLEB). The WLEB is the subject of ongoing agricultural management studies connected to recurring harmful algal blooms in western Lake Erie, and these events are influenced by regional precipitation intensity (Michalak et al., 2013). Our analysis utilizes modelled output from one global model ensemble and two dynamically downscaled regional model ensembles. We compare output between a historical period (1980–1999) and high

emissions scenario experiments for a mid-century period (2041–2060). We quantify changes in precipitation intensity and seasonality in the defined regions using daily and monthly rates to inform future climate change adaptation planning. Moreover, we highlight areas of confidence and uncertainty for the different ensembles to summarize the value of the multi-scale analysis.

3.2 Methods

The seasonal timing and daily magnitude of precipitation events are two metrics that can be used to quantify precipitation impacts. We use a suite of gridded observation products, RCM output, and global climate model output to assess present-day and future projections of precipitation in the Great Lakes region. We evaluate models during a historical time period, defined in this study as 1980–1999 based on overlapping data availability of observations and NARCCAP regional climate simulations (Mearns et al., 2013). For the future time period, we evaluate 2041–2060 based on NARCCAP time-slice experiment. We evaluate the seasonal cycle of precipitation [e.g. December–January–February (DJF), March–April–May (MAM), June–July–August (JJA), and September–October–November (SON)] for the historical period to understand model biases and also for the mid-century period to understand future changes in seasonality. To assess extreme precipitation, we use the maximum 1-day precipitation which is a common metric used to understand changes in intensity between the two time periods and model ensembles.

3.2.1 Precipitation observations

Modelled historical climate data is evaluated with the Climate Prediction Center's (CPC) Daily US Unified Precipitation data set between 1980 and 1999. The CPC Unified Precipitation data set uses distance weighting and optimal interpolation methods to resolve observations from over

30000 global observation stations to a 0.25˚×0.25˚ gridded product (Chen et al., 2008). The 20-year historical time period was selected based on the revised definition of climatological time period by the World Meteorological Organization from a 30-year average to a 20-year average (Arguez and Vose, 2011) and the intersection with RCM simulations.

3.2.2 Global climate model data

Twelve atmosphere–ocean (AO) models of the CMIP5 (Taylor et al., 2012) comprise the global climate model ensemble (Table 3.1), with model data accessed through the Earth System Grid Federation's PCMDI, DKRZ, and NCAR nodes. For the future, we selected the Representative Concentration Pathway 8.5 (RCP 8.5) experiment, as present-day emissions are currently following this emissions projection (Peters et al., 2013). Only CMIP5 AO models with daily temporal output for the present-day and RCP 8.5 experiments were selected. The AO configuration is defined to include interactive atmosphere, land surface, ocean, and sea ice models as well as aerosol components, and captures water cycle feedbacks with the atmosphere (Flato et al., 2013).

3.2.3 Regional climate model data

RCMs, i.e. dynamical downscaling, have the potential advantage of preserving physical and dynamical relationships between variables, thus reducing the issue of stationarity associated with statistical downscaling (Gutierrez et al., 2013). These regional, higher resolution simulations require global climate model data or reanalysis data for lateral boundary conditions. For our analysis, we use ten regional NARCCAP simulations that provided daily precipitation for the present-day and future time periods at 50km resolution for the A2 emissions scenario (Table 3.1). NARCCAP output was accessed through the Earth System Grid Federation PCMDI and

NCAR nodes as 3-h precipitation fluxes, which were converted to daily precipitation rates (mm day^{-1}). The full NARCCAP ensemble includes twelve simulations, but two of the simulations (WRFG-CCSM and HRM3-GFDL) use different treatment of the lakes in present day and future conditions, making the comparison of present day and future precipitation not possible given our focus region. In addition to the NARCCAP RCM ensemble, we also evaluate two RCM simulations at 25km resolution (RCM-HiRes) with the RegCM4 (Giorgi et al., 2012), which uses two different CMIP5 GCM RCP 8.5 simulations as boundary conditions (Bryan et al., 2015) (Table 3.1).

3.2.4 Spatial and temporal averaging

The gridded observations, global ensembles, and regional ensembles were analysed for the GLB (40˚–50˚N, 75˚–95˚W), and the WLEB (40˚–43˚N, 82˚–85.5˚W; Figure 3.1). Each simulation was spatially averaged over the GLB and WLEB regions, with the number of grid cells within each region for each simulation detailed in Table 3.1 to highlight the range of resolution within the global and regional models. Daily precipitation data were downloaded for the global model simulations, and 3-h precipitation data from the NARCCAP and RCM-HiRes were downloaded and aggregated to a daily basis for present-day (1980–1999) and future (2041–2060) precipitation intensity. We note that two NARCCAP ensemble members (CRCM-CCSM and MM5I-CCSM) did not simulate the complete year for 1999 and for these two members we use the present-day period of 1980–1998. For seasonal climatology, daily data were averaged to monthly for both the historical and future periods. Differences in precipitation rates between the present-day and future time periods were calculated from the monthly climatologies. For intensity, daily precipitation rate probabilities were sorted into 15 bins ranging from 0 to 90 mm day^{-1}. To account for the spatial variability within the GLB and WLEB averaging regions,

maximum precipitation rates within each region were also evaluated using 20 bins ranging from 0 to 500 mm day^{-1}. For the WLEB, seasonal and daily spring biases were calculated for the historical period to inform run-off sensitivity modeling for the Maumee watershed located in northwestern Ohio. Over the historical period, precipitation events >24 mm day^{-1} (99th percentile) were considered 'extreme' for the Maumee watershed based on comparisons with daily gauge precipitation data between 1981 and 1999.

3.3 Evaluation of precipitation seasonality and intensity

3.3.1 Precipitation seasonality

3.3.1.1 Observed historical precipitation (1980–1999)

Observed seasonal precipitation for the GLB and the WLEB subregions show a clear unimodal pattern with a summer maximum (Figures 3.2(a) and 3.3(a), respectively). For the period 1980–1999, observed annual precipitation over the GLB is 832.6 mm with an annual minimum during late winter (30.6 mm month^{-1} in February) and maximum during summer (99.0 mm month^{-1} in June and 99.4 mm month^{-1} in July) (Figure 3.2(a)). The seasonal cycle is similar in the WLEB region, with peak precipitation (97.1 and 97.8 mm month^{-1} in June and July, respectively) and the mean minimum precipitation is higher (46.7 mm month^{-1} in February; Figure 3.3(a)). Over the WLEB, total annual precipitation of 908.2 mm is slightly higher than the GLB region average. For the GLB, the summer season (JJA) includes the largest fraction (over one-third) of the averaged annual precipitation (294.6 mm), with just less than one-fourth annual precipitation occurring in spring (198.7 mm; MAM). Summer also contains the highest fraction of WLEB

Table 3.1: Global and regional model ensemble details.

Model type and emission scenario	Atmospheric horizontal resolution	Grid points (latitude× longitude=total)		Lake mask	Lake temperature	Lake ice[a]
Global, RCP 8.5	(latitude×longitude, °)	WLEB	GLB			
ACCESS1.0	1.25×1.875	3×2=6	9×11=99	No		
ACCESS1.3	1.25×1.875	3×2=6	9×11=99	No		
CCSM4	0.9×1.25	4×3=12	11×17=187	No		
CESM1-CAM5	0.9×1.25	4×3=12	11×17=187	No		
CMCC-CM	0.75×0.75	4×5=20	14×27=378	Yes	1D[b]	Yes
CMCC-CMS	1.875×1.875	2×2=4	6×11=66	Yes	1D	Yes
CSIRO-Mk3.6.0	1.875×1.875	2×2=4	6×11=66	No		
EC-EARTH	1.125×1.125	2×4=8	9×18=162	Yes	Interp[c]	No
FGOALS-g2	2.8125×2.8125	1×1=1	4×7=28	No		
HadGEM2-AO	1.25×1.875	3×2=6	9×11=99	No		
MIROC5	1.4×1.4	2×2=4	7×14=98	No		
MRI-CGCM3	1.125×1.125	2×4=8	9×18=162	No		
Regional, SRES A2 (RCM-driving GCM)	(latitude×longitude, km)					
CRCM-CGCM3	50×50	9×8=72	30×38=1140	Yes	1D	Yes
CRCM-CCSM	50×50	9×8=72	30×38=1140	Yes	1D	Yes
ECP2-GFDL	50×50	9×8=72	31x39=1209	Yes	Interp	No
EPC2-HadCM3	50×50	9×8=72	31×39=1209	Yes	Interp	No
HRM3-HadCM3	50×50	8×7=56	28×35=980	Yes	Interp	No
MM5I-CCSM	50×50	8×6=48	26×33=858	Yes	Interp	No
MM5I-HadCM3	50×50	8×6=48	26×33=858	Yes	Interp	No
RCM3-CGCM3	50×50	7×7=49	27×34=918	Yes	Interp	No
RCM3-GFDL	50×50	7×7=49	27×34=918	Yes	Interp	No
WRFG-CGCM3	50×50	8×6=48	26×33=858	Yes	Interp	Yes
Regional, RCP 8.5	(latitude×longitude, km)					
RCM4-HadGEM	25×25	15×14=210	53×68=3604	Yes	Interp	No
RCM4-GFDL	25×25	15×14=210	53×68=3604	Yes	Interp	No

[a]Lake ice present in Great Lakes region. [b]1D lake model for inland water points (Goyette *et al.*, 2000).

[c]Lake surface temperature interpolated from nearest lake point (if in parent GCM) or from the nearest sea surface temperature (e.g. from coastal regions).

precipitation (284.8 mm), however spring contains over one-fourth of its total precipitation (236.9 mm) (Table 3.2).

3.3.1.2 Modelled historical precipitation (1980–1999)

We compare simulated annual and seasonal precipitation from the global and regional ensembles with CPC observations averaged over 1980–1999 (Figures 3.2 and 3.3; Table 3.2). For the GLB over the historical period, 11 of the 12 CMIP5 members and eight of the ten NARCCAP members simulate more annual precipitation than the observed historical value, while both RCM-HiRes members have a negative or dry bias. The GLB averaging region has wet biases in both spring and winter in all 12 CMIP5 models and all ten NARCCAP models (Figures 3.2a-b). In both RCM-HiRes members, the seasonality of the modelled precipitation is relatively flat as noted by Bryan *et al.* (2015), with a positive winter bias and a negative summer bias. All of the models in the region exhibit a positive winter bias, while the summer bias in these simulations may be due to a weak parameterization of convective precipitation. All ensemble members show a wet bias in DJF precipitation ranging from 19.7mm (17.3%) to 108.3mm (95.2%) (Figures 3.2a-c), although this may be in part attributed to the low observed values in the region influenced by gauge error for solid phase precipitation (Legates and Willmott, 1990). For example, gauge corrections based on the Legates and Willmott data can increase winter precipitation in the Great Lakes region by up to 0.5 mm day^{-1}. The CMIP5 ensemble mean overestimates MAM precipitation by 61.0 mm (30.7%), with individual wet model biases ranging between 2.3 mm (1.2%) and 112.2 mm (56.5%). Similar to the global models, the NARCCAP ensemble mean shows a positive bias in MAM of 50.4 mm (25.4%) but with a narrower range in the model bias (18.3–96.0 mm). All NARCCAP models show a late spring/early summer (MJJ) peak that is stronger than observed (Figure 3.2b), and indicates that this ensemble shifts precipitation earlier in the season than observed and produces too much precipitation. In JJA, the inter-ensemble model spread grows, with 14 of the 24 total models

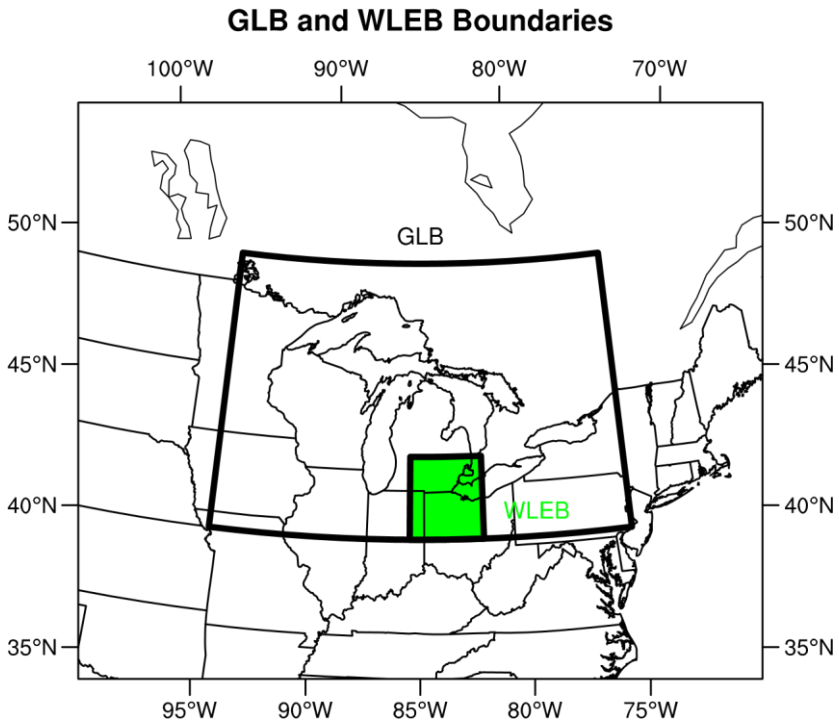

Figure 3.1: Boundaries representing the GLB and WLEB. The GLB includes the US Great Lakes states (U.S.) and Canada, and the WLEB includes the geographic extent of the watersheds that drain into the western basin of Lake Erie, including southeastern Michigan, northwestern Ohio, and northeastern Indiana.

exhibiting a summer dry bias and the rest exhibiting a wet bias (Figures 3.2a-c). As the summer progresses into fall, the intermodel CMIP5 spread narrows and individual model biases are reduced. In late summer/early fall (ASO), the NARCCAP ensemble reduces precipitation closer to observed, but then precipitation increases again in the winter, a feature not evident in the observations (Figure 3.2b). For the RCM-HiRes simulations, there is very little amplitude in the seasonal cycle, as discussed in Bryan *et al.* (2015). This leads to a comparatively small spring dry (negative) bias of 5.8 mm (−2.9%) in the ensemble mean, although this is largely due to the flat seasonal cycle relative to the increase in winter to spring precipitation (Figure 3.2c).

For the WLEB region, most models also have a wet annual bias with the exception of one CMIP5 model (CSIRO), one NARCCAP model (CRCM-CCSM), and the RCM-HiRes simulations (Table 3.2; Figures 3.3a-c). The seasonal bias is strongest in MAM for all model ensemble means, with a positive bias of 69.9 mm (29.5%) for CMIP5, a positive 60.1 mm (25.4%) bias for NARCCAP, and dry bias of 27.8 mm (−11.7%) for RCM-HiRes. The bias of individual CMIP5 members is similar to the larger region, falling between 4.7 mm (2.0%) and 122.9 mm (51.9%), likely due to the differing model processes and wide range of spatial resolution in this ensemble. Similar to the GLB, the NARCCAP ensemble produces MAM precipitation that ranges close to the CMIP5 models, from 12.1 mm (5.1%) and 112.4 mm (47.4%) for individual model members (Figure 3.3c). Unlike the other ensembles, the RCM-HiRes shows a dry bias over land in the region (Bryan *et al.*, 2015) with individual members showing a dry bias of 18.3 mm (−7.7%) and 37.2 mm (−15.7%; Figure 3.3e).

3.3.1.3 Modelled future precipitation (2041–2060)

With knowledge of the biases in the historical simulations, we examine the relative percent change in seasonal precipitation for mid-century (2041–2060) for the GLB and the WLEB, respectively (Figures 3.2d-f and 3.3d-f, respectively). For the GLB, the annual relative change in precipitation is typically positive and does not differ much between ensembles (CMIP5: −0.7 to 16.1%, NARCCAP: 4.7–10.6%, RCM-HiRes: 6.7–14.3%; Figures 3.2d-f). The projected increase in annual precipitation is similar for the WLEB region, however the increase is slightly higher in the global and regional ensembles (CMIP5: −5.4 to 17.8%, NARCCAP: 0.0–13.9%, RCM-HiRes: 0.8–12.9%; Figures 3.3d-f).

During spring and winter, precipitation is generally projected to increase across all ensemble members within both regions (Figures 3.2 and 3.3). Ensemble mean changes in MAM precipitation are small (7.0–14.7%) for the GLB, with individual models ranging between 1.4 and 30.0% for the CMIP5 ensemble, −1.6 to 12.7% for the NARCCAP ensemble, and 12.5–17.0% for the Hi-Res ensemble. For the WLEB, the spring ensemble mean changes have a smaller range (8.4–12.8%) with more member variability (CMIP5: −3.6 to 33.6%, NARCCAP: 1.5–19.2%, Hi-Res: 9.8–15.8%). The magnitude of winter precipitation change for the CMIP5 ensemble mean is similar for both regions (GLB: 17.4%; WLEB: 17.9%). The NARCCAP and RCM-HiRes ensemble means, present a lower increase than CMIP5 for the GLB (11.1 and 13.6%, respectively). The regional models' magnitude of increase is slightly higher for the WLEB (11.5, 14.0%; Figures 3.3d-f).

The greatest spread in the simulated future precipitation occurs in JJA, with some models showing decreases in future summer precipitation and some showing relative increases compared to the historical period (Figures 3.2 and 3.3). Although the ensemble mean changes show increases ranging from 0.9 to 8.8% in the GLB, in the WLEB, this range is −1.4 to +1.6%. For both the GLB and WLEB, 8 out of the 12 CMIP5 models show an increase in JJA precipitation (GLB: 0.2–9.3%, WLEB: 1.3–14.1%), while four show relative decreases (GLB: 0.2–19.0% decrease, WLEB: 1.0–20% decrease) (Figures 3.2d and 3.3d). For the regional NARCCAP ensemble, there is more variability between members although there is a similar spread in JJA between regions, with seven models predicting an increase in GLB precipitation and four models predicting an increase for the WLEB (GLB: 0.5–13.4%, WLEB: 2.5–16.4%, Figures 3.2 and 3.3d). The range of predicted decrease is also similar from three models in the

GLB and six models for the WLEB (GLB: 0.3–7.6 decrease, WLEB: 3.5–12.7% decrease, Figures 3.2 and 3.3d). The RCM-HiRes simulations are also split on the change in JJA precipitation for the WLEB (−8.4 decrease and 9.7% increase), leading to a near zero change in precipitation in the ensemble mean whereas they both indicate an increase for the GLB (4.9 and 12.8%; Figures 3.2 and 3.3f). Overall, the response of seasonal precipitation at the mid-century time period is similar across both regions with most ensemble members, with ensemble means indicating an increase between 8.5 and 12.6% in the spring and 11.5 and 18% in the winter for the WLEB (Figures 3.2 and 3.3). The overall response of precipitation to the future climate scenarios is more variable during the summer and early fall, depending on the ensemble and member. However, we note that this increase is slightly smaller than the model bias in these seasons. This result is consistent with Hayhoe et al. (2010), who used two statistical downscaling techniques for precipitation in the Chicago and Great Lakes area and found that that winter and spring precipitation may increase up to 20% before end of century (2070–2099) under the similar A2 (or moderate) emissions scenario. Possible explanations for these changes are explored in Section 3.4.

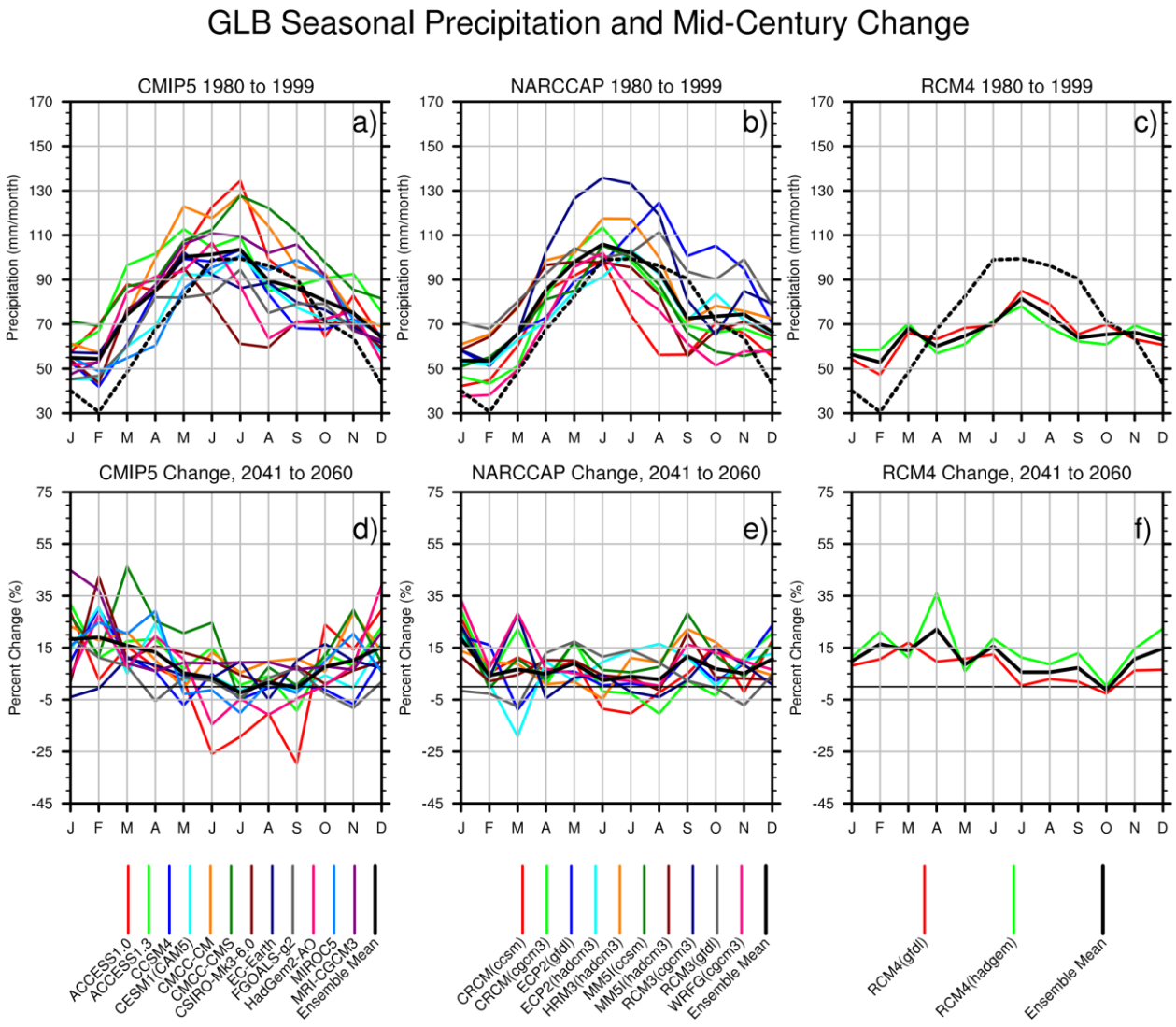

Figure 3.2: Monthly averages for the historical period (1980–1999) spatially averaged over the GLB for (a) the CMIP5 ensemble, (b) the NARCCAP ensemble, and (c) the RCM-HiRes ensemble. Individual model members in coloured lines, the multi-model average in solid black lines, and the CPC observed precipitation in black dotted lines. Monthly average changes projected for mid-century (2041–2060) normalized to a percent change from the historical period for (d) the CMIP5 ensemble, (e) the NARCCAP ensemble, and (c) the RCM-HiRes ensemble.

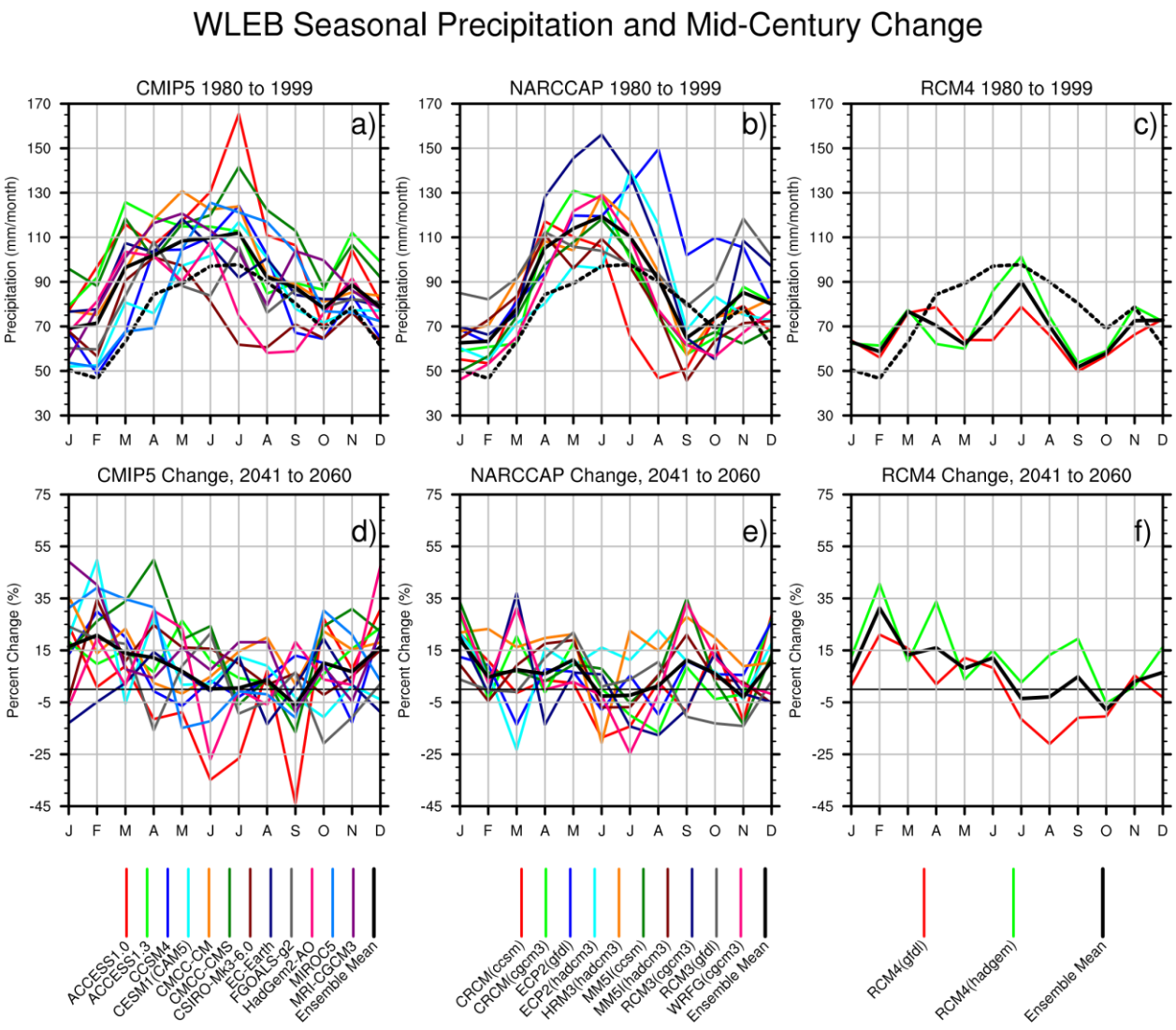

Figure 3.3: As for Figure 3.2, but for the WLEB.

3.3.2 Precipitation intensity

3.3.2.1 Observed historical period precipitation intensity (1980–1999)

We examine daily precipitation rates (or precipitation intensity) over the historical period with probability density functions, dividing daily precipitation into 15 equally spaced bins spanning 0–90 mm day^{-1}. We define three categories of events: small (0–5 mm day^{-1}), moderate (6–23 mm day^{-1}), and extreme events (≥24 mm day^{-1}). Simulated precipitation intensity is compared

with daily CPC gridded observations, although we note that using a gridded product for intensity may smooth out individual stations that may experience higher, localized rainfall. However, this product provides continuous coverage of historical data for evaluation and a daily precipitation value that is spatially consistent with a model grid cell.

In the GLB region (Figures 3.4a-d), all ensemble members generally capture the observed intensities in all seasons except for DJF, where the models overestimate daily precipitation. For DJF, this suggests that the seasonal wet bias (Section 3.3.1.2) is due to both more precipitation during the moderate events in most of the models (e.g. 6–23 mm day^{-1}) as well as the simulation of higher intensity events by some model members (≥24 mm day^{-1}) (Figure 3.4d). Other seasons, such as MAM, show that the models capture the frequency of moderate events (6–23 mm day^{-1}) but some model members simulate additional high intensity events (≥24 mm day^{-1}) (Figure 3.4a). The same pattern is evident in JJA (Figure 3.4b) and SON (Figure 3.4c). When comparing the model type in both MAM and DJF, the global models produce more intense events than the regional models (Figures 3.4a-d). For the RCM-HiRes ensemble, the spatially averaged precipitation shows lower mean probability values, consistent with the previously described summer season dry bias (Figure 3.4b).

For the WLEB subregion, simulated intensities are higher (up to 90 mm day^{-1}) than the GLB because of spatial averaging techniques (e.g. the WLEB subregion is $3^{\circ}\times3.5^{\circ}$ and the GLB is $10^{\circ}\times20^{\circ}$). With fewer grid cells, more of the individual grid intensities are captured with a smaller averaging region, increasing the regionally averaged intensity (Figures 3.5a-d). All model ensembles generally capture the JJA and SON moderate range intensities (e.g. 6–23 mm

Table 3.2: WLEB annual precipitation (mm), spring precipitation (MAM; mm), and spring intensity (mm day−1) for observed, global CMIP5 model members, NARCCAP model members, and RCM high resolution model members.

Observations							
CPC	Annual precipitation(mm)		Spring(MAM) precipitation(mm)		MAMintensity, %(≥24 mm day^{-1})		
	908.2		236.9		0.2		
Models							
	Present(1980–1999)						Future(2041–2065)
	Annual precipitationbias		MAMprecipitation bias		MAMintensitybias		MAMintensitychange, mm day^{-1} (≥24 mm day^{-1})
	mm	%	mm	%	mm day^{-1} (≥24 mm day^{-1})	mm day^{-1} (≥24 mm day^{-1})	
CMIP5							
ACCESS1	372.4	41.0	102.9	43.5	1.0	475.0	0.6
ACCESS3	321.9	35.4	122.9	51.9	1.3	600.0	0.9
CCSM4	100.5	11.1	39.2	16.6	0.2	75.0	0.0
CESM1-CAM5	73.4	8.1	17.1	7.2	0.7	300.0	0.3
CMCC-CM	266.3	29.3	107.3	45.3	2.6	1175.0	0.1
CMCC-CMS	393.7	43.3	98.0	41.4	2.3	1075.0	2.3
CSIRO-Mk3-6.0	−16.3	−1.8	52.0	22.0	0.3	125.0	0.8
EC-Earth	201.3	22.2	92.1	38.9	0.8	375.0	0.2
FGOALS-g2	85.7	9.4	43.1	18.2	1.3	600.0	0.2
HadGem2-AO	75.0	8.3	58.5	24.7	0.9	436.7	1.2
MIROC5	131.0	14.4	4.7	2.0	0.9	425.0	0.9
MRI-CGCM3	226.9	25.0	101.2	42.7	1.6	725.0	0.4
NARCCAP							
CRCM(ccsm)	−0.5	0.0	72.8	30.7	0.2	110.5	0.1
CRCM(cgcm3)	108.6	12.0	67.1	28.3	0.3	125.0	0.4
ECP2(gfdl)	317.8	35.0	57.9	24.5	0.7	325.0	0.3
ECP2(hadcm3)	108.0	11.9	12.1	5.1	0.4	181.1	0.7
HRM(hadcm3)	165.2	18.2	66.8	28.2	1.4	666.7	1.8
MM5I(ccsm)	36.4	4.0	43.2	18.2	0.3	136.8	0.4
MM5I(hadcm3)	55.3	6.1	53.6	22.6	1.4	666.7	0.7
RCM3(cgcm3)	303.1	33.4	112.4	47.4	0.6	275.0	0.2
RCM3(gfdl)	252.1	27.8	73.0	30.8	0.1	50.0	1.3
WRF(cgcm3)	49.5	5.4	42.6	18.0	0.3	150.0	0.7
RCM4(*HiRes*)							
RCM4(gfdl)	−114.7	−12.6	−18.3	−7.7	0.3	125.0	0.2
RCM4(hadgem)	−59.5	−6.6	−37.2	−15.7	0.4	181.1	0.1

day^{-1}) but again have individual members that simulate higher intensity events that reach up to 83 mm day^{-1} (Figures 3.5b-c). For MAM and DJF, the models overestimate the observed

precipitation in the 18–41 mm day^{-1} range as well as simulating additional, high intensity events (Figures 3.5a-d).

For extreme intensity values in the WLEB (≥24 mm day^{-1}, informed by historically modelled streamflow data for the Maumee Basin), the relative error in historical spring (MAM) probabilities ranged from 75 to 1175% for CMIP5, 50 to 667% for NARCCAP, and 125 to 181% for RCM-HiRes (Table 3.2). As in the GLB region, there are several CMIP5 model members that show more intense events than the regional models in MAM and JJA (Figures 3.5a-b). Summer in the WLEB shows good agreement with historically observed probabilities for small to moderate events (≤24 mm day^{-1}), however the simulations include higher events that are not present in the observations (Figure 3.5b). The CMIP5 mean exceeds the historical range by eight bins, equating to almost 48mm (6mm per bin) or 1.9 inches (Figure 3.5b). However, the associated probabilities indicate a low frequency of these events with values close to 0.1%, or 1.8 events per 20 years (Figure 3.5b).

3.3.2.2 Future Precipitation Intensity (2041–2060)

We examine the change in daily precipitation rate probabilities between the historical (1980–1999) and future (2041–2060) periods for the three ensembles (Figures 3.4e-h and 3.5e-h). We calculate the change in probability as the difference of the future probability with that of the historical probability. For example, from the ~1800 days included in MAM over 20 years, a typical extreme event may have a 1% probability. This is equivalent to about 18 events over the 20-year period for that season. If the probability of such an extreme event increased relatively by 0.1%, that would increase total MAM extreme events by 1.8 events between the

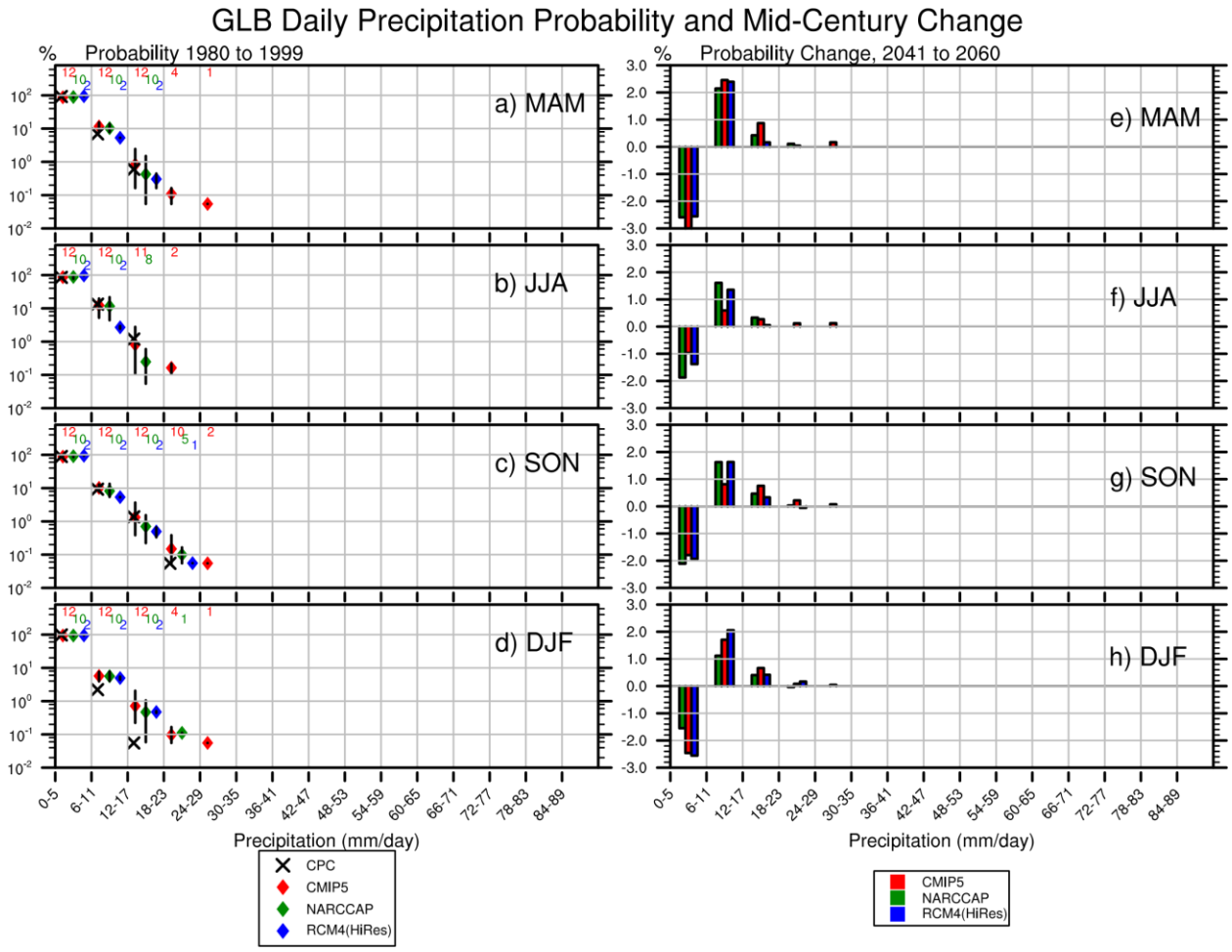

Figure 3.4: Historical (1980–1999) probabilities of precipitation events (binned every 6 mm day−1) spatially averaged over the GLB for (a) MAM, (b) JJA, (c) SON, and (d) DJF. Mid-century (2041–2060) projections of probability change for each bin, calculated as the difference from historical values for the GLB for (d) MAM, (e) JJA, (f) SON, and (g) DJF. Precipitation bins are averaged for each ensemble, including the CMIP5 ensemble (red), the NARCCAP ensemble (green), and the RCM-HiRes ensemble (blue). Numbers above each bin denote the total number of model members that simulated precipitation in that bin. CPC observations are denoted with a black X.

20-year periods. For small precipitation events, the GLB ensemble means show negative changes across all seasons (1.0–3.4% decrease in probability; Figures 3.4e-h). The WLEB ensemble means for small events show a similar result for the spring and winter seasons, however with a slightly smaller range (0.9–1.9% decrease), while summer and fall have a mixed sign of change (Figures 3.5e-h).

For each of the GLB ensemble means, moderate daily precipitation events across all seasons show the largest positive change (1.0–3.4%), with extreme events showing no change (Figure 3.4e-h). This is in part due to the spatial averaging used in this study, where averaging over a large region causes a relatively sharp drop off in the tail end of the probability distribution function (24–90 mm day^{-1}) for each ensemble. As compared to the GLB, the WLEB ensemble means show less consensus for the sign of moderate events, with about half of the models showing overall positive changes (0.1–0.7%) for spring and winter extreme events. This translates to a projected increase of about 1–12 more events over the 20-year mid-century period (Figures 3.5e-h).

3.4 Discussion

To place these results in context, we discuss several factors related to the spatial averaging employed in this study, the climate model resolution and the model representation of physical processes such as lakes to understand model biases and projections of future precipitation in the GLB and WLEB regions.

3.4.1. Spatial averaging effects

Spatial averaging across regions effectively smooths the extreme daily events, especially for the GLB region. For example, GLB intensity values (Figures 3.4a-d) are lower than the WLEB (Figures 3.5a-d) and may under-represent the intense events in the overall GLB region, suggesting that the larger spatial extent of the GLB may reduce the calculated precipitation

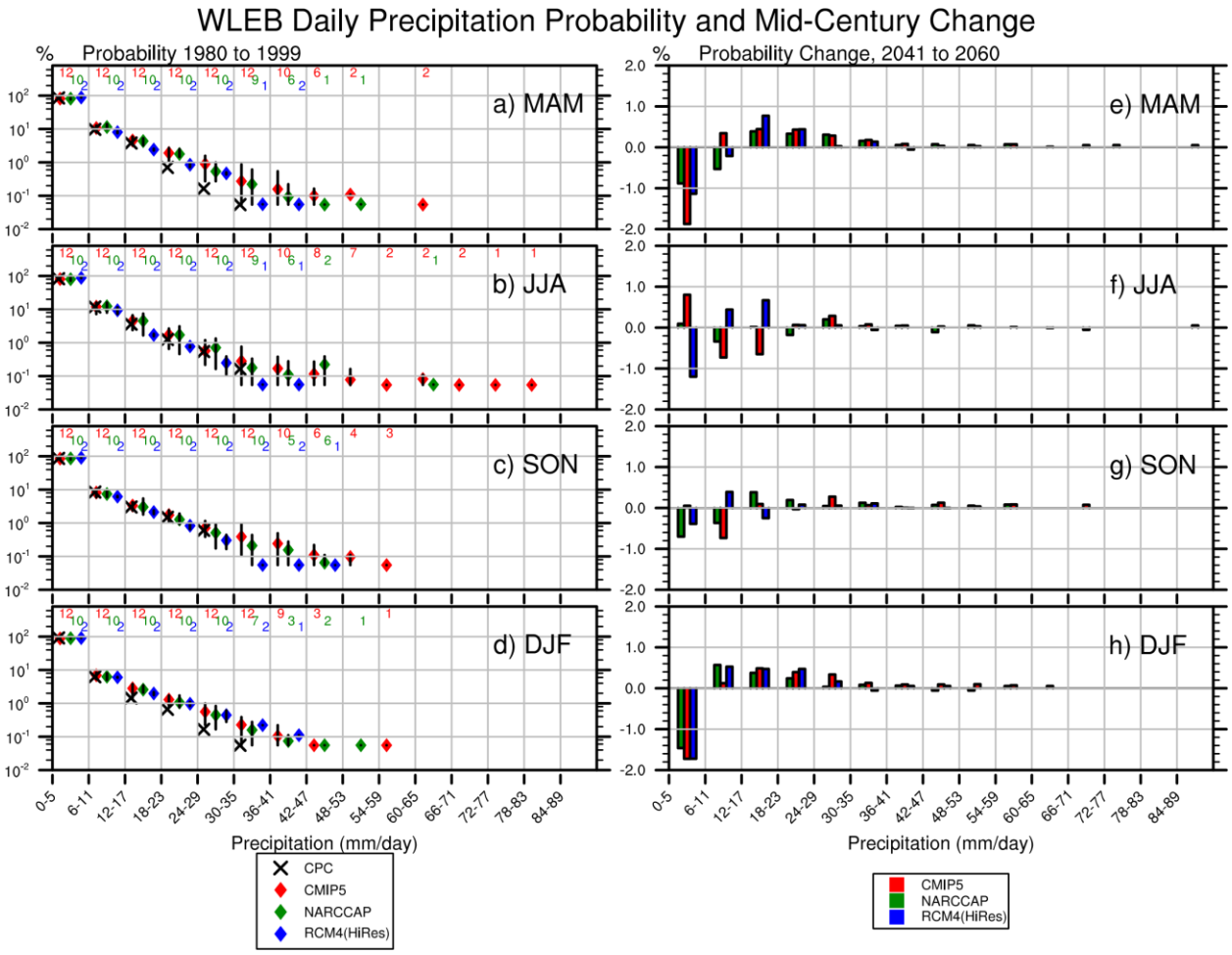

Figure 3.5: As for Figure 3.4, but for the WLEB region.

intensity. To understand how the spatial averaging affects the calculation of the extremes, we evaluate the maximum daily precipitation rates across each region. The maximum daily precipitation intensity is defined as the greatest intensity that occurs within any individual grid cell in the region during the selected season over all years. The probability distribution of these maxima shows the likelihood of the maximum possible precipitation that can occur within each averaging region (Figure 3.6 for the GLB and Figure 3.7 for the WLEB). For example, in the GLB in MAM, observations show a 0.05% probability in the 150–174 mm day^{-1} bin, which indicates that at least one grid cell in the GLB reached a daily precipitation value in this range.

This probability is equivalent to about one spring event of this intensity over the 20-year averaging period (1980–1999). This provides a metric for the spatial distribution of precipitation intensity at any point within the region and can be useful to compare with the regional averages (Figures 3.4 and 3.5). Over the GLB region, CMIP5 models tend to underestimate the maximum probability values (Figures 3.6a-d). Generally, the regional model ensembles (NARCCAP and RCM-HiRes) simulate a larger number of extreme events that more accurately captures the maximum daily precipitation distribution (Figures 3.6e-l). The dynamically downscaled models do tend to have some models that overestimate the maximum intensity, most notably in the spring (Figures 3.6e-i) and summer (Figures 3f-j). In the fall, not all NARCCAP ensemble members capture the event range and only one model (HRM3-HadCM3) extends beyond the historical CPC range (Figure 3.6g) while the HiRes members are split for larger event sizes (above 50 mm day^{-1}; Figure 3.6k). In the winter, the NARCCAP ensemble shows a spread around historical probabilities (Figure 3.6h) while the HiRes members have more occurrences of extreme events above 50 mm day^{-1} (Figure 3.6l). In the WLEB region (Figure 3.7), the dynamically downscaled models also show an improvement over the global models in the simulation of intense precipitation. However, NARCCAP extends the range beyond CPC probabilities for all WLEB seasons (Figures 3.7e-f), while the HiRes shows a higher intensities for WLEB summer and winter (Figures 3.7j-l). The tendency for the NARCCAP models to produce large extremes in excess of observed values has been noted in other studies that evaluated the model performance over the entire United States (Caldwell, 2010; Kawazoe and Gutowski, 2013b; Wehner, 2013). Here, these results show that the regional models produce some grid cells with very high intensity events (e.g. >250 mm day^{-1} in JJA), but overall, the finer resolution models better capture the high intensity events across the two regions.

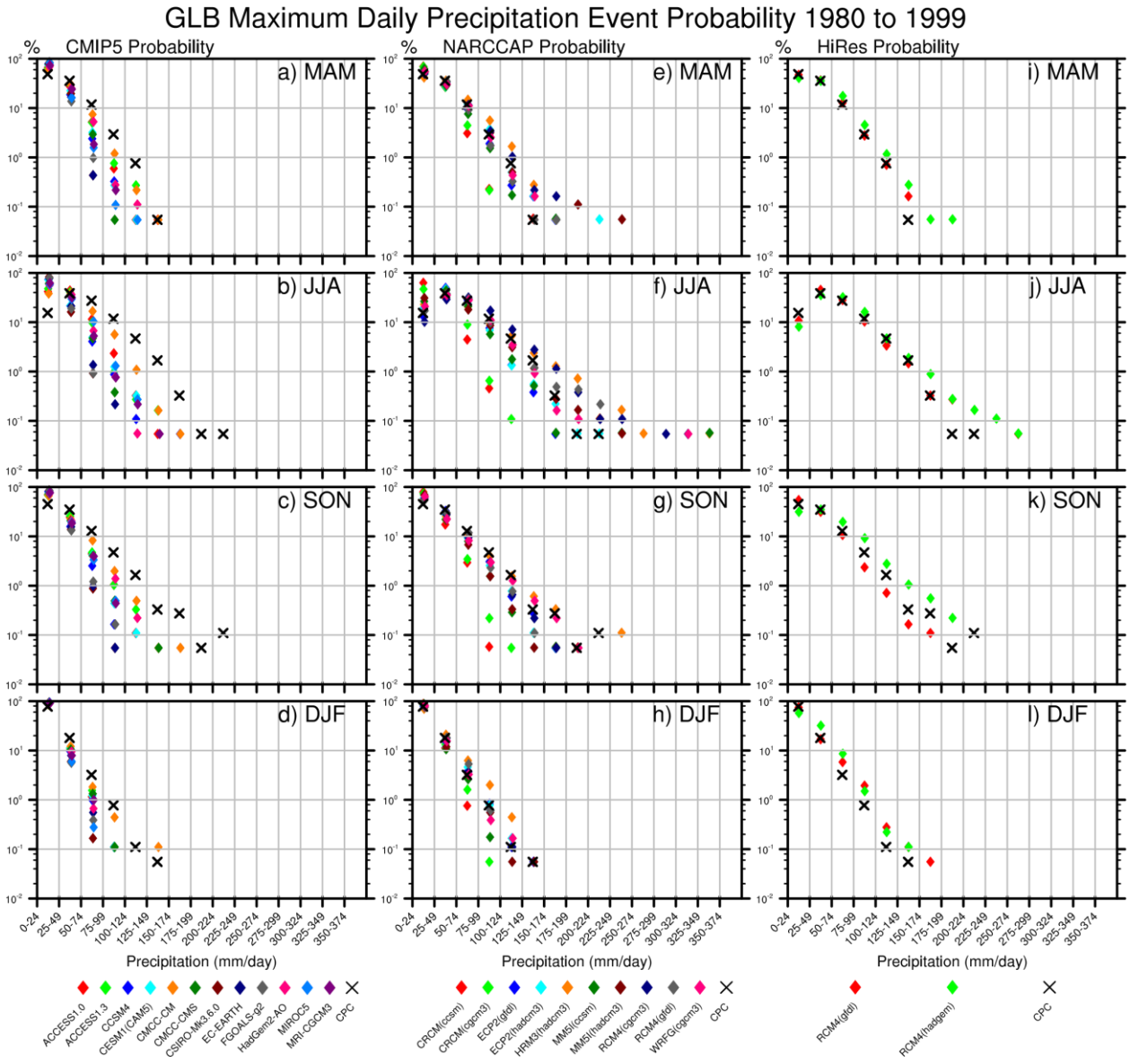

Figure 3.6: Maximum probabilities for each precipitation size (bins spaced every 6 mm day^{-1}) extracted from the GLB region before averaging. Ensemble probability distribution functions are shown for each season; (a–d) CMIP5, (e–h) NARCCAP, and (i–l) RCM-HiRes. CPC observations are denoted with a black X.

To further evaluate the effects of area averaging, we also examined the spatial distribution of the 99th percentile precipitation (considering rain days on which the precipitation was over 1 mm day^{-1}) in the WLEB region to determine if certain grid points have substantially higher

precipitation extremes. Evaluation of seasonal averages shows no appreciable spatial pattern in seasons outside of DJF. Figure 3.8 shows the 99th percentile for the ten NARCCAP models and the CPC observations. In several of the NARCCAP members, and to some extent in the observations, the 99th percentile precipitation is largest near the lakes, suggesting these larger extremes are related to the production of lake effect snow in winter. For some models, the lake temperatures are interpolated from the nearest sea surface temperatures (SST). Bryan et al. (2015) showed that southern Great Lakes SSTs lake temperatures were biased warm compared to observations when using this method, enhancing precipitation near the lake in this model. Examination of the patterns of the GCMs did not reveal similar lake effects (not shown), likely because the grid spacing is too large to simulate lake-precipitation feedbacks or the lakes are absent, as discussed below.

3.4.2 Resolution effects

Another potential factor in the differences in precipitation intensity is the climate model resolution. In the GLB region, the CMIP5 ensemble mean has higher intensities than the dynamically downscaled models (Figures 3.4a-d) and this effect is magnified for the WLEB (Figures 3.5a-d). Within the CMIP5 ensemble, the CMCC-CMS model consistently places non-zero probabilities in higher intensity bins beyond those of the historical record for both regions (individual model members not shown in Figures 3.4 and 3.5).

For the WLEB we evaluated two simulations with the CMCC model, the CMS version (1.875° resolution, which resolves the stratosphere) and the finer CMCC-CM (0.75° resolution, the

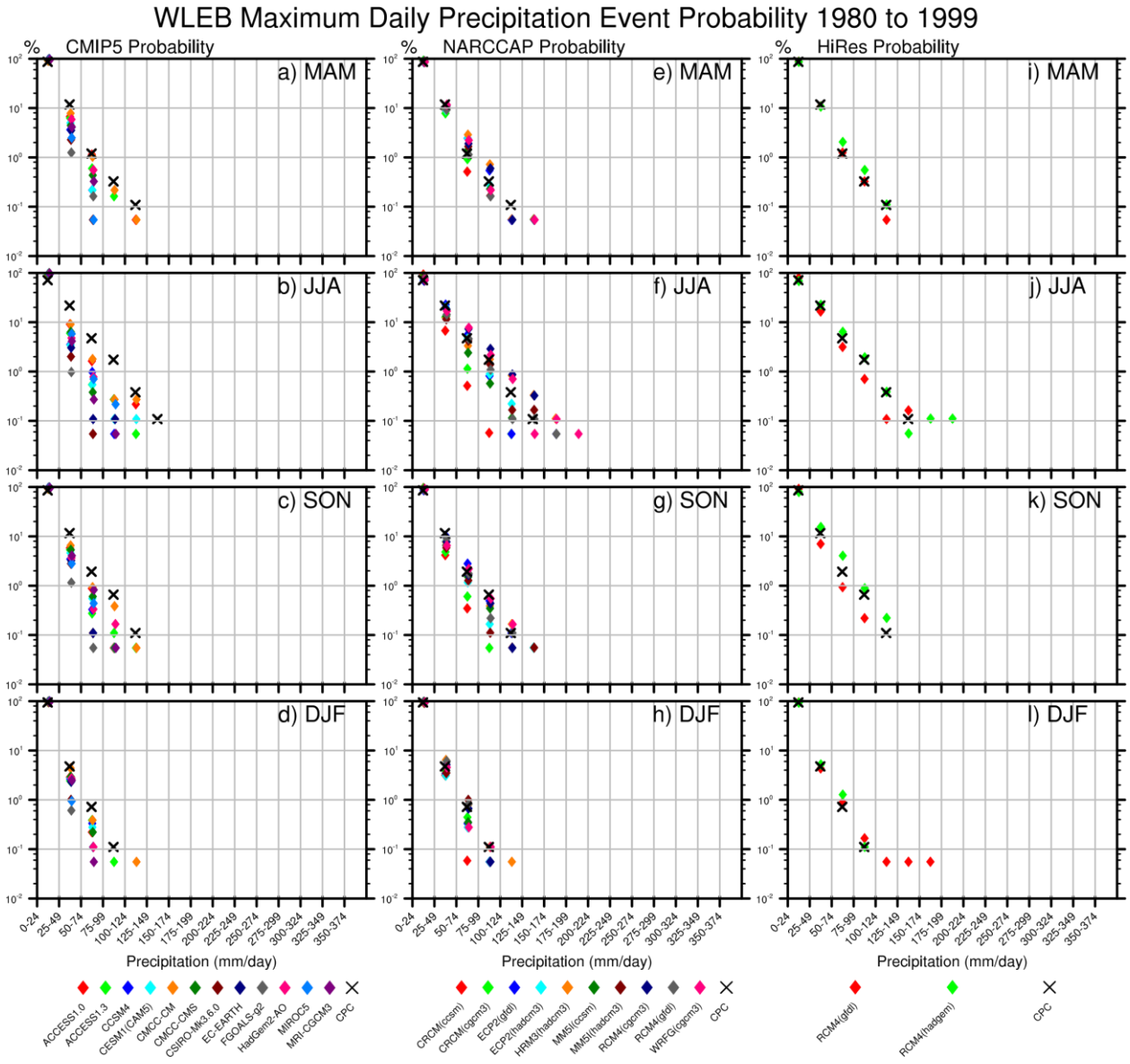

Figure 3.7: Maximum probabilities for each precipitation size (bins spaced every 6 mm day^{-1}) extracted from the WLEB region before averaging. Ensemble probability distribution functions are shown for each season; (a–d) CMIP5, (e–h) NARCCAP, and (i–l) RCM-HiRes. CPC observations are denoted with a black X.

highest resolution CMIP5 model in our ensemble). While these model versions have several parameterization differences, the increase in horizontal spatial resolution does not explain the historical bias for intense daily events. The two resolution versions show similar bias in the spring extreme event probability (1075 and 1175% respectively; Table 3.2). However, CCSM4

and CESM1-CAM5 (0.9˚×1.25˚ each) are also relatively high resolution in our CMIP5 ensemble (187 grid cells for the WLEB), but show a larger difference in extreme event probability bias (75 and 300%, respectively; Table 3.2). Interestingly, the CSIRO model, which has a coarser resolution equal to the CMCC-CMS model (1.875˚), has less bias for extreme daily events (125 and 1075%, respectively; Table 3.2) and also exhibits a lower bias for MAM seasonal precipitation than CMCC-CMS (22.0 and 41.4%, respectively; Table 3.2). While it is not surprising that the models produce very different precipitation distributions due to large number of variable parameterizations in the model (e.g. convective precipitation, microphysics, and land surface), the comparison here shows that higher resolution alone within the CMIP5 ensemble does not improve the precipitation intensity bias simulated in the region. This is consistent with other studies, e.g. Kawazoe and Gutowski (2013a) found that CMIP5 model resolution could not explain biases in precipitation intensity over the upper Mississippi region in the winter. Additionally, six global models show relatively low bias for spring precipitation (CCSM4 at 16.6%, CESM1 at 7.2%, CSIRO at 22.0%, FGOALS at 18.2%, HadGEM2 at 24.7%, and MIROC at 2.0%, respectively; Table 3.2), which is similar to several of the regional models for this metric (about 7–25%; Table 3.2).

For the WLEB spring and summer seasons (Figures 3.5a-b), observed intensities reach up to 30–35 mm day^{-1}. However, ten of the CMIP5 models place probabilities in the next available bin (36–41 mm day^{-1}) for spring, summer, and fall (nine models for winter), showing that most of the CMIP5 ensemble overemphasizes the magnitude of intense events by at least 6 mm day^{-1} (0.2 inch day^{-1}) for these seasons. Multiple models go beyond this lower end bias and have non-zero probabilities in even higher bin ranges, with half of the CMIP5 ensemble

represented in the 42–47 mm day^{-1} range for spring and fall, eight models for summer and three models for winter producing a bias of at least 12 mm day^{-1} (0.5 inch day^{-1}). Further, seven models in the CMIP5 ensemble place non-zero probabilities in the 48–53 mm day^{-1} range giving a bias of at least 18 mm day^{-1} for the summer period. In contrast, the regionally averaged RCM simulations overall do not exhibit such a high intensity, with lower average probabilities across all seasons in both regions. This suggests that the maximum probabilities with very high intensities (Figures 3.6 and 3.7) are likely occurring over a very small number of grid cells at different times and locations, and these grid cells do not affect the overall regional average (Figures 3.4 and 3.5). For example, HRM-HadCM (Figure 3.8k) shows that a grid cell north of Lake Erie (1 of 56 grid cells in the WLEB region in this model, or 1.78% of the model grid cells) has the highest precipitation over the WLEB 12% of the time.

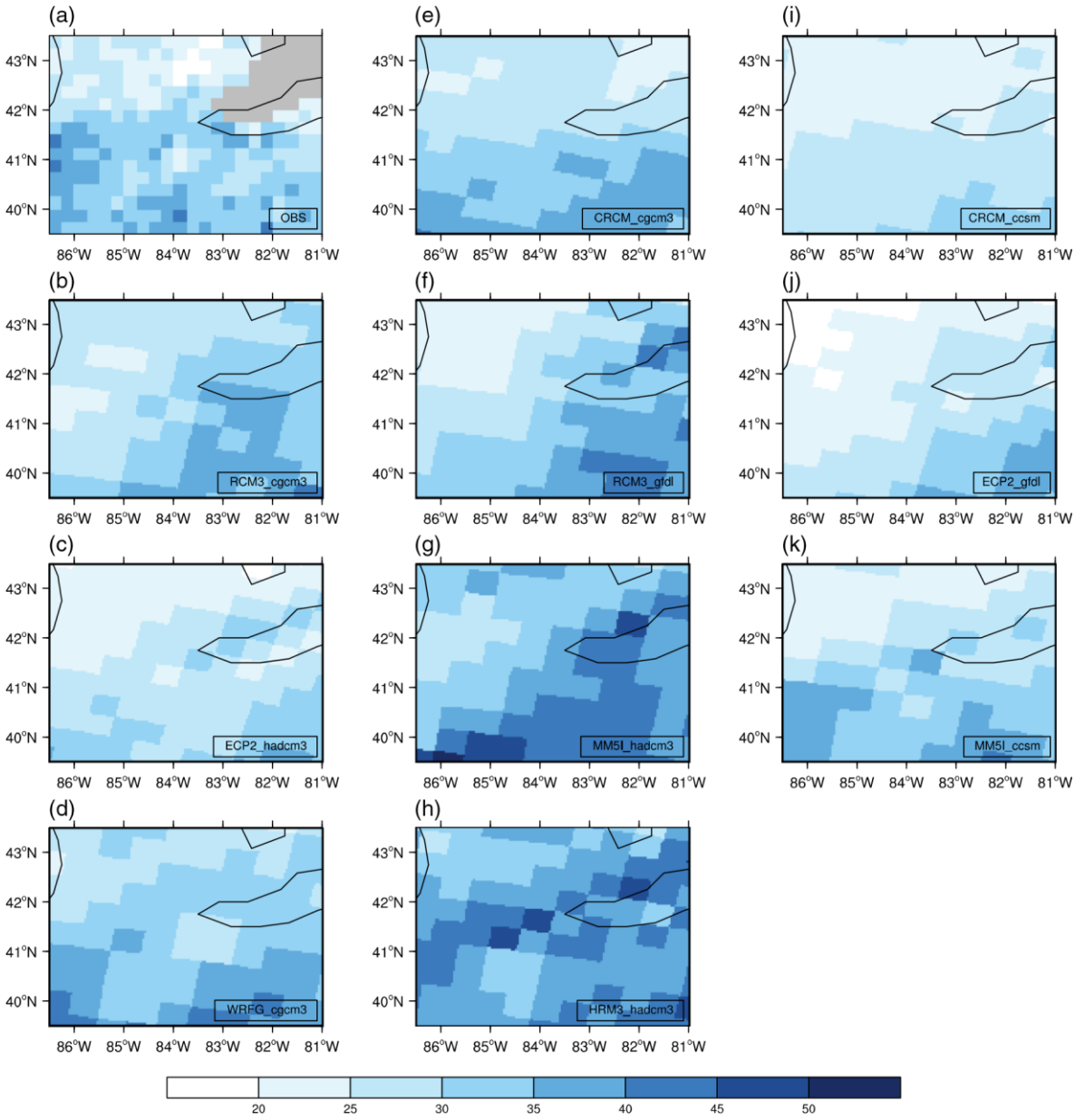

Figure 3.8: The 99th percentile DJF precipitation (mm day^{-1}) (for days with >1 mm day^{-1} of precipitation) over the WLEB grid cells for (a) observations and (b–k) the NARCCAP ensemble members (Table 3.1), including (b) RCM3-CGCM3, (c) EPC2-HadCM3, (d) WRFG-CGCM3, (e) CRCM-CGCM3, (f) RCM3-GFDL, (g) MM5I-HadCM3, (h) HRM3-HadCM3, (i) CRCM-CCSM, (j) EPC2-GFDL, and (k) MM5I-CCSM. Darker colors indicate higher values of extreme precipitation within that grid cell.

3.4.3 Lake representation

Even if topographic features such as the lakes are better resolved at higher resolution, physical parameterizations may not result in better evaluation with observations (Caldwell, 2010; Rauscher et al., 2010). The representation of lakes in the region is known to play an important role in regional precipitation (Notaro et al., 2013; Suriano and Leathers, 2016). One advantage of higher resolution models would be to include these important features at the lower model boundary condition, but resolution alone does not determine whether or not the surface is represented as bodies of water. In most of the global model members of the CMIP5 ensemble (9 of the 12 models), the Great Lakes are not differentiated from land (Table 3.1). In the NARCCAP ensemble, the lakes are represented in terms of land cover but have different treatment of lake processes that drive lake temperatures and the presence of ice. For example, most of the NARCCAP models do not use a lake model and interpolate lake surface temperatures from nearby sea surface temperatures (Table 3.1). As a result, there is no prognostic calculation of lake ice coverage. Three members of the NARCCAP ensemble (CRCM-CGCM3, CRCM-CCSM, and WRFG-CGCM3) simulate dynamic lake ice across the Great Lakes.

We group model members across the multiple ensembles used in this study to understand the role of lake representation in the simulation of regional precipitation. The 15 models that represent lakes include 3 CMIP5 models (Table 3.1), and all 12 regional scale models (10 NARCCAP and 2 RCM HiRes). The ensemble without lakes includes the remaining nine CMIP5 models (Table 3.1). For the historical period, the multi-model average seasonal cycle between the models that include lakes *versus* those that do not is similar over the GLB (Figures 3.9a-c), yet there is much more variability among the members of seasonal precipitation in the lake ensemble. Both sets of

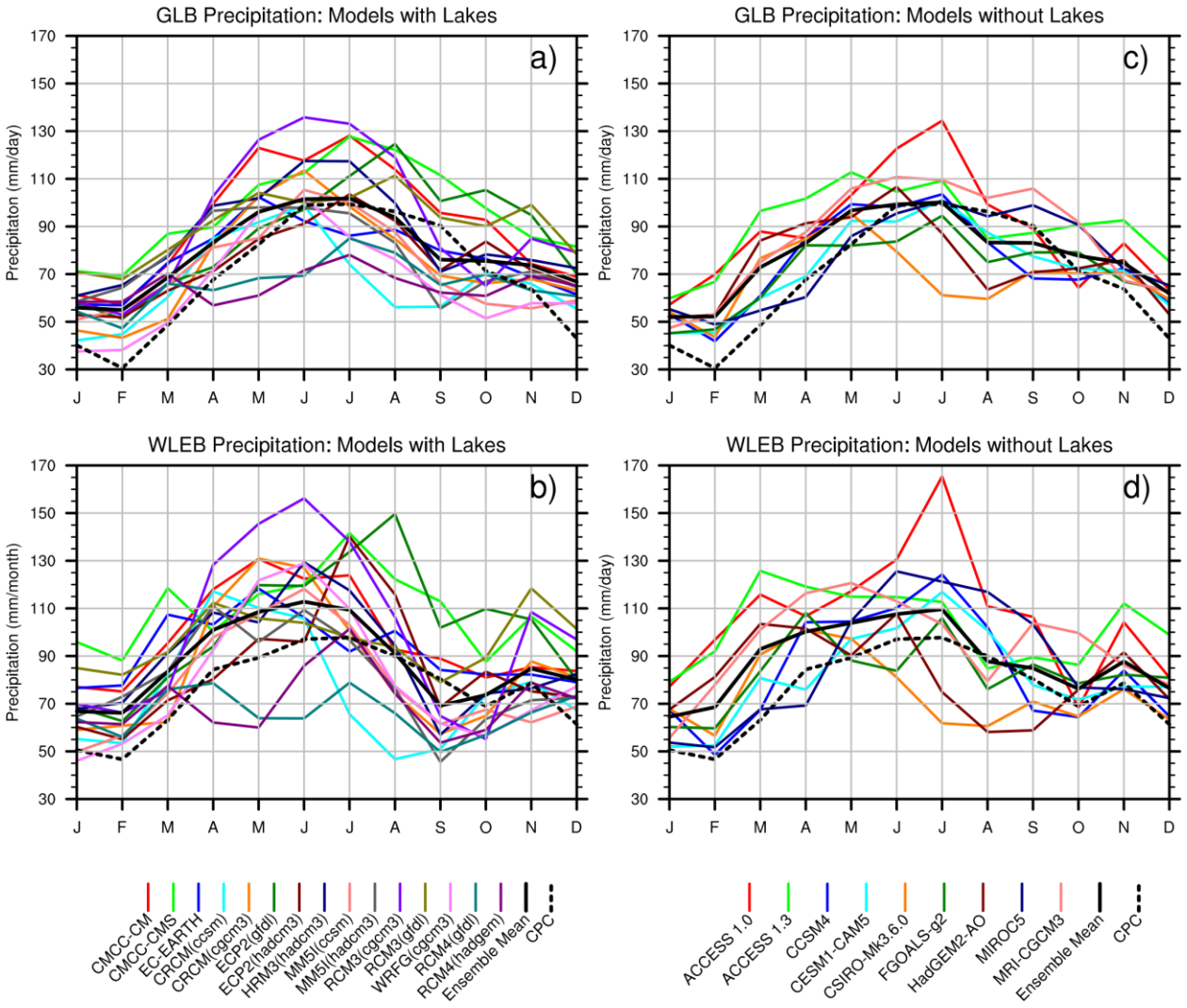

Figure 3.9: Monthly averages for the historical period (1980–1999) spatially averaged over the GLB and WLEB. CPC values displayed in dashed lines. (a, b) Models with lakes; including three of the CMIP5 AO models, as well as the complete NARCCAP and Hi-Res ensembles (Table 3.1). (c, d) Models without lakes; including eight of the CMIP5 AO models (Table 3.1).

models show wet biases in the winter and spring for the GLB, as well as slight dry bias in the late summer and early fall. The model bias improvement due to the lakes is inconsistent across seasons, with the spring bias slightly reduced by the models that include lakes (from a bias of 53.9 to 49.3mm, for models without lakes and with lakes, respectively) and the winter bias slightly increased (from 52.4 to 64.0mm).

For the WLEB, there are greater differences in monthly precipitation between the simulations with lakes (Figure 3.9b) and without lakes (Figure 3.9d). The summer–fall transition period shows a different response, with a small dry ASO bias for the models with lakes (0.4 mm below the historical mean) while the models without lakes have a wet bias of 20.9 mm (Figure 3.9b-d), suggesting that the lake feedback during this transition period is weak. Both sets of models still overestimate winter precipitation across both regions by 54.4 mm for models with lakes and 51.0 mm for models without lakes (Figure 3.9c-d). This wet bias could be attributed to the lack of dynamic lake ice in many simulations, which would suppress winter precipitation (Wright et al., 2013). In addition, the lack of dynamic lake ice could also affect the projected change in precipitation, where less ice in the future may lead to greater winter precipitation.

The NARCCAP ensemble also explores the differences between local parameterizations and driving large-scale global conditions. For example, the difference in precipitation between the two similar RCM3 simulations from the NARCCAP ensemble (RCM3-CGCM3 and RCM3-GFDL, Figure 3.9b) is larger than between GCM models with lakes, with the RCM3-CGCM3 showing a large springtime precipitation bias of over 60 mm (Figure 3.9b). Other model pairs with different boundary conditions (e.g. ECP2-GFDL and ECP2-HadCM3; CRCM-CCSM and CRCM-CGCM3; MM5I-CCSM and MM5I-HadCM3) also show that the driving boundary conditions play an important role. In the CRCM simulations that have the most complex lake treatment, the summer drying in the WLEB is more pronounced in the CRCM-CCSM simulation (47 mm in August as compared to the observed value of 90 mm) than in the CRCM-CGCM3 simulation (74 mm; Figure 3.9b). Interestingly, the other regional model driven by the CCSM (MM5I-CCSM) does not have such a strong summer dry bias and is similar to the CRCM-

CGCM3 member. This suggests that while the driving global boundary conditions are important, the interactions between the regional and local processes may be the dominant driver in determining precipitation rates. Overall, this suggests that the inclusion of lakes alone does not necessarily improve model simulations of precipitation, and that the accurate representation of lake processes (e.g. Notaro et al., 2013; Mallard et al., 2015) and their interactions with large-scale dynamics are as important as including the lakes themselves.

3.5 Conclusions

We evaluate the simulation of seasonal and daily precipitation for a suite of climate models at varying resolutions for present-day and future conditions, and use resolution and configuration options to understand model biases and the range in simulated future changes in precipitation. Using seasonality as a metric, each ensemble shows positive (wet) winter and spring biases for the historical period, with greater intermodel variability in the summer and fall. At mid-century, most models show an increase in spring season precipitation of 7–18%, in agreement with prior studies in the Midwest using the CMIP3 ensemble and other RCMs (e.g. Hayhoe et al., 2010; Vavrus and Behnke, 2014). All model ensembles including both the global CMIP5 simulations and regional simulations show a mixed signal for future summer drying. Compared to historical daily precipitation intensity, all models overestimate the observed intense precipitation events in winter and spring. Mid-century projection consensus for each region shows small increases in moderate and intense daily spring events.

This analysis highlights model biases in the region and informs the application of future climate data to specific problems. Potentially, these results highlight the need to understand the

springtime bias evident in almost all of the global models and can contribute to improved representations of regional processes feedbacks and physical features. The advantage of increased resolution between the global and regional ensembles depends largely on location, boundary conditions, and physical parameterizations. For the Great Lakes region, increased resolution shows benefits in resolving daily precipitation events for the spring period as well as for the spring and summer periods in the WLEB. However for other seasons and at longer temporal averaging, boundary conditions and physical parameterizations may still play an important role in understanding and reducing the regional bias in simulated precipitation. Further analysis is needed to determine the dynamical drivers of the spring wet biases that are consistent in the global and regional models, understand how these biases affect future projections of precipitation in the region, and relay these insights to aid adaptation planning around the GLB.

References

Arguez, A. and Vose, R. S.: The definition of the standard WMO climate normal: The key to deriving alternative climate normals, Bull. Am. Meteorol. Soc., 92(6), 699–704, doi:10.1175/2010BAMS2955.1, 2011.

Bryan, A. M., Steiner, A. L. and Posselt, D. J.: Regional modeling of surface-atmosphere interactions and their impact on Great Lakes hydroclimate, J. Geophys. Res., 1044–1064, doi:10.1002/2014JD022316, 2015.

Caldwell, P.: California Wintertime Precipitation Bias in Regional and Global Climate Models, J. Appl. Meteorol. Climatol., 49(10), 2147–2158, doi:10.1175/2010JAMC2388.1, 2010.

Chen, M., Shi, W., Xie, P., Silva, V. B. S., Kousky, V. E., Higgins, R. W. and Janowiak, J. E.: Assessing objective techniques for gauge-based analyses of global daily precipitation, J. Geophys. Res. Atmos., 113(4), 1–13, doi:10.1029/2007JD009132, 2008.

Cherkauer, K. a. and Sinha, T.: Hydrologic impacts of projected future climate change in the Lake Michigan region, J. Great Lakes Res., 36(SUPPL. 2), 33–50, doi:10.1016/j.jglr.2009.11.012, 2010.

Giorgi, F., Coppola, E., Solmon, F., Mariotti, L., Sylla, M. B., Bi, X., Elguindi, N., Diro, G. T., Nair, V., Giuliani, G., Turuncoglu, U. U., Cozzini, S., Güttler, I., O'Brien, T. A., Tawfik, A. B., Shalaby, A., Zakey, A. S., Steiner, A. L., Stordal, F., Sloan, L. C. and Brankovic, C.: RegCM4: Model description and preliminary tests over multiple CORDEX domains, Clim. Res., 52(1), 7–29, doi:10.3354/cr01018, 2012.

Goyette, S., McFarlane, N. a. and Flato, G. M.: Application of the Canadian regional climate model to the Laurentian great lakes region: Implementation of a lake model, Atmosphere-Ocean, 38(3), 481–503, doi:10.1080/07055900.2000.9649657, 2000.

Gronewold, A. D. and Stow, C. A.: Water Loss from the Great Lakes, Science, 343(6175), 1084–1085, doi:10.1126/science.1249978, 2014.

Gronewold, A. D., Fortin, V., Lofgren, B., Clites, A., Stow, C. a. and Quinn, F.: Coasts, water levels, and climate change: A Great Lakes perspective, Clim. Change, 120(4), 697–711, doi:10.1007/s10584-013-0840-2, 2013.

Gula, J. and Peltier, W.R.: Dynamical downscaling over the Great Lakes Basin of North America using the WRF regional climate model: The impact of the great lakes system on regional greenhouse warming, J. Clim., 25(21), 7723–7742, doi:10.1175/JCLI-D-11-00388.1, 2012.

Gutiérrez, J. M., San-Martín, D., Brands, S., Manzanas, R. and Herrera, S.: Reassessing statistical downscaling techniques for their robust application under climate change conditions, J. Clim., 26(1), 171–188, doi:10.1175/JCLI-D-11-00687.1, 2013.

Hayhoe, K., VanDorn, J., Croley, T., Schlegal, N. and Wuebbles, D.: Regional climate change projections for Chicago and the US Great Lakes, J. Great Lakes Res., 36(SUPPL. 2), 7–21, doi:10.1016/j.jglr.2010.03.012, 2010.

Khaliq, M. N., Sushama, L., Monette, A. and Wheater, H.: Seasonal and extreme precipitation characteristics for the watersheds of the Canadian Prairie Provinces as simulated by the NARCCAP multi-RCM ensemble, Clim. Dyn., 44(1–2), 255–277, doi:10.1007/s00382-014-2235-0, 2015.

Legates, D. R. and Willmott, C. J.: Gauge-Corrected , Global Precipitation, Int. J., 10, 1990.

Mallard, M. S., Nolte, C. G., Spero, T. L., Bullock, O. R., Alapaty, K., Herwehe, J. A., Gula, J. and Bowden, J. H.: Technical challenges and solutions in representing lakes when using WRF in downscaling applications, Geosci. Model Dev., 8(4), 1085–1096, doi:10.5194/gmd-8-1085-2015, 2015.

Mearns, L. O., Sain, S., Leung, L. R., Bukovsky, M. S., McGinnis, S., Biner, S., Caya, D., Arritt, R. W., Gutowski, W., Takle, E., Snyder, M., Jones, R. G., Nunes, A. M. B., Tucker, S., Herzmann, D., McDaniel, L. and Sloan, L.: Climate change projections of the North American Regional Climate Change Assessment Program (NARCCAP), Clim. Change, 120(4), 965–975, doi:10.1007/s10584-013-0831-3, 2013.

Meehl, G. A., Covey, C., Delworth, T., Latif, M., McAvaney, B., Mitchell, J. F. B., Stouffer, R. J. and Taylor, K. E.: The WCRP CMIP3 multi-model dataset: a new era in climate change research Bulletin of the American Meteorological Society, Bull. Am. Meteorol. Soc., 88(September), 1383–1394, doi:10.1175/BAMS-88-9-1383, 2007.

Mallard, M. S., Nolte, C. G., Bullock, O.R., Spero, T. L., and Gula, J.: Using a coupled lake model with WRF for dynamical downscaling, J. Geophys. Res., 119(12), 7193–7208, doi:10.1002/2014JD021785, 2014.Melillo, J. M., Richmond, T. (T. C. and Yohe, Eds., G. W.: Climate Change Impacts in the United States:The Third National Climate Assessment., 2014.

Michalak, A. M., Anderson, E. J., Beletsky, D., Boland, S., Bosch, N. S., Bridgeman, T. B., Chaffin, J. D., Cho, K., Confesor, R., Daloglu, I., Depinto, J. V, Evans, M. A., Fahnenstiel, G. L., He, L., Ho, J. C., Jenkins, L., Johengen, T. H., Kuo, K. C., Laporte, E., Liu, X., McWilliams, M. R., Moore, M. R., Posselt, D. J., Richards, R. P., Scavia, D., Steiner, A. L., Verhamme, E., Wright, D. M. and Zagorski, M. a: Record-setting algal bloom in Lake Erie caused by agricultural and meteorological trends consistent with expected future conditions., Proc. Natl. Acad. Sci. U. S. A., 110(16), 6448–6452, doi:10.1073/pnas.1216006110, 2013.

Mishra, V. and Cherkauer, K. a.: Influence of cold season climate variability on lakes and wetlands in the Great Lakes region, J. Geophys. Res. Atmos., 116(12), 1–21, doi:10.1029/2010JD015063, 2011.

Notaro, M., Zarrin, A., Vavrus, S. and Bennington, V.: Simulation of heavy lake-effect snowstorms across the great lakes basin by RegCM4: Synoptic climatology and variability, Mon. Weather Rev., 141(6), 1990–2014, doi:10.1175/MWR-D-11-00369.1, 2013.

Notaro, M., Bennington, V. and Lofgren, B.: Dynamical downscaling-based projections of great lakes water levels, J. Clim., 28(24), 9721–9745, doi:10.1175/JCLI-D-14-00847.1, 2015.

Patz, J. a., Vavrus, S. J., Uejio, C. K. and McLellan, S. L.: Climate Change and Waterborne Disease Risk in the Great Lakes Region of the U.S., Am. J. Prev. Med., 35(5), 451–458, doi:10.1016/j.amepre.2008.08.026, 2008.

Peters, G. P., Andrew, R. M., Boden, T., Canadell, J. G., Ciais, P., Le Quéré, C., Marland, G., Raupach, M. R. and Wilson, C.: The challenge to keep global warming below 2 C, Nat. Clim., 3(January), 2–3, doi:10.1038/nclimate1766, 2013.

Rauscher, S. a., Coppola, E., Piani, C. and Giorgi, F.: Resolution effects on regional climate model simulations of seasonal precipitation over Europe, Clim. Dyn., 35(4), 685–711, doi:10.1007/s00382-009-0607-7, 2010.

Taylor, K. E., Stouffer, R. J. and Meehl, G. A.: An overview of CMIP5 and the experiment design, Bull. Am. Meteorol. Soc., 93(4), 485–498, doi:10.1175/BAMS-D-11-00094.1, 2012.

Vavrus, S. J. and Behnke, R. J.: A comparison of projected future precipitation in Wisconsin using global and downscaled climate model simulations: implications for public health, Int. J. Climatol., 34(10), 3106–3124, doi:10.1002/joc.3897, 2014.

Wehner, M. F.: Very extreme seasonal precipitation in the NARCCAP ensemble: model performance and projections, Clim. Dyn., 40(1–2), 59–80, doi:10.1007/s00382-012-1393-1, 2013.

Wilby, R. L., Wigley, T. M. L., Conway, D., Jones, P. D., Hewitson, B. C., Main, J. and Wilks, D. S.: Statistical downscaling of general circulation model output: A comparison of methods, Water Resour. Res., 34(11), 2995, doi:10.1029/98WR02577, 1998.

Wright, D. M., Posselt, D. J. and Steiner, A. L.: Sensitivity of lake-effect snowfall to lake ice cover and temperature in the great lakes region, Mon. Weather Rev., 141(2), 670–689, doi:10.1175/MWR-D-12-00038.1, 2013.

Chapter 4 Conceptualizing uncertainty in harmful algal bloom modeling for ecosystem service planning in Western Lake Erie.

4.1 Introduction

4.1.1 Harmful Algal Blooms and the Western Lake Erie Basin

Algae blooms are prevalent in freshwater and coastal systems across the globe, reoccurring each year with a range of societal and environmental impacts (Hudnell and Dortch, 2008). Algal blooms can be categorized as "harmful" by growing to sizes that cause a severe reduction in oxygen in aquatic systems, or hypoxia events, which damage surrounding biodiversity (Paerl et al., 2001; Watson et al., 2016). Harmful algal blooms (HABs) can include toxin-producing cyanobacteria, also termed toxic algal blooms or TABs. HABs and TABs put drinking water and recreational water at risk of contamination, especially in the North American Great Lakes where the cyanobacterium Microcystis dominates – producing the neurotoxin Microcystin (Galen et al., in review; Jetoo et al., 2015; Loftin et al., 2016; Carmichael et al., 2016). Algal blooms are caused by a range of environmental factors which can be exacerbated directly and indirectly by human activity such as local agricultural practices that influence nutrient runoff into waterways, and fossil fuel burning which contributes to global climate change. Eutrophication, or the process of excess nutrients being loaded into water systems, is one pathway for the enhancement of algae growth. Climate change has already begun to influence regional drivers of HABs, as atmospheric warming affects summer water temperature and salinity that drive lake circulation dynamics, as well as atmospheric dynamics that drive regional weather (Dale et al., 2006; Edwards et al., 2006; Paerl and Huisman, 2008). Changes in water temperature (Paerl & Huisman, 2008; Kosten

et al., 2012), water column mixing (Huber et al., 2012), irradiance (Litchman, 1998), lake hydrologic regime and residence time (Elliott, 2010), and introduction of invasive species (Vanderploeg et al., 2001) influence bloom size and toxicity. Tracking climate change impacts to HABs and TABs will also depend on the response of individual plankton communities (Wells et al., 2015).

The Midwest region of the United States is a unique intersection of the factors for HAB growth with strong seasonal shifts in temperature and precipitation as well as agricultural lands that contribute nutrients connected to Great Lakes water bodies through multiple rivers and watersheds. Algae growth and hypoxia events within the Great Lakes peaked in the 1970s, declined through the 1990s, and has experienced a resurgence since 2000 (Winter et al., 2011; Zhou et al, 2013; Scavia et al., 2014). Specifically, the Western Basin of Lake Erie is prone to annual HAB growth in part due to its shallow depth which leads to faster heating and reduced vertical mixing of the water. In the last 20 years Western Lake Erie has seen record breaking HABs and toxic algal blooms (Rinta-Kanto et al., 2005; Steffen et al., 2014). Agricultural runoff, in particular phosphorus and nitrogen laden fertilizer, has been identified as a source of nutrients to Lake Erie which can predispose the system to HABs and TABs (Watson et al. 2016). The Maumee river is the primary source of nutrients for Western Lake Erie, showing increasing trends in nitrates and dissolved phosphorus, despite declines in total phosphorus since 1990 (Stow et al., 2015). Other total phosphorus sources include the Detroit River, where loading is based on shoreline proximity and flow channel, and the St. Clair River where the long-term loading trend reflects the decline in Lake Huron (Burniston et al., 2018; Scavia et al., 2019). Extreme spring precipitation can contribute regionally to agricultural surface run-off, which

loads nutrients into Western Lake Erie, fueling late-summer HABs (Michalak et al., 2013; Basile et al., 2017).

HAB location, duration, and toxicity level can have impacts that cascade across ecosystem services including provisioning (commercial fishing, drinking water, water for the energy sector) and cultural categories (recreation, nature and viewscape enjoyment, historical interests, spiritual fulfilment; Allan et al., 2017). For example, Lake Erie provides a source of municipal drinking water for 11 million people (United States Environmental Protection Agency, https://www.epa.gov/greatlakes/lake-erie). During the summer of 2014, a HAB containing the neurotoxin Microcystin surrounded the raw water intake for Toledo, Ohio resulting in a three day "do not drink" water ban for city residents (Bullerjahn et al, 2016). Lake Erie also provides recreational services which contribute over $10 billion per year to the regional economy including $2 billion from sports fishing (Allan et al., 2017). Lake Erie HABs negatively impact these recreational services as well. Palm-Forster et al. (2016) modeled beach closures surrounding Lake Erie HABs, finding that closure of just 6 western basin beaches of 67 total Lake Erie beaches would result in over a quarter of a million dollars lost per day (modeled as economic welfare loss in 2015 dollar value). Likewise, Wolf et al., (2017) estimated that between 2011 to 2014 fishing license sales in Lake Erie dropped 10% to 13% when algal conditions surpassed the World Health's Organization's moderate health risk advisory threshold (20,000 cyanobacteria cells/mL).

4.1.2 HABs mitigation vs. adaptation for Lake Erie ecosystem services.

Planning and response actions for Western Lake Erie HABs depends on the stakeholder perspective. Interactions between climate and farm management can change the direction of future nutrient loading (increase or decrease) by altering the streamflow, crop growth, and nutrient loading (Kalcic et al., 2019). Between 2012 and 2018, The Great Lakes Environmental Research Laboratory collected water samples across Western Lake Erie for HAB monitoring and forecasting. Over that period, average annual values of total dissolved phosphorus ranged from 45 to 105 µg/L, however maximum annual values reached over 1000 µg/L highlighting phosphorus transfer that occurs in large pulses (Figure 4.1a). Consequently the focus on HAB mitigation emphasizes actions by stakeholders in the agricultural sector– known as agricultural best management practices (BMPs) which help control the amount of soil, water and nutrients in run-off from farm fields. Examples of best management practices include cover crops which maintain soil structure during non-growing season periods, buffer zones comprising plants placed at the edge of fields to limit erosion and provided filtration, and adjustments to tile drainage to reduce diminish runoff (Kalcic et al., 2015; Kalcic et al., 2019; Williamson et al., 2019; USGS, https://www.usgs.gov/centers/glri/science/agriculture-best-management-practices?qt-science_center_objects=0#qt-science_center_objects). Wetlands and filter strips may also be used for adjacent and in-stream filtering of phosphorus, however nutrient saturation of wetlands may reduce their effectiveness over time (Currie et al., 2017; Kieta et al., 2018). Policies that include harmful algal bloom mitigation include the Canada-USA Great Lakes Water Quality Agreement, the Canada-Ontario agreement and the Western Basin of Lake Erie Collaborative agreement (Watson et al., 2016; https://www.michigan.gov/documents/snyder/Western_Basin_of_Lake_Erie_Collaborative_Agr

eement--Lieutenant_Governor_491709_7.pdf). In June 2019, government officials from Michigan, Ohio and Ontario reaffirmed nutrient reduction targets first announced in 2015: A 40% total load reduction in total and dissolved reactive phosphorus by 2025 (compared to 2008 levels) with the interim goal of a 20 percent reduction by 2020 (https://www.michigan.gov/whitmer/0,9309,7-387-90499-499932--,00.html).

Reoccurring HABs within the Western Lake Erie Basin also necessitate adaptation planning to avoid wasted resources from year to year. However, with current forecasting and observation techniques, stakeholders have mostly responded with short-term actions once algal blooms form, whether through beach and marina closures, adjusting water quality treatment, or in decreased tourism and fishing. One issue in communicating algal bloom impacts to regional stakeholders (residents, resource managers, business owners, etc.) is the range of definitions used to describe the blooms –nuisance, harmful, and toxic. The implications of these definitions have more complexity as they can encompass a range of safety thresholds. For example, toxicity impacts cross multiple sectors and depend on the level of toxin concentration. In 2015, the Environmental Protection Agency's (EPA) developed drinking water quality thresholds for two cyanotoxins (microcystins and cylindrospermopsin) and updated its recreational water quality threshold in 2018 (EPA, https://www.epa.gov/cyanohabs/epa-drinking-water-health-advisories-cyanotoxins). From 2012-2018, between 20-40% of GLERL water samples contained Microcystin concentrations that exceeded the EPA limit for infants and pre-school children (0.3 µg/L for children 6 years old and younger). This threshold is the most stringent as 1.6 µg/L is the drinking water limit for school-age children through adults and the recreational water use threshold is 8.0 µg/L.

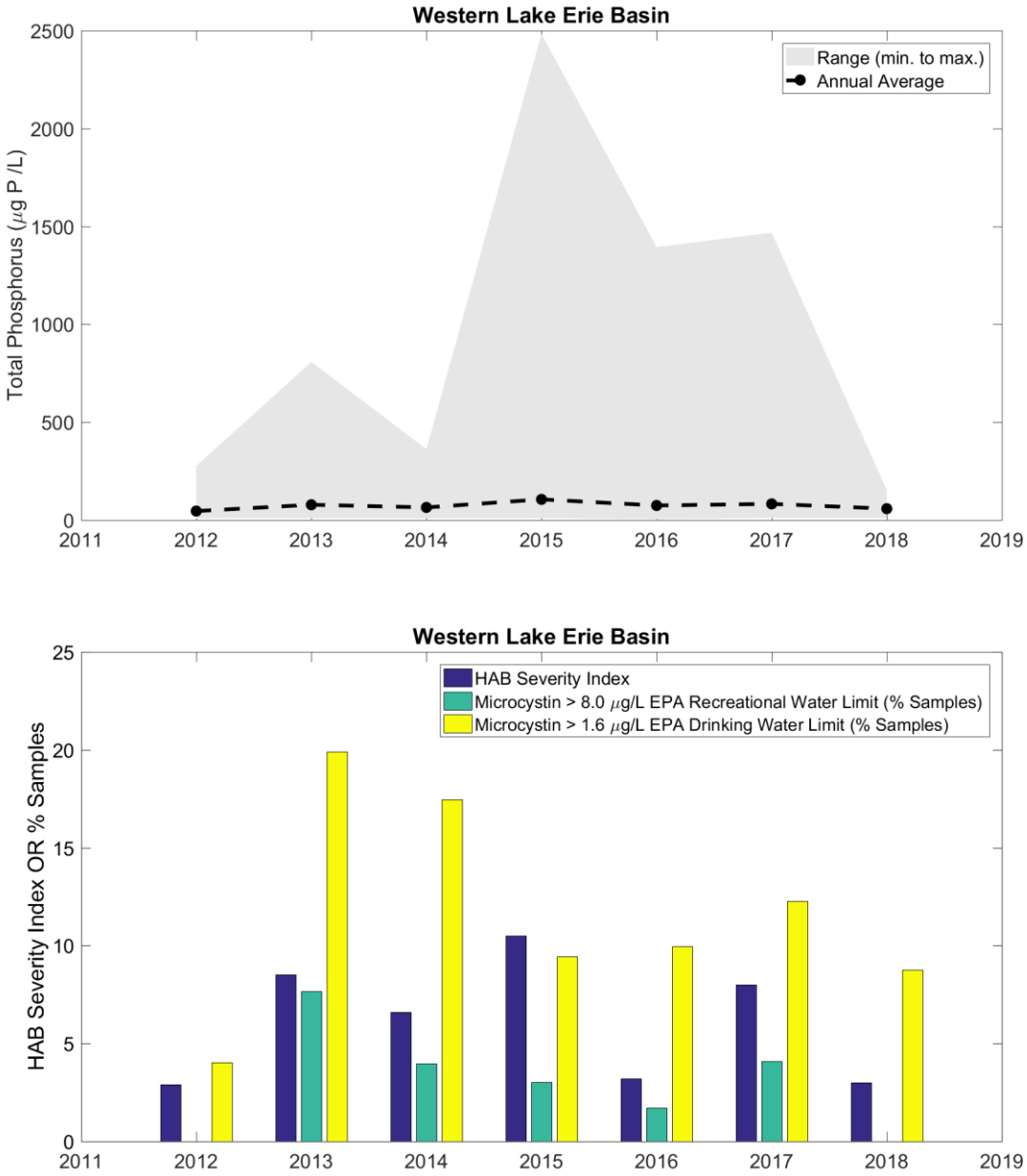

Figure 4.1: HAB severity index and water quality data from 2012 to 2018. (See Supplemental for number of samples per year and station locations). (a) Annual average total phosphorus sites in Western Lake Erie. Minimum and maximum values are shown in gray colorfill. (b) Severity index which accounts for spring-summer bioavailable phosphorus to predict peak 30-day bloom biomass. Percentage of water samples that exceed EPA safety thresholds.

The large threshold range for water quality advisories and range of possible toxicity impacts can be difficult to capture in HAB products, such as the annual HAB severity index in NOAA's

seasonal outlook. Each year, NOAA in partnership with Heidelburg University, LimnoTech and the Great Lakes Environmental Research Laboratory, produces a severity forecast for Western Lake Erie, taking into account bioavailable phosphorus in late spring and early summer to predict peak 30-day bloom biomass. In 2014 a moderate HAB severity index of 6.6 was issued, and water quality samples showed that exceedance of the safe drinking threshold was a factor of 5 higher than that of the recreational water quality threshold (Stumpf, 2019; Figure 4.1b). The 2014 HAB resulted in the Toledo Water crisis due to the bloom location near a municipal water intake area which overwhelmed the treatment facility (Jetoo et al., 2015). In 2015, the HAB index indicated a severe bloom year (10.5, highest index from 2001-2018) and twice as many samples were taken as in 2014 (Stumpf, 2019; Figure 4.1b, Table 2). The 2015 samples showed water quality exceedance at a factor of 3 higher than that for recreational water quality, but at an overall low frequency (< 10% of the samples; Figure 4.1b). Note that toxicity levels may decrease from the in-lake concentrations after water has been treated for municipal water supplies, but measures and compliance vary between plants, facts that prompt discussion of centralized water safety planning (Jetoo et al., 2015). Conversely, recreational waters do not have large scale containment or treatment measures, and thus rely on warnings system to communicate HAB hazards to the public. For example, recreational beaches in Ohio don't officially close due to the presence of HABs, but informational signs are posted at state park beaches and boat ramps that describe the blooms and advise people avoid contact with the blooms (Ohio EPA, https://epa.ohio.gov/HAB-Algae#147744473-advisories). Depending on the cyanotoxin level, additional Ohio public health advisories are posted and drinking water warnings may be issued (Ohio EPA, https://epa.ohio.gov/HAB-Algae#147744473-advisories). Furthermore, due to the variety of HAB impacts and responses, cross-sectoral communication is

infrequent or nonexistent. Thus, public outreach and stakeholder input is vital to understanding the range of adaptation actions, knowledge sources, data needs, and consideration of uncertainty in HAB impact planning.

4.1.3 Modeling HABs in the Western Lake Erie Basin

There is a multitude of research surrounding the growth of harmful algal blooms for Western Lake Erie. Much of the focus for model prediction and policy has been the mitigation of runoff and nutrient loading into the lake. Three projects from this larger field of work directly preceded Coastal SEES work to incorporation climate information and stakeholder needs into nutrient load projections in Western Lake Erie; 1. the Ecological Forecasting (ECOFOR) project focused on Soil Water Assessment Testbed model development for the Maumee watershed, 2. the Water, Climate and Sustainability (WCS) project achieved climate-SWAT coupling for the Western Lake Erie region, and 3. the NOAA Coastal Ocean Climate Applications (COCA) brought together regional stakeholders to co-develop scenarios for mitigating Maumee basin nutrient loading that could be tested using coupled simulations. Specifically, the COCA project included three brainstorming workshops, where discussions covered agricultural practices (e.g., crop rotations, type and timing, fertilizer applications, adoption of best management practices) in the basin as well as feasible scenarios for nutrient management and how to best disseminate research outputs (Kalcic et al., 2019). Top scenario priorities identified by stakeholders included fertilizer application rate and location, placement of vegetative filter strips and wetlands, as well as cover crops type and rotation. Incorporation of stakeholder feedback within the limits of available modeling techniques led to changes in how modelers accounted for fertilizer type and seasonal application, tile drain density, wetland coverage, filter strip widths and watershed coverage, as

well as watershed crop percentages. Modeling scales are currently a challenge for mitigation decision making as precipitation and land processes are heavily simplified in model representations. However stakeholders found the descriptions of mid-21st century precipitation changes to be useful context for discussion of nutrient mitigation actions.

The Coastal SEES project goal is to extending climate-watershed coupling to include HAB simulations while engaging stakeholders from the adaptation space. Following the model of Lemos et al., 2012, work is being done within the Coastal SEES Lake Erie project to investigate user perceptions of HAB forecasts and subsequently the potential of co-production in forecast creation. Understanding how forecasts fits users' decision-making and how forecasts interplay with other available information provides a basis to consider the effects of co-production on scaling of information and decisions. Workshop feedback shows that information used for HAB responses includes peer experiences as well as the NOAA HAB tracker and bulletin (Coastal SEES, 2018). Seasonal forecasts were described as potentially useful products to communicate the threat of HABs – but not for day to day decisions (Coastal SEES, 2018). To increase usability of HAB forecasting, stakeholders described needs for confidence descriptions for late season forecasts and a mid-century focus from climate projections (Coastal SEES, 2018). Inclusion of toxicity, spring and autumn forecasts, and an increase in the frequency of HAB updates were also identified as areas for improvement (Coastal SEES, 2018). This stakeholder input captures the mismatch of available HAB information with differing scales and scope of adaptation decisions.

Current HAB forecasting frameworks incorporate projected nutrient loads with meteorological conditions to track the location and size of algal blooms to inform affected stakeholder communities, as well as sample to understand the toxicity of the bloom (Wynne et al., 2013). However, HAB models are not set up for direct incorporation of climate scenario output. Many complex meteorological and hydrological interactions that influence the bloom formation are affected by a changing climate. Pulses of nutrients to river and in-lake systems vary from year to year with environmental and human drivers. Compounding the effect of seasonal runoff is release of previously accumulated dissolved reactive phosphorus (DRP) by within lake processes on a decadal scale (Ho and Michalak, 2017). Additionally, nutrient type and reactive state can invoke differences in HAB development as some algae communities utilize phosphorus and others preferentially use nitrogen, while dissolved reactive phosphorus can be more bioavailable for cyanobacterial use (Anderson et al., 2002; Newell et al., 2019). Understanding changes to extreme precipitation, and subsequent land runoff, in the Western Lake Erie Basin can inform planning for future algal bloom impacts, however this involves resolving processes at different scales including cold versus warm season precipitation, lake circulation and moisture flux within the region.

New techniques linking model simulations together are being developed to understand the role of climate on HAB changes in Western Lake Erie. However each modeling step contains inherent uncertainty. Here we discuss configuration of climate, watershed and HAB models as well as caveats to current methods aimed at uncertainty management. We propose four pathways to conceptualize uncertainty across model coupling. Section 4.2 will focus on model structure, sources of uncertainty, and methods of uncertainty management. Section 4.3 will describe

conceptual pathways for characterizing climate-watershed-HAB modeling and Section 4.4 will discuss strategies to address modeling gaps with stakeholder needs

4.2 Characterizing uncertainty for climate, watershed and HAB modeling

Satellite and ground observations are available to validate model behavior for a historical period, however data availability in both space and time and measurement accuracy can limit both global and regional variable comparisons. Alongside model validation, characterizing sources of uncertainty allows decision makers to contextualize model output for the issue of concern. Moreover, accurate simulation of the historical period does not automatically translate to fidelity in model projections, that is, the model could be getting to the correct historical picture for the wrong reasons such as the cancellation of variable errors against each other, or incomplete understanding of underlying variable interactions. To characterize uncertainty across model configurations, we follow the Hawkins and Sutton (2009) categorization of uncertainty by model forcing, structure, and internal variability.

4.2.1 Forcing scenario

Forcing scenario, or the set of conditions around which the model simulations evolve, include initial information for simulation spin-up and transient information that is accessed over the full time period of the simulation. Climate model simulations have been forced by scenarios based on policy, energy, and population choices that affect carbon dioxide concentrations. More recently, large scale Earth system model simulations have been guided by radiative pathways for the 21st century that detail additional radiation absorbed and re-emitted to Earth's surface by atmospheric

carbon dioxide compared to preindustrial radiative balance at the top of the atmosphere (IPCC, 2014).

The Soil and Water Assessment Tool (SWAT), simulates water, sediments and agricultural chemical yields based on land use and land management practices (Arnold et al., 2012; Gassman et al., 2007). For the Great Lakes region, SWAT includes assumptions about farming practices – what they are and where they take place, for example the percent area of the basin with cover crops and the type of cover crop can be fixed in the model. Great Lakes simulations using SWAT are highly calibrated to local measurements of runoff, streamflow and nutrient loads, with the goal of testing land use changes that reduce in-river and in-lake nutrients. Recently SWAT has been used to probe best management practices (BMPs) in around the Great Lakes for nutrient load reductions over time and how nutrients break down or not in waterways. For example, the use of filter strips or wetland to reduce the amount of nutrients at the edge of agricultural fields or within the lake (Kalcic et al., 2019; Merriman et al., 2018; Merriman et al., 2018).

4.2.2 Model structure

Mode structure refers to model components (grid spacing, time-step, variable calculations, sub-grid process representation) that shape simulation responses to the choice of forcing scenario. Earth system models (models with coupled climate system components, i.e. land, atmosphere, ocean, etc.), show different responses of global average temperature and precipitation to changes in atmospheric radiation as a result of increasing atmospheric carbon dioxide in the 21st century (IPCC, 2014). Within regional precipitation projections for the Great Lakes, structural uncertainty can manifest in physical parameterizations of lake effect snow, lake ice dynamics, and evapotranspiration (Basile et al., 2017; Bryan et al., 2015). Many earth system models do not

include representation of inland lake dynamics (Briley et al., 2017). For finer scale models that do include lakes, lake parameterization and lake model coupling have been ongoing areas of model development for the Great Lakes region (Charusombat et al., 2018; Conrick et al., 2015; Mallard et al., 2015; Notaro et al., 2015; Xiao et al., 2016). Structural uncertainty in SWAT arises from the use of many input parameters (~100 depending on the watershed), which complicates model evaluation and makes knowledge of the individual system of study an asset (Arnold et al., 2012). Current research defines cropland agriculture, mussel species filter feeding, and lake sedimentation as nutrient sources that predispose the Western Lake Erie Basin to toxic algal blooms (Heisler et al., 2008; Newell et al., 2019; Steffen et al., 2014; Vanderploeg et al., 2001). These small scale and heterogeneous nutrient sources may not be captured in ground measurements, thus introducing a layer of uncertainty to toxicity modeling techniques that incorporate nutrient loading input (Bertani et al., 2016; Sayers et al., 2019).

4.2.3 Internal variability

Internal variability is defined as non-forcing related fluctuations within models. For example, atmospheric wave oscillations and circulation patterns can affect the Great Lakes region by driving changes in lake ice cover and winter temperature extremes (Assel and Rodionov, 1998; Bai et al., 2015; Fu and Steinschneider, 2019; Ghanbari and Bravo, 2008; Holman et al., 2014; Rodionov and Assel, 2010; Wang et al., 2012). However, earth system models contain climate states that are simplifications of reality based on choices of model design and simulation setup. Thus, model climate fluctuations may not be timed in the same way that they occur in the real world contributing to simulation uncertainty. Further, the Soil Water Assessment Tool (SWAT) is calibrated to historical datasets which can lead to uncertainty surrounding streamflow patterns

under future climate change. Testing the influence of historical climate period on the SWAT model for a Northern Michigan watershed basin revealed that the choice of climatic datasets led to differences in parameter validation (Wu et al., 2007). Representing the complex and annually varying environmental interactions that affect algae growth rates are challenges for HAB model development (Obenour et al., 2014). Algal blooms are traceable once they form, but HAB initiation, duration, and toxicity remain sources of uncertainty for forecast modeling that are related to environmental variability.

4.2.4 Management of model uncertainty

Calibration of a full climate model is nearly impossible due to the large amount of simulated variables. Further, climate model resolution, or the size of the grid cells, can vary considerably across different climate models, leading to uncertainty arising in missing processes. For global models, smaller scale processes are not accounted for at the grid level of even the finest resolution models, and are added using parameterizations –whereby sub-grid processes are represented by an average value or probability of occurrence (McFarlane, 2011). Regional scale climate models are examples of dynamical downscaling, where the use of finer grid resolution is aimed at better representation of local phenomena. However, regional models do require information from global models along domain boundaries.

Climate model uncertainty can compound watershed model uncertainty depending on variable responses to climate forcing. Precipitation and temperature changes under a range of future climate scenarios have been shown to impact the hydrologic responses in agricultural watersheds (Christiansen et al., 2014; Ficklin et al., 2009; Kalcic et al., 2019). Depending on the study

timeframe, model simulations can be analyzed when spread in scenario uncertainty is minimal. For example, despite following separate forcing scenarios for radiation, Intergovernmental Panel on Climate Change (IPCC) climate model projections of temperature mostly align until 2050 (IPCC, 2014). Additionally, bias correction has been repeatedly used to constrain the structural uncertainty of climate model data in watershed studies when reliable observations are available, especially for precipitation and temperature input to hydrological models (El-Khoury et al., 2015; Gao et al., 2019; Glavan et al., 2015; Kang et al., 2015; Liu et al., 2015; Maraun, 2013; Shrestha et al., 2017; Teng et al., 2015; Troin et al., 2015; Vaghefi et al., 2013; Wagner et al., 2015; Zhang et al., 2015) but bias correction is not as consistently used in studies specific to the Great Lakes region. Bias correction employs statistical techniques to match modeled variable relationships, such as mean and variance to present-day observations. Present day biases are then assumed to persist in future model simulations. Common implementations of bias correction of climate models include Bias Corrected Spatial Disaggregation (BCSD) that adjusts model data to match historical statistical distributions (quantile mapping; Wood et al., 2004; Thrasher et al., 2013), LOcalized Constructed Analogs (LOCA) by spatial matching daily observations and model output (Pierce et al., 2014; Pierce and Cayan, 2016), and Bias Corrected Constructed Analogs (BCCA) which first use quantile mapping before constructing analogs (Maurer et al., 2010). However caution should be used in understanding the final impact of each technique (Maraun, 2015; Thrasher et al., 2012), as the climate is not a stationary system.

Over the last decade, satellite data has provided an important observational constraint on the shape, size, location and trend of harmful algal blooms in Lake Erie (Becker et al, 2009; Sayers et al., 2016; Sayers et al., 2019; Soontiens et al., 2019; Wynne et al., 2008; Wynne et al., 2011;

Wynne and Stumpf, 2015;). The Great Lakes Environmental Research Laboratory (GLERL) and the Cooperative Institute for Great Lakes Research (CIGLR) run NOAA Great Lakes Harmful Algal Blooms (HABs) and Hypoxia program which uses an integrated approach for understanding the environmental drivers of HABs and hypoxia for prediction of events. Seasonal dynamics are examined using satellite images, remote sensing, buoys, a monitoring program in Lake Erie, Saginaw Bay, and Lake Huron, and genetic techniques. Remote sensing data has been coupled to HAB transport models, leading to the development of a Lake Erie HAB forecast system (Wynne et al., 2013). Manning et al. (2019) used satellite-derived concentrations within a statistical model to demonstrate forecasts of sub-basin bloom severity toward better understanding of shoreline ecosystem service impact. Algorithms have been developed to associate satellite imagery with bloom toxicity by relating image pigmentation to species type (Wynne et al., 2011; Vincent et al., 2004), although these methods are still very uncertain with limited water samples for validation (Binding et al., 2019; Bridgeman et al., 2013; Stumpf et al., 2016).

Since current HAB modeling does not explicitly account for climate, co-production could be an avenue to managing model uncertainty. Co-production, or two-way communication between knowledge producers and users that target iteration on science questions, methods or applications, has emerged as a practical way to address the lack of usability of climate information (Kirchhoff et al. 2013; Lemos et al. 2019). Co-production moves toward problem driven research with high user participation, which is relevant to planning for HAB impacts under climate change where different stakeholders have different data needs (Figure 4.2; Kirchhoff et al., 2013). Co-production on climate science knowledge encompasses multiple

modes of interaction (contractual, consultative, collaborative, and collegial), and can take shape through several research approaches depending on available resources such as time, funding and

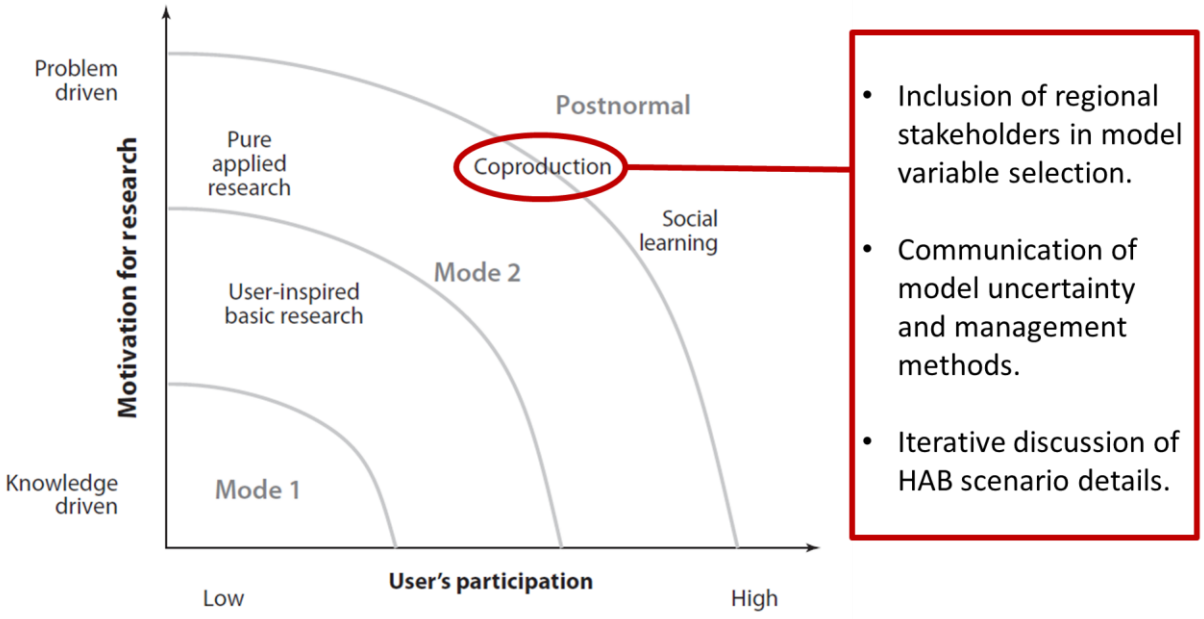

Figure 4.2: Examples of co-production for HAB impacts. Figure modified from Kirchhoff et al., 2013.

training (Meadow et al., 2015). Scenario planning, or problem-solving through development of possible futures, follows an iterative process involving problem identification (orientation), system assessment (exploration), scenario creation (synthesis), and scenario testing (action and monitoring; Peterson et al., 2003; Weeks et al., 2011). Scenario creation for HABs is one way to incorporate expert judgment on model uncertainty as well as stakeholder knowledge of HAB responses

4.2.5 Conceptualizing uncertainty for climate-watershed-HAB model chains

Communication of climate impacts involves explanation of model and expert sources of uncertainty (Patt, 2007). In bridging the gap between HAB modeling decision-making in

Western Lake Erie, model coupling must be examined for the ways it treats underlying uncertainties. Here we develop an uncertainty framework with four pathways that conceptualize uncertainty based on current methods used in modeling chains (Figure 4.3):

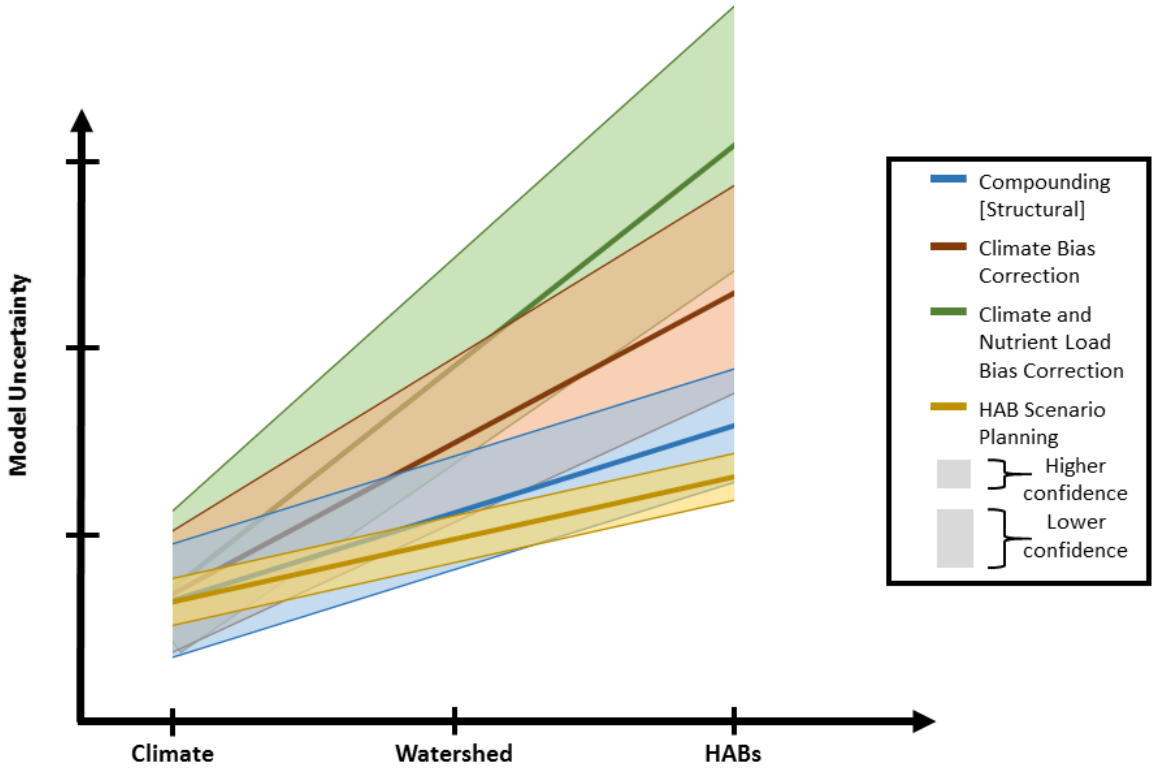

Figure 4.3: Conceptual uncertainty in climate-watershed-HAB model chain. Solid lines represent uncertainty pathways for compounding model structures, bias correction methods, and scenario planning. Confidence range on each pathway is shown in colorfill. A narrower confidence range indicates better understanding of the pathway methods or the addition of expert judgement.

Compounding Structural Uncertainty: In this pathway structural uncertainty from one modeling step (climate, watershed, HAB modeling) directly carries over to the next. This type of uncertainty could manifest through lake parameterizations in climate models, precipitation

magnitude timing, watershed model calibration and parameterizations, and/or timing of peak HAB growth.

Climate Bias Correction: By introducing climate bias correction prior to use in watershed models, both initial uncertainty and error in the modeling chain increase as future variable relationships will likely not be the same as historical trends.

Climate and Nutrient Load Bias Correction: This pathway describes the use of bias corrected values for both climate input into watershed modeling, and nutrient load input for HAB modeling. Bias correcting at each step increases uncertainty at all modeling stages, and leads to the largest error range due to non-stationarity similar to bias correction in pathway #2.

HAB Scenario Planning: The scenario planning pathway combines modeling projections with expert judgement from within each field to form descriptions of future change. For example, a scenario could provide details such as summer temperature increases, probability of spring precipitation intensity, changes to watershed nutrient loads, probability of future HAB duration and location, changes to seasonal water use, and potential effects of future policy change (see detailed description below). Introducing the enhanced understanding of regional climate and watershed dynamics reduces both the overall uncertainty and the amount of error, however there is still overlap with the error range of the compounding pathway.

4.3 Discussion

The conceptual HAB uncertainty framework presented here relates confidence intervals to model structure, bias correction and expert judgement. The compounding uncertainty pathway shows the highest overall uncertainty at the end of the model chain, however the error range is constrained because physical processes are explicitly represented in each modeling step –that is there is non-negligible error on the uncertainty due to choices of model structure, however the error is lower than if uncertainty were managed with statistics (Figure 4.3). Conversely, bias correction reduces uncertainty for present-day relationships, but doesn't account for changing variable relationships into the future, which increases the error of the final output leading to reduced confidence in the technique (Figure 4.3). Dynamical downscaling in climate modeling allows for the tracking of structural uncertainty through changes in grid resolution and sub-grid parameterization (such as convective precipitation processes), while maintaining some fidelity to real world relationships over time with the guiding laws of physics. However dynamical downscaling of regional climate models is also subject to errors in guiding global model input that should be considered alongside other forms of structural uncertainty. Statistical bias correction aims at reducing uncertainty but instead may obscure errors in both historical statistics and model simulations under assumptions of stationarity, which has ethical implications for decision-making as we move into new and previously unexperienced climate regimes (Hewitson et al., 2014).

In the scenario planning pathway, both overall uncertainty and the error range decrease because expert judgement can contextualize model structures and scenarios for regional processes. For example, within the Great Lakes region, the difference in heating rates between land, water, and

air affects circulation patterns and moisture fluxes lead to enhanced cold season precipitation, lake effect rain/snow, moisture recycling, and winter cyclone strengthening (Anderson et al., 2018; Baijnath-Rodino et al., 2018; Corcoran et al., 2019; Fujisaki-Manome et al., 2017; Lang et al., 2018; Notaro and Holman, 2013; Scott and Huff, 1996; Wright et al., 2013; Xiao et al., 2018). Therefore precipitation output could be analyzed and recommend by researchers based on evaluation of climate model structure. Stakeholders can also provide expertise on land management practices, which improves parameter selection guiding regional watershed model simulations. As a result of COCA stakeholder workshops, stakeholder feedback led to changes in how SWAT modelers accounted for fertilizer type and application, tile drain density, wetland coverage, filter strip widths and watershed coverage, as well as watershed crop percentages (Kalcic et al., 2019). Similarly, iterative engagement could potentially lead to co-produced seasonal metrics for ranking climate models, SWAT calibration, and development of a HAB model ensemble. However HAB adaptation involves stakeholders with varying capacity and response options across spatial scales (e.g. closing a beach for multiple days versus moving a business to another lake location) which need to be considered in scenario development, especially in discussion of model information.

4.4 Conclusions

Enhanced application of climate information requires framing of uncertainty for different disciplines and stakeholders (Gettelman and Rood, 2016). However, a predominant challenge for the scientific community is to communicate current and future climate uncertainty to decision makers (Webster, 2003). Within the Great Lakes region there are multiple initiatives that work at the boundary of HAB research and decision-making, including the Great Lakes Environmental

Research Laboratory (GLERL), Heidelburg University, LimnoTech and the Ohio Sea Grant. Each year, NOAA and partners include a likely range on the HAB severity forecast for Western Lake Erie, and provide past index values dating to 2002 for historical context. During the active season (June-October), the HAB Tracker is used to produce bi-weekly bulletins detail current cyanobacteria bloom location, as well as 3-day forecasts of bloom development, transport, and decline (Rowe et al., 2016; https://tidesandcurrents.noaa.gov/hab/lakeerie.html#). Each bulletin contains expert analysis and summary to interpret the forecast and figures presented. However, communication of how uncertainty is managed in modeling remains a gap as techniques develop to project HAB impacts under climate changes in Western Lake Erie. Multidisciplinary modeling has potential to advance the current state of HAB prediction and continue stakeholder engagement on adaptation issues. Integrating stakeholder feedback into model simulation output is one way to co-produce usable information for HAB decision-making. Characterizing the sources of uncertainty in model simulation chains can be utilized for modeler-stakeholder discussion on HAB adaptation including HAB scenario planning. However, descriptions uncertainty management throughout the coupling process should be used as additional guidance for model confidence. Iterative engagement with stakeholders can extend the results of Coastal SEES workshop feedback in construction of model chain simulations

References

Agriculture Best Management Practices: https://www.usgs.gov/centers/glri/science/agriculture-best-management-practices?qt-science_center_objects=0#qt-science_center_objects, last access: 04 October, 2019.

Allan, J. D., Manning, N. F., Smith, S. D. P., Dickinson, C. E., Joseph, C. A. and Pearsall, D. R.: Ecosystem services of Lake Erie: Spatial distribution and concordance of multiple services, J. Great Lakes Res., 43(4), 678–688, doi:10.1016/j.jglr.2017.06.001, 2017.

Anderson, E. J., Fujisaki-Manome, A., Kessler, J., Lang, G. A., Chu, P. Y., Kelley, J. G. W., Chen, Y. and Wang, J.: Ice forecasting in the next-generation Great Lakes Operational Forecast System (GLOFS), J. Mar. Sci. Eng., 6(4), doi:10.3390/jmse6040123, 2018.

Arnold, J. G., Kiniry, J. R., Srinivasan, R., Williams, J. R., Haney, E. B. and Neitsch, S. L.: Input/Output Documentation Soil & Water Assessment Tool, available from: https://swat.tamu.edu/media/69296/swat-io-documentation-2012.pdf, 2012.

Assel, R. and Rodionov, S.: Atmospheric teleconnections for annual maximum ice cover on the Laurentian Great Lakes, Int. J. Climatol., 18(4), 425–442, doi:10.1002/(sici)1097-0088(19980330)18:4<425::aid-joc258>3.3.co;2-h, 1998.

Bai, X., Wang, J., Austin, J., Schwab, D. J., Assel, R., Clites, A., Bratton, J. F., Colton, M., Lenters, J., Lofgren, B., Wohlleben, T., Helfrich, S., Vanderploeg, H., Luo, L. and Leshkevich, G.: A record-breaking low ice cover over the Great Lakes during winter 2011/2012: combined effects of a strong positive NAO and La Niña, Clim. Dyn., 44(5–6), 1187–1213, doi:10.1007/s00382-014-2225-2, 2015.

Baijnath-Rodino, J. A. and Duguay, C. R.: Assessment of coupled CRCM5–FLake on the reproduction of wintertime lake-induced precipitation in the Great Lakes Basin, Theor. Appl. Climatol., (Eccc 2017), doi:10.1007/s00704-019-02799-8, 2019.

Baijnath-Rodino, J. A., Duguay, C. R. and LeDrew, E.: Climatological trends of snowfall over the Laurentian Great Lakes Basin, Int. J. Climatol., 38(10), 3942–3962, doi:10.1002/joc.5546, 2018.

Basile, S. J., Rauscher, S. A. and Steiner, A. L.: Projected precipitation changes within the Great Lakes and Western Lake Erie Basin: a multi-model analysis of intensity and seasonality, Int. J. Climatol., 37(14), 4864–4879, doi:10.1002/joc.5128, 2017.

Becker, R. H., Sultan, M. I., Boyer, G. L., Twiss, M. R. and Konopko, E.: Mapping cyanobacterial blooms in the Great Lakes using MODIS, J. Great Lakes Res., 35(3), 447–453, doi:10.1016/j.jglr.2009.05.007, 2009.

Bertani, I., Obenour, D. R., Steger, C. E., Stow, C. A., Gronewold, A. D. and Scavia, D.: Probabilistically assessing the role of nutrient loading in harmful algal bloom formation in western Lake Erie, J. Great Lakes Res., 42(6), 1184–1192, doi:10.1016/j.jglr.2016.04.002, 2016.

Binding, C. E., Zastepa, A. and Zeng, C.: The impact of phytoplankton community composition on optical properties and satellite observations of the 2017 western Lake Erie algal bloom, J. Great Lakes Res., 45(3), 573–586, doi:10.1016/j.jglr.2018.11.015, 2019.

Bridgeman, T. B., Chaffin, J. D. and Filbrun, J. E.: A novel method for tracking western Lake Erie Microcystis blooms, 2002-2011, J. Great Lakes Res., 39(1), 83–89, doi:10.1016/j.jglr.2012.11.004, 2013.

Briley, L.J., Ashley, W.S., Rood, R.B. and Krmenec, A.: The role of meteorological processes in the description of uncertainty for climate change decision-making. Theor. Appl. Climatol., 127(3-4), 643-654, doi:10.1007/s00704-015-1652-2, 2017.

Bryan, A. M., Steiner, A. L. and Posselt, D. J.: Regional modeling of surface-atmosphere interactions and their impact on Great Lakes hydroclimate, J. Geophys. Res., 120(3), 1044–1064, doi:10.1002/2014JD022316, 2015.

Bullerjahn, G. S., McKay, R. M., Davis, T. W., Baker, D. B., Boyer, G. L., D'Anglada, L. V., Doucette, G. J., Ho, J. C., Irwin, E. G., Kling, C. L., Kudela, R. M., Kurmayer, R., Michalak, A. M., Ortiz, J. D., Otten, T. G., Paerl, H. W., Qin, B., Sohngen, B. L., Stumpf, R. P., Visser, P. M. and Wilhelm, S. W.: Global solutions to regional problems: Collecting global expertise to address the problem of harmful cyanobacterial blooms. A Lake Erie case study, Harmful Algae, 54, 223–238, doi:10.1016/j.hal.2016.01.003, 2016.

Burniston, D., Dove, A., Backus, S. and Thompson, A.: Nutrient concentrations and loadings in the St. Clair River–Detroit River Great Lakes Interconnecting Channel, J. Great Lakes Res., 44(3), 398–411, doi:10.1016/j.jglr.2018.02.005, 2018.

Carmichael, W. W. and Boyer, G. L.: Health impacts from cyanobacteria harmful algae blooms: Implications for the North American Great Lakes, Harmful Algae, 54, 194–212, doi:10.1016/j.hal.2016.02.002, 2016.

Charusombat, U., Fujisaki-Manome, A., Gronewold, A. D., Lofgren, B. M., Anderson, E. J., Blanken, P. D., Spence, C., Lenters, J. D., Xiao, C., Fitzpatrick, L. E. and Cutrell, G.: Evaluating and improving modeled turbulent heat fluxes across the North American Great Lakes, Hydrol. Earth Syst. Sci., 22(10), 5559–5578, doi:10.5194/hess-22-5559-2018, 2018.

Christiansen, D. E., Walker, J. F. and Hunt, R. J.: Basin-scale simulation of current and potential climate changed hydrologic conditions in the Lake Michigan Basin, United States, Sci. Investig. Rep., 86, doi:10.3133/sir20145175, 2014.

Coastal SEES: Notes from a workshop titled The Future of Harmful Algal Blooms held on October 26, 2018, Ottawa National Wildlife Refuge, Oak Harbor, OH, 2018.

Conrick, R., Reeves, H. D. and Zhong, S.: The dependence of QPF on the choice of boundary- and surface-layer parameterization for a lake-effect snowstorm, J. Appl. Meteorol. Climatol., 54(6), 1177–1190, doi:10.1175/JAMC-D-14-0291.1, 2015.

Corcoran, M. C., Thomas, E. K. and Boutt, D. F.: Event-Based Precipitation Isotopes in the Laurentian Great Lakes Region Reveal Spatiotemporal Patterns in Moisture Recycling, J. Geophys. Res. Atmos., 124(10), 5463–5478, doi:10.1029/2018JD029545, 2019.

Currie, S. J., Vanzomeren, C. M. and Berkowitz, J. F.: Utilizing Wetlands for Phosphorus Reduction in Great Lakes Watersheds : A Review of Available Literature Examining Soil Properties and Phosphorus Removal Efficiency, U.S. Army Engineer Research and Development Center, Vicksburg, MS, Available from: www.erdc.usace.army.mil., 120 pp., 2017.

Dale, B., Edwards, M. and Reid, P. C.: Climate Change and Harmful Algal Blooms, Ecol. Harmful Algae, 189(Hallegraeff 1993), 367–378, doi:10.1007/978-3-540-32210-8_28, 2006.

Edwards, M., Johns, D. G., Leterme, S.C., Svendsen, E., and Richardson, A.J.: Regional climate change and harmful algal blooms in the northeast Atlantic, Limnol. Oceanogr., 51(2), 820–829, 2006.

El-Khoury, A., Seidou, O., Lapen, D. R. L., Que, Z., Mohammadian, M., Sunohara, M. and Bahram, D.: Combined impacts of future climate and land use changes on discharge, nitrogen and phosphorus loads for a Canadian river basin, J. Environ. Manage., 151, 76–86, doi:10.1016/j.jenvman.2014.12.012, 2015.

Elliott, J. A.: The seasonal sensitivity of Cyanobacteria and other phytoplankton to changes in flushing rate and water temperature, Glob. Chang. Biol., 16(2), 864–876, doi:10.1111/j.1365-2486.2009.01998.x, 2010.

EPA Drinking Water Health Advisories for Cyanotoxins: https://www.epa.gov/cyanohabs/epa-drinking-water-health-advisories-cyanotoxins, last access: 21 September 2019.

Ficklin, D. L., Luo, Y., Luedeling, E. and Zhang, M.: Climate change sensitivity assessment of a highly agricultural watershed using SWAT, J. Hydrol., 374(1–2), 16–29, doi:10.1016/j.jhydrol.2009.05.016, 2009.

Fu, W. and Steinschneider, S.: A diagnostic-predictive assessment of winter precipitation over the Laurentian Great Lakes: Effects of ENSO and other teleconnections, J. Hydrometeorol., 20(1), 117–137, doi:10.1175/JHM-D-18-0128.1, 2019.

Fujisaki-Manome, A., Fitzpatrick, L. E., Gronewold, A. D., Anderson, E. J., Lofgren, B. M., Spence, C., Chen, J., Shao, C., Wright, D. M. and Xiao, C.: Turbulent heat fluxes during an extreme lake-effect snow event, J. Hydrometeorol., 18(12), 3145–3163, doi:10.1175/JHM-D-17-0062.1, 2017.

Gao, J., Sheshukov, A. Y., Yen, H., Douglas-Mankin, K. R., White, M. J. and Arnold, J. G.: Uncertainty of hydrologic processes caused by bias-corrected CMIP5 climate change projections with alternative historical data sources, J. Hydrol., 568(July 2018), 551–561, doi:10.1016/j.jhydrol.2018.10.041, 2019.

Gassman, P.W., Reyes, M.R., Green, C.H. and Arnold, J.G.: The soil and water assessment tool: historical development, applications, and future research directions., Transactions of the ASABE, 50(4), 1211-1250, doi:10.13031/2013.23637, 2007.

Gettelman, A. and Rood, R. B.: Demystifying Climate Models, Earth Syst. Data Model., 2(2011), 282, doi:10.1007/978-3-662-48959-8, 2016.

Ghanbari, R. N. and Bravo, H. R.: Coherence between atmospheric teleconnections, Great Lakes water levels, and regional climate, Adv. Water Resour., 31(10), 1284–1298, doi:10.1016/j.advwatres.2008.05.002, 2008.

Glavan, M., Ceglar, A. and Pintar, M.: Assessing the impacts of climate change on water quantity and quality modelling in small Slovenian Mediterranean catchment - lesson for policy and decision makers, Hydrol. Process., 29(14), 3124–3144, doi:10.1002/hyp.10429, 2015.

Hawkins, E. and Sutton, R.: The potential to narrow uncertainty in regional climate predictions, Bull. Am. Meteorol. Soc., 90(8), 1095–1107, doi:10.1175/2009BAMS2607.1, 2009.

He, X., Liu, Y. L., Conklin, A., Westrick, J., Weavers, L. K., Dionysiou, D. D., Lenhart, J. J., Mouser, P. J., Szlag, D. and Walker, H. W.: Toxic cyanobacteria and drinking water: Impacts, detection, and treatment, Harmful Algae, 54, 174–193, doi:10.1016/j.hal.2016.01.001, 2016.

Heisler, J., Glibert, P. M., Burkholder, J. M., Anderson, D. M., Cochlan, W., Dennison, W. C., Dortch, Q., Gobler, C. J., Heil, C. A., Humphries, E., Lewitus, A., Magnien, R., Marshall, H. G., Sellner, K., Stockwell, D. A., Stoecker, D. K. and Suddleson, M.: Eutrophication and harmful algal blooms: A scientific consensus, Harmful Algae, 8(1), 3–13, doi:10.1016/j.hal.2008.08.006, 2008.

Hewitson, B.C., Daron, J., Crane, R.G., Zermoglio, M.F. and Jack, C.: Interrogating empirical-statistical downscaling. Climatic Change, 122(4), 539-554, doi:10.1007/s10584-013-1021-z, 2014.

Ho, J. C. and Michalak, A. M.: Phytoplankton blooms in Lake Erie impacted by both long-term and springtime phosphorus loading, J. Great Lakes Res., 43(3), 221–228, doi:10.1016/j.jglr.2017.04.001, 2017.

Holman, K. D., Lorenz, D. J. and Notaro, M.: Influence of the background state on Rossby wave propagation into the great lakes region based on observations and model simulations, J. Clim., 27(24), 9302–9322, doi:10.1175/JCLI-D-13-00758.1, 2014.

Huber, V., Wagner, C., Gerten, D. and Adrian, R.: To bloom or not to bloom: Contrasting responses of cyanobacteria to recent heat waves explained by critical thresholds of abiotic drivers, Oecologia, 169(1), 245–256, doi:10.1007/s00442-011-2186-7, 2012.

Hudnell, H.K. and Dortch, Q.: A synopsis of research needs identified at the interagency, international symposium on cyanobacterial harmful algal blooms (ISOC-HAB). in: Cyanobacterial harmful algal blooms: state of the science and research needs, Springer, New York, NY, 17-43, doi:10.1007/978-0-387-75865-7_2, 2008.

IPCC: Climate Change 2014: Synthesis Report. Contribution of Working Groups I, II and III to the Fifth Assessment Report of the Intergovernmental Panel on Climate Change [Core Writing Team, R.K. Pachauri and L.A. Meyer (eds.)]. IPCC, Geneva, Switzerland, 151 pp, 2014.

Jetoo, S., Grover, V. I. and Krantzberg, G.: The toledo drinking water advisory: Suggested application of the water safety planning approach, Sustain., 7(8), 9787–9808, doi:10.3390/su7089787, 2015.

Kalcic, M. M., Frankenberger, J. and Chaubey, I.: Spatial Optimization of Six Conservation Practices Using Swat in Tile-Drained Agricultural Watersheds, J. Am. Water Resour. Assoc., 51(4), 956–972, doi:10.1111/1752-1688.12338, 2015.

Kalcic, M. M., Muenich, R. L., Basile, S., Steiner, A. L., Kirchhoff, C. and Scavia, D.: Climate Change and Nutrient Loading in the Western Lake Erie Basin: Warming Can Counteract a Wetter Future, Environ. Sci. Technol., doi:10.1021/acs.est.9b01274, 2019.

Kang, B., Kim, Y. Do, Lee, J. M. and Kim, S. J.: Hydro-environmental runoff projection under GCM scenario downscaled by Artificial Neural Network in the Namgang Dam watershed, Korea, KSCE J. Civ. Eng., 19(2), 434–445, doi:10.1007/s12205-015-0580-0, 2015.

Kieta, K. A., Owens, P. N., Lobb, D. A., Vanrobaeys, J. A. and Flaten, D. N.: Phosphorus dynamics in vegetated buffer strips in cold climates: A review, Environ. Rev., 26(3), 255–272, doi:10.1139/er-2017-0077, 2018.

Kirchhoff, C.J., Lemos, M.C. and Dessai, S.: Actionable knowledge for environmental decision making: broadening the usability of climate science. Annual review of environment and resources, 38, doi:10.1146/annurev-environ-022112-112828, 2013.

Kosten, S., Huszar, V. L. M., Bécares, E., Costa, L. S., van Donk, E., Hansson, L. A., Jeppesen, E., Kruk, C., Lacerot, G., Mazzeo, N., De Meester, L., Moss, B., Lürling, M., Nõges, T., Romo, S. and Scheffer, M.: Warmer climates boost cyanobacterial dominance in shallow lakes, Glob. Chang. Biol., 18(1), 118–126, doi:10.1111/j.1365-2486.2011.02488.x, 2012.

Lake Erie: https://www.epa.gov/greatlakes/lake-erie, last access: 04 October, 2019.

Lang, C. E., McDonald, J. M., Gaudet, L., Doeblin, D., Jones, E. A. and Laird, N. F.: The influence of a lake-to-lake connection from lake huron on the lake-effect snowfall in the vicinity

of Lake Ontario, J. Appl. Meteorol. Climatol., 57(7), 1423–1439, doi:10.1175/JAMC-D-17-0225.1, 2018.

Leaders pledge water quality improvements for Lake Erie: https://www.michigan.gov/whitmer/0,9309,7-387-90499-499932--,00.html, last access: 04 October, 2019.

Lemos, M.C., Wolske, K.S., Rasmussen, L.V., Arnott, J.C., Kalcic, M. and Kirchhoff, C.J.: The Closer, the Better? Untangling Scientist–Practitioner Engagement, Interaction, and Knowledge Use. Weather Clim. Soc., 11(3), 535-548, doi:10.1175/WCAS-D-18-0075.1, 2019.

Litchman, E.: Population and community responses of phytoplankton to fluctuating light, Oecologia, 117(1–2), 247–257, doi:10.1007/s004420050655, 1998.

Liu, W., Zhang, A., Wang, L., Fu, G., Chen, D., Liu, C. and Cai, T.: Projecting streamflow in the Tangwang River basin (China) using a rainfall generator and two hydrological models, Clim. Res., 62(2), 79–97, doi:10.3354/cr01261, 2014.

Loftin, K. A., Graham, J. L., Hilborn, E. D., Lehmann, S. C., Meyer, M. T., Dietze, J. E. and Griffith, C. B.: Cyanotoxins in inland lakes of the United States: Occurrence and potential recreational health risks in the EPA National Lakes Assessment 2007, Harmful Algae, 56, 77–90, doi:10.1016/j.hal.2016.04.001, 2016.

Mallard, M. S., Nolte, C. G., Bullock, O.R., Spero, T. L., and Gula, J.: Using a coupled lake model with WRF for dynamical downscaling, J. Geophys. Res., 119(12), 7193–7208, doi:10.1002/2014JD021785, 2014.

Mallard, M. S., Nolte, C. G., Spero, T. L., Bullock, O. R., Alapaty, K., Herwehe, J. A., Gula, J. and Bowden, J. H.: Technical challenges and solutions in representing lakes when using WRF in downscaling applications, Geosci. Model Dev., 8(4), 1085–1096, doi:10.5194/gmd-8-1085-2015, 2015.

Manning, N. F., Wang, Y. C., Long, C. M., Bertani, I., Sayers, M. J., Bosse, K. R., Shuchman, R. A. and Scavia, D.: Extending the forecast model: Predicting Western Lake Erie harmful algal blooms at multiple spatial scales, J. Great Lakes Res., 45(3), 587–595, doi:10.1016/j.jglr.2019.03.004, 2019.

Maraun, D.: Bias Correction, Quantile Mapping, and Downscaling: Revisiting the Inflation Issue, J. Clim., 26(6), 2137–2143, doi:10.1175/JCLI-D-12-00821.1, 2013.

Maraun, D.: Bias Correcting Climate Change Simulations - a Critical Review, Curr. Clim. Chang. Reports, 2(4), 211–220, doi:10.1007/s40641-016-0050-x, 2016.

Maurer, E. P., Hidalgo, H. G., Das, T., Dettinger, M. D. and Cayan, D. R.: The utility of daily large-scale climate data in the assessment of climate change impacts on daily streamflow in California, Hydrol. Earth Syst. Sci., 14(6), 1125–1138, doi:10.5194/hess-14-1125-2010, 2010.

McFarlane, N.: Parameterizations: representing key processes in climate models without resolving them. Wiley Interdisciplinary Reviews: Climate Change, 2(4), 482-497, doi:10.1002/wcc.122, 2011.

Meadow, A.M., Ferguson, D.B., Guido, Z., Horangic, A., Owen, G. and Wall, T.: Moving toward the deliberate coproduction of climate science knowledge. Weather Clim. Soc., 7(2), 179-191, doi:10.1175/WCAS-D-14-00050.1, 2015.

Merriman, K. R., Daggupati, P., Srinivasan, R., Toussant, C., Russell, A. M. and Hayhurst, B.: Assessing the impact of site-specific BMPs using a spatially explicit, field-scale SWAT model with edge-of-field and tile hydrology and water-quality data in the Eagle Creek Watershed, Ohio., Water, 10(10), 1299, doi:10.3390/w10101299, 2018.

Merriman, K. R., Russell, A. M., Rachol, C. M., Daggupati, P., Srinivasan, R., Hayhurst, B. A. and Stuntebeck, T. D.: Calibration of a field-scale soil and water assessment tool (SWAT) model with field placement of best management practices in Alger Creek, Michigan, Sustain., 10(3), 1–23, doi:10.3390/su10030851, 2018.

Michalak, A. M., Anderson, E. J., Beletsky, D., Boland, S., Bosch, N. S., Bridgeman, T. B., Chaffin, J. D., Cho, K., Confesor, R., Daloglu, I., Depinto, J. V, Evans, M. A., Fahnenstiel, G. L., He, L., Ho, J. C., Jenkins, L., Johengen, T. H., Kuo, K. C., Laporte, E., Liu, X., McWilliams, M. R., Moore, M. R., Posselt, D. J., Richards, R. P., Scavia, D., Steiner, A. L., Verhamme, E., Wright, D. M. and Zagorski, M. A: Record-setting algal bloom in Lake Erie caused by agricultural and meteorological trends consistent with expected future conditions., Proc. Natl. Acad. Sci. U. S. A., 110(16), 6448–6452, doi:10.1073/pnas.1216006110, 2013.

Newell, S. E., Davis, T. W., Johengen, T. H., Gossiaux, D., Burtner, A., Palladino, D. and McCarthy, M. J.: Reduced forms of nitrogen are a driver of non-nitrogen-fixing harmful cyanobacterial blooms and toxicity in Lake Erie, Harmful Algae, 81(January), 86–93, doi:10.1016/j.hal.2018.11.003, 2019.

Notaro, M., Holman, K., Zarrin, A., Fluck, E., Vavrus, S. and Bennington, V.: Influence of the laurentian great lakes on regional climate, J. Clim., 26(3), 789–804, doi:10.1175/JCLI-D-12-00140.1, 2013.

Notaro, M., Bennington, V. and Vavrus, S.: Dynamically downscaled projections of lake-effect snow in the Great Lakes basin, J. Clim., 28(4), 1661–1684, doi:10.1175/JCLI-D-14-00467.1, 2015.

Obenour, D. R., Gronewold, A. D., Stow, C. A. and Scavia, D.: Water Resources Research, J. Am. Water Resour. Assoc., 5(3), 2–2, doi:10.1111/j.1752-1688.1969.tb04897.x, 2014.

Ohio Algae Information for Recreational Waters: https://epa.ohio.gov/HAB-Algae#147744473-advisories, last access: 04 October, 2019.

Paerl, H. W. and Huisman, J.: Blooms like it hot, Science, 320(5872), 57–58, doi:10.1126/science.1155398, 2008.

Paerl, H. W., Fulton, R. S., Moisander, P. H. and Dyble, J.: Harmful freshwater algal blooms, with an emphasis on cyanobacteria., Sci. World. J., 1, 76–113, doi:10.1100/tsw.2001.16, 2001.

Palm-Forster, L. H., Lupi, F. and Chen, M.: Valuing lake erie beaches using value and function transfers, Agric. Resour. Econ. Rev., 45(2), 270–292, doi:10.1017/age.2016.15, 2016.

Patt, A.: Assessing model-based and conflict-based uncertainty, Glob. Environ. Chang., 17(1), 37–46, doi:10.1016/j.gloenvcha.2006.10.002, 2007.

Peterson, G.D., Cumming, G.S. and Carpenter, S.R.: Scenario planning: a tool for conservation in an uncertain world. Conserv. Biol., 17(2), 358-366, doi:10.1046/j.1523-1739.2003.01491.x, 2003.

Pierce, D. W. and Cayan, D. R.: Downscaling humidity with Localized Constructed Analogs (LOCA) over the conterminous United States, Clim. Dyn., 47(1–2), 411–431, doi:10.1007/s00382-015-2845-1, 2016.

Pierce, D. W., Cayan, D. R. and Thrasher, B. L.: Statistical downscaling using localized constructed analogs (LOCA), J. Hydrometeorol., 15(6), 2558–2585, doi:10.1175/JHM-D-14-0082.1, 2014.

Rinta-Kanto, J. M., Ouellette, A. J. A., Boyer, G. L., Twiss, M. R., Bridgeman, T. B. and Wilhelm, S. W.: Quantification of toxic Microcystis spp. during the 2003 and 2004 blooms in western Lake Erie using quantitative real-time PCR, Environ. Sci. Technol., 39(11), 4198–4205, doi:10.1021/es048249u, 2005.

Rodionov, S. and Assel, R.: Atmospheric teleconnection patterns and severity of winters in the Laurentian Great Lakes basin, Atmos. - Ocean, 38(4), 601–635, doi:10.1080/07055900.2000.9649661, 2000.

Rowe, M.D., Anderson, E.J., Wynne, T.T., Stumpf, R.P., Fanslow, D.L., Kijanka, K., Vanderploeg, H.A., Strickler, J.R. and Davis, T.W.: Vertical distribution of buoyant Microcystis blooms in a Lagrangian particle tracking model for short-term forecasts in Lake Erie., J. Geophys. Res.-Oceans, 121(7), 5296-5314, doi:10.1002/2016JC011720, 2016.

Sayers, M., Fahnenstiel, G. L., Shuchman, R. A. and Whitley, M.: Cyanobacteria blooms in three eutrophic basins of the Great Lakes: a comparative analysis using satellite remote sensing, Int. J. Remote Sens., 37(17), 4148–4171, doi:10.1080/01431161.2016.1207265, 2016.

Sayers, M. J., Grimm, A. G., Shuchman, R. A., Bosse, K. R., Fahnenstiel, G. L., Ruberg, S. A. and Leshkevich, G. A.: Satellite monitoring of harmful algal blooms in the Western Basin of Lake Erie: A 20-year time-series, J. Great Lakes Res., 45(3), 508–521, doi:10.1016/j.jglr.2019.01.005, 2019.

Scavia, D., David Allan, J., Arend, K. K., Bartell, S., Beletsky, D., Bosch, N. S., Brandt, S. B., Briland, R. D., Daloğlu, I., DePinto, J. V., Dolan, D. M., Evans, M. A., Farmer, T. M., Goto, D., Han, H., Höök, T. O., Knight, R., Ludsin, S. A., Mason, D., Michalak, A. M., Peter Richards, R., Roberts, J. J., Rucinski, D. K., Rutherford, E., Schwab, D. J., Sesterhenn, T. M., Zhang, H. and Zhou, Y.: Assessing and addressing the re-eutrophication of Lake Erie: Central basin hypoxia, J. Great Lakes Res., 40(2), 226–246, doi:10.1016/j.jglr.2014.02.004, 2014.

Scavia, D., Bocaniov, S. A., Dagnew, A., Long, C. and Wang, Y. C.: St. Clair-Detroit River system: Phosphorus mass balance and implications for Lake Erie load reduction, monitoring, and climate change, J. Great Lakes Res., 45(1), 40–49, doi:10.1016/j.jglr.2018.11.008, 2019.

Scott, R. W. and Huff, F. A.: Impacts of the Great Lakes on regional climate conditions, J. Great Lakes Res., 22(4), 845–863, doi:10.1016/S0380-1330(96)71006-7, 1996.

Shrestha, M., Acharya, S. C. and Shrestha, P. K.: Bias correction of climate models for hydrological modelling – are simple methods still useful?, Meteorol. Appl., 24(3), 531–539, doi:10.1002/met.1655, 2017.

Soontiens, N., Binding, C., Fortin, V., Mackay, M. and Rao, Y. R.: Algal bloom transport in Lake Erie using remote sensing and hydrodynamic modelling: Sensitivity to buoyancy velocity and initial vertical distribution, J. Great Lakes Res., 45(3), 556–572, doi:10.1016/j.jglr.2018.10.003, 2019.

Steffen, M. M., Belisle, B. S., Watson, S. B., Boyer, G. L. and Wilhelm, S. W.: Status, causes and controls of cyanobacterial blooms in Lake Erie, J. Great Lakes Res., 40(2), 215–225, doi:10.1016/j.jglr.2013.12.012, 2014.

Stow, C. A., Cha, Y., Johnson, L. T., Confesor, R. and Richards, R. P.: Long-Term and Seasonal Trend Decomposition of Maumee River Nutrient Inputs to Western Lake Erie, Environ. Sci. Technol., 49(6), 3392–3400, doi:10.1021/es5062648, 2015.

Stumpf, R. P., Davis, T. W., Wynne, T. T., Graham, J. L., Loftin, K. A., Johengen, T. H., Gossiaux, D., Palladino, D. and Burtner, A.: Challenges for mapping cyanotoxin patterns from remote sensing of cyanobacteria, Harmful Algae, 54, 160–173, doi:10.1016/j.hal.2016.01.005, 2016.

Stumpf, R. P.: NOAA_Lake Erie 2002-2018 (HAB Severity Index dataset), NOAA, received through email correspondence, 2019.

Teng, J., Potter, N. J., Chiew, F. H. S., Zhang, L., Wang, B., Vaze, J. and Evans, J. P.: How does bias correction of regional climate model precipitation affect modelled runoff?, Hydrol. Earth Syst. Sci., 19(2), 711–728, doi:10.5194/hess-19-711-2015, 2015.

Thrasher, B., Maurer, E. P., McKellar, C. and Duffy, P. B.: Technical Note: Bias correcting climate model simulated daily temperature extremes with quantile mapping, Hydrol. Earth Syst. Sci., 16(9), 3309–3314, doi:10.5194/hess-16-3309-2012, 2012.

Troin, M., Velázquez, J. A., Caya, D. and Brissette, F.: Comparing statistical post-processing of regional and global climate scenarios for hydrological impacts assessment: A case study of two Canadian catchments, J. Hydrol., 520, 268–288, doi:10.1016/j.jhydrol.2014.11.047, 2015.

Vaghefi, A S., Mousavi, S. J., Abbaspour, K. C., Srinivasan, R. and Arnold, J. R.: Integration of hydrologic and water allocation models in basin-scale water resources management considering crop pattern and climate change: Karkheh River Basin in Iran, Reg. Environ. Chang., 15(3), 475–484, doi:10.1007/s10113-013-0573-9, 2013.

Vanderploeg, H. A., Liebig, J. R., Carmichael, W. W., Agy, M. A., Johengen, T. H., Fahnenstiel, G. L. and Nalepa, T. F.: Zebra mussel (Dreissena polymorpha) selective filtration promoted toxic Microcystis blooms in Saginaw Bay (Lake Huron) and Lake Erie, Can. J. Fish. Aquat. Sci., 58(6), 1208–1221, doi:10.1139/f01-066, 2001.

Vincent, R. K., Qin, X., McKay, R. M. L., Miner, J., Czajkowski, K., Savino, J. and Bridgeman, T.: Phycocyanin detection from LANDSAT TM data for mapping cyanobacterial blooms in Lake Erie, Remote Sens. Environ., 89(3), 381–392, doi:10.1016/j.rse.2003.10.014, 2004.

Wagner, P. D., Reichenau, T. G., Kumar, S. and Schneider, K.: Development of a new downscaling method for hydrologic assessment of climate change impacts in data scarce regions and its application in the Western Ghats, India, Reg. Environ. Chang., 15(3), 435–447, doi:10.1007/s10113-013-0481-z, 2015.

Wang, J., Bai, X., Hu, H., Clites, A., Colton, M. and Lofgren, B.: Temporal and spatial variability of Great Lakes ice cover, 1973-2010, J. Clim., 25(4), 1318–1329, doi:10.1175/2011JCLI4066.1, 2012.

Watson, S. B., Miller, C., Arhonditsis, G., Boyer, G. L., Carmichael, W., Charlton, M. N., Confesor, R., Depew, D. C., Höök, T. O., Ludsin, S. A., Matisoff, G., McElmurry, S. P., Murray, M. W., Peter Richards, R., Rao, Y. R., Steffen, M. M. and Wilhelm, S. W.: The re-eutrophication of Lake Erie: Harmful algal blooms and hypoxia, Harmful Algae, 56, 44–66, doi:10.1016/j.hal.2016.04.010, 2016.

Weeks, D., Malone, P. and Welling, L.: Climate change scenario planning: a tool for managing parks into uncertain futures. Park Science, 28(1), 26-33, 2011.

Wells, M. L., Trainer, V. L., Smayda, T. J., Karlson, B. S. O., Trick, C. G., Kudela, R. M., Ishikawa, A., Bernard, S., Wulff, A., Anderson, D. M. and Cochlan, W. P.: Harmful algal blooms and climate change: Learning from the past and present to forecast the future, Harmful Algae, 49, 68–93, doi:10.1016/j.hal.2015.07.009, 2015.

Western Basin of Lake Erie Collaborative Agreement: https://www.michigan.gov/documents/snyder/Western_Basin_of_Lake_Erie_Collaborative_Agreement--Lieutenant_Governor_491709_7.pdf, last access: 04 October, 2019.

Williamson, T. N., Dobrowolski, E. G., Meyer, S. M., Frey, J. W. and Allred, B. J.: Delineation of tile-drain networks using thermal and multispectral imagery—Implications for water quantity and quality differences from paired edge-of-field sites, J. Soil Water Conserv., 74(1), 1–11, doi:10.2489/jswc.74.1.1, 2019.

Winter, J. G., Desellas, A. M., Fletcher, R., Heintsch, L., Morley, A., Nakamoto, L. and Utsumi, K.: Algal blooms in Ontario, Canada: Increases in reports since 1994, Lake Reserv. Manag., 27(2), 105–112, doi:10.1080/07438141.2011.557765, 2011.

Wolf, D., Georgic, W. and Klaiber, H. A.: Reeling in the damages: Harmful algal blooms' impact on Lake Erie's recreational fishing industry, J. Environ. Manage., 199, 148–157, doi:10.1016/j.jenvman.2017.05.031, 2017.

Wood, A. W., Leung, L. R., Sridhar, V. and Lettenmaier, D. P.: Hydrologic implications of dynamical and statistical approaches to downscaling climate model outputs, Clim. Change, 62(1–3), 189–216, doi:10.1023/B:CLIM.0000013685.99609.9e, 2004.

Wright, D. M., Posselt, D. J. and Steiner, A. L.: Sensitivity of lake-effect snowfall to lake ice cover and temperature in the great lakes region, Mon. Weather Rev., 141(2), 670–689, doi:10.1175/MWR-D-12-00038.1, 2013.

Wu, K. and Johnston, C. A.: Hydrologic response to climatic variability in a Great Lakes Watershed: A case study with the SWAT model, J. Hydrol., 337(1–2), 187–199, doi:10.1016/j.jhydrol.2007.01.030, 2007.

Wynne, T. T., Stumpf, R. P., Tomlinson, M. C., Warner, R. A., Tester, P. A., Dyble, J. and Fahnenstiel, G. L.: Relating spectral shape to cyanobacterial blooms in the Laurentian Great Lakes, Int. J. Remote Sens., 29(12), 3665–3672, doi:10.1080/01431160802007640, 2008.

Wynne, T. T., Stumpf, R. P., Tomlinson, M. C., Schwab, D. J., Watabayashi, G. Y. and Christensen, J. D.: Estimating cyanobacterial bloom transport by coupling remotely sensed imagery and a hydrodynamic model Published by : Wiley on behalf of the Ecological Society of America Stable URL : https://www.jstor.org/stable/41416689 Estimating cyanobacterial bloom t, , 21(7), 2709–2721, 2011.

Wynne, T. T., Stumpf, R. P., Tomlinson, M. C., Fahnenstiel, G. L., Dyble, J., Schwab, D. J. and Joshi, S. J.: Evolution of a cyanobacterial bloom forecast system in western Lake Erie: Development and initial evaluation, J. Great Lakes Res., 39(S1), 90–99, doi:10.1016/j.jglr.2012.10.003, 2013.

Wynne, T. T. and Stumpf, R. P.: Spatial and Temporal Patterns in the Seasonal Distribution of Toxic Cyanobacteria in Western Lake Erie from 2002–2014, Toxins, 7(5), 1649–1663, doi:10.3390/toxins7051649, 2015.

Xiao, C., Lofgren, B. M., Wang, J. and Chu, P. Y.: Improving the lake scheme within a coupled WRF-lake model in the Laurentian Great Lakes, J. Adv. Model. Earth Syst., 8(4), 1969–1985, doi:10.1002/2016MS000717, 2016.

Xiao, C., Lofgren, B. M. and Wang, J.: WRF-based assessment of the Great Lakes' impact on cold season synoptic cyclones, Atmos. Res., 214(June), 189–203, doi:10.1016/j.atmosres.2018.07.020, 2018.

Zhang, X., Booij, M. J. and Xu, Y. P.: Improved simulation of peak flows under climate change: Postprocessing or composite objective calibration?, J. Hydrometeorol., 16(5), 2187–2208, doi:10.1175/JHM-D-14-0218.1, 2015.

Zhou, Y., Obenour, D. R., Scavia, D., Johengen, T. H. and Michalak, A. M.: Spatial and temporal trends in Lake Erie hypoxia, 1987-2007, Environ. Sci. Technol., 47(2), 899–905, doi:10.1021/es303401b, 2013.

Chapter 5 Conclusions

There is an ethical urgency to address climate change impacts on society. Communication of uncertainty associated with climate model structure can aid interpretation of model output for key processes at regional and global scales. However, communication alone is not sufficient; iterative collaboration between producers and users of climate information can contribute to well-informed mitigation and adaptation strategies. Model uncertainty is tied to the nature of the process of interest, the scale of the model simulation, and how processes are simplified from reality. This dissertation work has evaluated model uncertainty associated with carbon dioxide uptake and release processes on land, regional precipitation patterns under climate change, as well as conceptualized uncertainty in coupling techniques for climate-watershed-HAB interactions. The following are chapter conclusions and recommended next steps for continued research.

Chapter 2

A more complete understanding of the land carbon sink – which will ultimately affect the rate of climate change – requires the ability to quantitatively simulate soil respiration processes for the present climate and the sensitivity of these processes to environmental variables, such as temperature. I used carbon fluxes from a novel biogeochemical testbed for input to an atmospheric transport model to track the evolution of atmospheric CO_2 from net primary production and heterotrophic respiration to evaluate three different models for heterotrophic respiration. Seasonal timeseries across six regions show that CO_2 release from soil heterotrophic

respiration contributes substantial spatial and temporal variability to atmospheric CO_2, and that model parameterization affects the magnitude and timing of these variations in a way that atmospheric CO_2 observations should be able to discriminate between model parameterizations. The CO_2 variations resulting from models with explicit microbial processes showed higher than observed interannual variability and temperature sensitivity. The variation among model formulations has implications for simulations of HR under climate change; if models are too sensitive to global temperature there will be larger releases of CO_2 to the atmosphere that are inconsistent with observed variable relationships. The regional influence of regional HR fluxes could also be tracked in patterns of global variability. Results here suggest there is a possible path to use atmospheric CO_2 observations together with productivity data, such as new observations of solar-induced chlorophyll fluorescence from satellites, to constrain hemispheric respiration.

Understanding regional sources of soil heterotrophic respiration will be necessary for holistic action in both the mitigation and adaptation spaces. Reducing uncertainty in the land sink through better measurement of global soil respiration would have policy implications for tracking and responding to increase in atmospheric CO_2. Through the Paris Agreement, countries have committed to mitigate fossil fuel emissions, with some pledging far reaching adaptation actions including reforestation and land use management. Regional accounting for land CO_2 uptake will then also have to take into account natural sources of CO_2 to the atmosphere for continued carbon budgeting and emissions tracking, especially if carbon tax policy is put in place.

Chapter 3

Regional problems require specific spatial and temporal information. Understanding changes to intense spring precipitation can inform planning for agricultural runoff into waterways and future algal bloom impacts within Western Lake Erie. I constructed three climate model ensembles to investigate precipitation changes at the mid-21st century over two spatial domains (Great Lakes Basin and Western Lake Erie Basin). I examined uncertainty through calculations of precipitation seasonality and intensity and investigate the impact of grid resolution on the model output. In general precipitation is a difficult process to model because cloud development occurs at spatial scales that are smaller than model grid spacing. Probability of historical spring rain events dropped off rapidly for the Great Lakes Basin, this is related to size of domain used in spatial averaging.

For the Western Lake Erie Basin model ensemble means overestimated the probability of intense daily events. Global model ensemble members underestimated historical probability of daily max precipitation in the Western Lake Erie Basin, whereas the bias was reduced in the regional model ensembles. Unexpectedly, the highest resolution ensemble displayed reduced precipitation seasonality and unobserved drying in spring and summer months, supporting the body of research that shows model representation of physical processes can factor into regional bias. Despite historical model biases for the domains examined, all models are based on principles of physics applied to the atmosphere. However, limitations in model structure should be taken into account, therefore precipitation changes are calculated in terms of relative change by mid-century and through shifts in probability distributions. Both global and regional models showed a shift in probability toward intense spring precipitation at mid-century, suggesting an increase in

the frequency precipitation events with potential to impact fertilizer runoff from agricultural land.

Chapter 4

Harmful algal blooms impact business, recreational areas, water quality and culture of Western Lake Erie. Adaptation planning for harmful algal blooms is distinct from mitigation planning in the different sources of data and timescales of action. Climate model data can be used as guidance on regional climate change questions however understanding underlying uncertainties and limitations is key to application. Current HAB forecasting frameworks do not directly use climate information, but new techniques are in development to couple climate projection information with watershed and HAB models. Synthesizing the state of harmful algal bloom literature and ongoing work from the Coastal SEES Lake Erie project, I posed four pathways for conceptualizing uncertainty within the model chain and discuss common methods used for uncertainty management, specifically dynamical and statistical downscaling. Statistical downscaling, or bias correction, is static to a past climate period which doesn't capture changing climate variable relationships under future conditions. Co-production of land management and HAB scenarios between scientists and practitioners can also be used to manage uncertainty while supporting creation of usable science.

The research presented in this dissertation includes opportunities for continued multidisciplinary collaboration and stakeholder engagement, detailed below. Opportunities also exist for university and research institution leadership in innovative coursework, research co-production, network building, and community outreach. Universities can strengthen student-driven knowledge

creation by funding organizational activities and fostering co-production with community-based groups. For example, University Climate Delegations to the provide students and researchers the chance to learn about and participate in the United Nations international negotiations (Basile et al., 2018 – Appendix C). Researchers also have opportunities to engage with several new climate reports in the fourth National Climate Assessment, the special report for Global Warming of 1.5°C from the Intergovernmental Panel on Climate Change, and the State of the Carbon Cycle Report 2018. Project Drawdown and the Global Carbon Project provide example avenues for interdisciplinary research applications. Next steps for furthering research into the science questions presented here include the following:

Next steps Q1: Can atmospheric CO_2 observations be used to analyze regional carbon flux signatures based on different soil model representations of microbial activity?

Utilizing CO_2 observations as a constraint to soil model respiration will require testing additional observational datasets in land model benchmarking and tracking metrics cohesively instead of in isolation. For example, incorporating satellite data of productivity and soil stock measurements into model validation allow for respiration flux signatures to be identified –while tracking the interannual variability and phasing of net primary productivity and respiration moves toward better mechanistic understanding of co-varying carbon flux responses to climate drivers. Additionally, developing model metrics for plant and root autotrophic respiration has implications for the phasing and offsets between productivity and soil heterotrophic respiration. Further, tracking the regional respiration into the 21st century under future radiative forcing to understand changes in seasonality and changing contributions to global variability.

Next steps Q2: How can changing precipitation patterns from a range of climate model simulations be interpreted for timescales relevant to ecosystem service planning?

For further quantification of precipitation bias for the Great Lakes, the development of cold season precipitation metrics can elucidate links to moisture availability and intense spring precipitation events. The comparison of regional parameterization presented here could be expanded to the recent iterations of climate model simulations such as the CORDEX regional model ensemble and the CMIP6 global model ensemble.

Next steps Q3: How can uncertainty be tracked in coupled climate, watershed, and harmful algal bloom modeling to inform ecosystem service adaptation decisions?

Tracking uncertainty through model chain experiments that test the four conceptual pathways presented in this dissertation is encapsulated in ongoing work of the Coastal SEES Lake Erie project. Developing model metrics, output variables, and report information that is designed in conjunction with stakeholders or based on feedback could increase the usability of HAB information for ecosystem decision-making. For example, further development of modeling HAB toxicity may include more attention to empirical information gathering and engagement with water quality managers. There is potential to define future HAB scenarios for Western Lake Erie based the incorporation of climate, watershed, and HAB projections. Continued collaboration with regional stakeholders would determine a range of impacts for each scenario

along with expert guidance to frame uncertainty surrounding future HAB changes in terms of confidence.

Appendices

Appendix A: Supplemental to Chapter 2

Table A.1: Marine Boundary Layer (MBL) stations within the NOAA Earth System Research Laboratory CO_2 sampling network (ESRL). These sites were selected for obtaining at least 50% data coverage over the analysis period of 1982 to 2010.

Region	Station	Acronym	Lat	Lon
60°–90°N	Alert, AK	ALT	82.5	-62.5
	Ny-Ålesund, Svalbard	ZEP	78.9	11.9
	Barrow, AK	BRW	71.3	-156.6
	Stórhöfði, Iceland	ICE	63.4	-20.0
23°–60°N	Mace Head, Ireland	MHD	53.3	-9.9
	Shemya, AK	SHM	52.7	174.1
	Terceira Island, Azores	AZR	38.8	-27.4
	Tudor Hill, Bermuda	BMW	32.3	-64.9
	Sand Island, Midway	MID	28.2	-177.4
	Key Biscayne, FL	KEY	25.7	-80.2
	Pacific Ocean, 25°N	POCN25	25.0	-135.0
0°–23°N	Pacific Ocean, 20°N	POCN20	20.0	-139.0
	Cape Kumukahi, HI	KUM	19.5	-154.8
	Pacific Ocean, 15°N	POCN15	15.0	-143.0
	Mariana Islands, Guam	GMI	13.4	144.8
	Ragged Point, Barbados	RPB	13.2	-59.4
	Pacific Ocean, 10°N	POCN10	10.0	-147.0
	Pacific Ocean, 5°N	POCN05	5.0	-151.0
	Christmas Island	CHR	1.7	-157.2
0°–23°S	Seychelles	SEY	-4.7	55.2
	Pacific Ocean 5°S	POCS05	-5.0	-159.0
	Ascension Island	ASC	-8.0	-14.4
	Pacific Ocean 10°S	POCS10	-10.0	-163.0
	Tutuila American Samoa	SMO	-14.2	-170.6
	Pacific Ocean 15°S	POCS15	-15.0	-167.0
	Pacific Ocean 20°S	POCS20	-20.0	-171.0
23°–60°S	Pacific Ocean 25°S	POCS25	-25.0	-174.0
	Pacific Ocean 30°S	POCS30	-30.0	-177.0
	Cape Grim, Australia	CGO	-40.7	144.7
	Crozet Island	CRZ	-46.5	51.9

60°–90°S	Palmer Station, Antarctica	PSA	-64.0	-64.0
	Syowa Antarctica	SYO	-69.0	39.6
	Halley Bay, Antarctica	HBA	-75.6	-26.5
	South Pole	SPO	-90.0	-24.8

Table A.2: Coefficient of variation for flux variables by latitude zone. All variables have been detrended using a third-order polynomial fit. For NEP, a negative sign represents flux into land and a positive sign represents a flux to the atmosphere from land.

Region	Model Flux	Mean Flux [Pg C yr^{-1}]	Flux Standard Deviation (STD) [Pg C yr^{-1}]	STD : Flux [%]
NHL 61°-90°N	CASA HR	3.94	0.08	2
	CORPSE HR	4.52	0.23	5
	MIMICS HR	3.96	0.09	2
	CASA NPP	4.07	0.09	2
	CASA NEP	-0.13	0.05	40
	CORPSE NEP	0.45	0.16	35
	MIMICS NEP	-0.11	0.08	76
NML 24°-60°N	CASA HR	22.73	0.24	0 1
	CORPSE HR	23.06	0.31	1
	MIMICS HR	22.88	0.48	2
	CASA NPP	23.15	0.28	1
	CASA NEP	-0.42	0.40	96
	CORPSE NEP	-0.09	0.46	505
	MIMICS NEP	-0.27	0.66	245
NT 1°-23°N	CASA HR	10.63	0.08	0 1
	CORPSE HR	10.63	0.10	1
	MIMICS HR	10.57	0.22	2
	CASA NPP	10.66	0.44	4
	CASA NEP	-0.03	0.48	1428
	CORPSE NEP	-0.03	0.47	1571
	MIMICS NEP	-0.09	0.62	732
ST 0°-23°S	CASA HR	14.26	0.10	0 1
	CORPSE HR	14.30	0.12	1
	MIMICS HR	14.24	0.29	2

	CASA NPP	14.52	0.57	4
	CASA NEP	-0.27	0.61	232
	CORPSE NEP	-0.22	0.58	262
	MIMICS NEP	-0.28	0.84	296
				0
SE 24°-90°N	CASA HR	3.72	0.05	1
	CORPSE HR	3.74	0.07	2
	MIMICS HR	3.74	0.08	2
	CASA NPP	3.77	0.26	7
	CASA NEP	-0.05	0.26	518
	CORPSE NEP	-0.03	0.24	810
	MIMICS NEP	-0.03	0.33	1135

Table A.3: Multiple linear regression coefficients (γ) and R2 are used to model interannual variability in heterotrophic respiration as a function of interannual variability in temperature, NPP, or preceding year NPP. All variables have been detrended and deseasonalized. We list statistically significant predictors of HR IAV, as determined by p-values from ANOVA.

Region	Model IAV	HR IAV Regression γ* , R^2		
		CASA-CNP Temperature IAV [Pg C y^{-1} K^{-1}]	CASA-CNP NPP Current year IAV [--]	CASA-CNP NPP Preceding year IAV [--]
NHL 61°-90°N	CASA HR	**0.16** , 0.64	**0.74** , 0.67	-0.14, 0.02
	CORPSE HR	**0.42**, 0.54	**2.22**, 0.77	-0.23, 0.01
	MIMICS HR	**0.13**, 0.32	**0.63**, 0.40	0.06, 0.00
	CASA-CNP NPP	**0.15**, 0.43		
NML 24°-60°N	CASA HR	**0.78**, 0.58	0.2, 0.05	0.33, 0.15
	CORPSE HR	**1.00**, 0.57	-0.28, 0.06	0.32, 0.08
	MIMICS HR	**1.74**, 0.70	**-0.90**, 0.27	0.05, 0.00
	CASA-CNP NPP	-0.38, 0.10		
NT 1°-23°N	CASA HR	0.17, 0.14	**-0.10**, 0.26	**0.12**, 0.45
	CORPSE HR	0.00, 0.00	-0.06, 0.07	**0.17**, 0.61
	MIMICS HR	**1.03**, 0.68	**-0.40**, 0.60	-0.03, 0.00
	CASA-CNP NPP	**-1.57**, 0.42		
ST 0°-23°S	CASA HR	**0.24**, 0.17	**-0.07**, 0.17	**0.12**, 0.41
	CORPSE HR	-0.01, 0.00	-0.01, 0.00	**0.17**, 0.61
	MIMICS HR	**1.50**, 0.87	**-0.46**, 0.79	0.03, 0.00
	CASA-CNP NPP	**-2.65**, 0.72		

SE 24°-90°N	CASA	0.00, 0.00	0.03, 0.03	**0.12**, 0.32
	CORPSE	-0.07, 0.04	0.09, 0.13	**0.17**, 0.36
	MIMICS	**0.32**, 0.42	**-0.26**, 0.65	-0.08, 0.04
	CASA-CNP NPP	**-1.11**, 0.52		

*bolded values are statistically significant ($p < 0.05$)

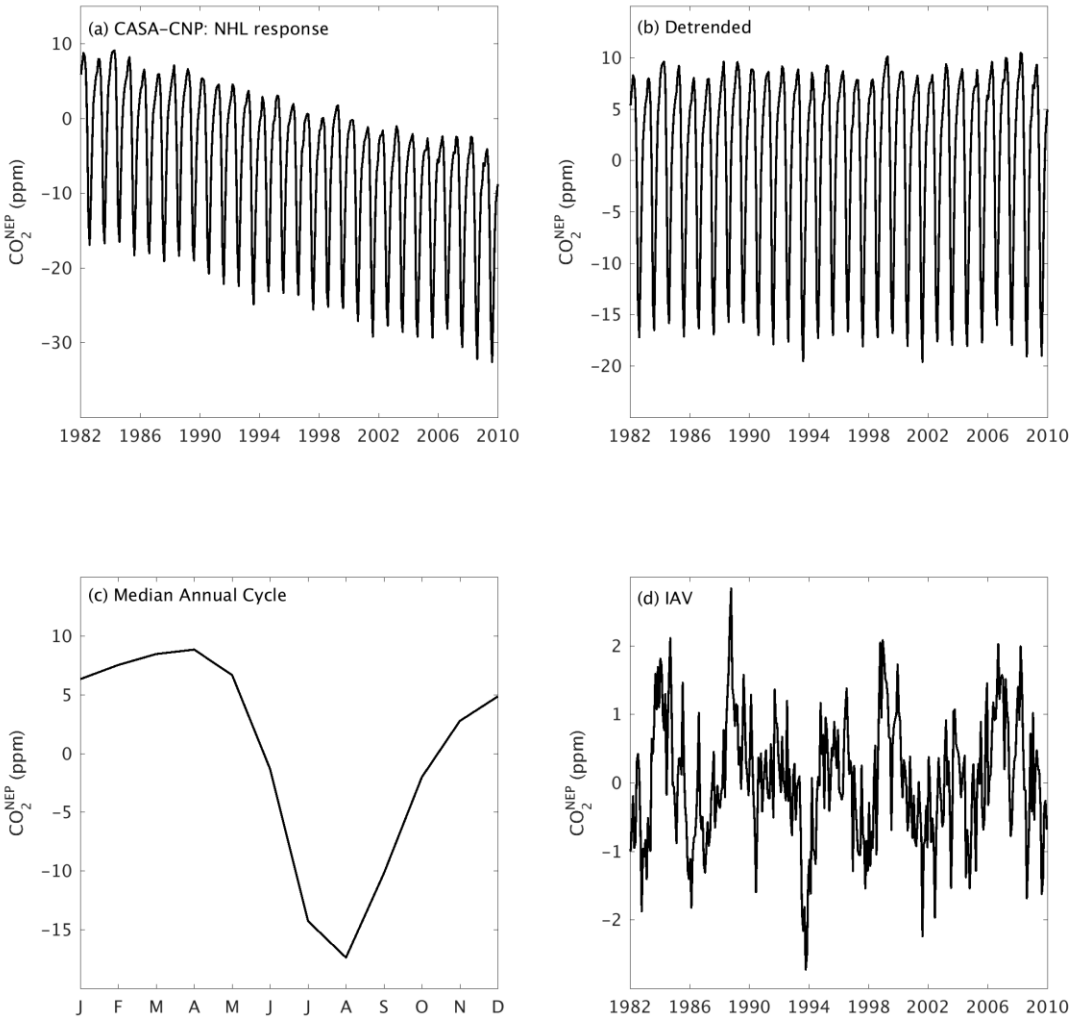

Figure A.1: Depiction of interannual variability (IAV) calculation. (a) Multi-site mean CASA-CNP CO_2^{NEP} in the Northern Hemisphere high latitudes (NHL) region for 1982 to 2010 ($CO_2^{NEP} = CO_2^{HR} + CO_2^{NPP}$). (b) Detrended CASA-CNP CO_2^{NEP} timeseries after removing a third-order polynomit fit. (c) Climatological annual cycle calculated using the median of monthly values over the analysis period. (d) CASA-CNP CO_2^{NEP} interannual variability calculated from removing the climatological annual cycle from each year in the detrended timeseries.

Appendix B: Supplemental to Chapter 4

Table B.1: Total number of measurements combined from station water samples in the Western Lake Erie Basin. Data collected by NOAA and retrieved from the National Centers of Environmental Information.

	Total Measurements						
	2012	2013	2014	2015	2016	2017	2018
Microcystin (particulate + dissolved)	124	196	252	530	472	514	400
Total Phosphorus	62	98	126	265	236	257	200

Table B.2: Harmful Algal Bloom (HAB) from 2002 to 2018. Data provided by Dr. Richard Stumpf of NOAA National Centers for Coastal Ocean Science.

	Harmful Algal Bloom Severity Index
2002	0.3
2003	4.1
2004	2.7
2005	0.3
2006	1.3
2007	0.9
2008	6.2
2009	5.1
2010	5.8
2011	10
2012	2.9
2013	8.5
2014	6.6
2015	10.5
2016	3.2
2017	8

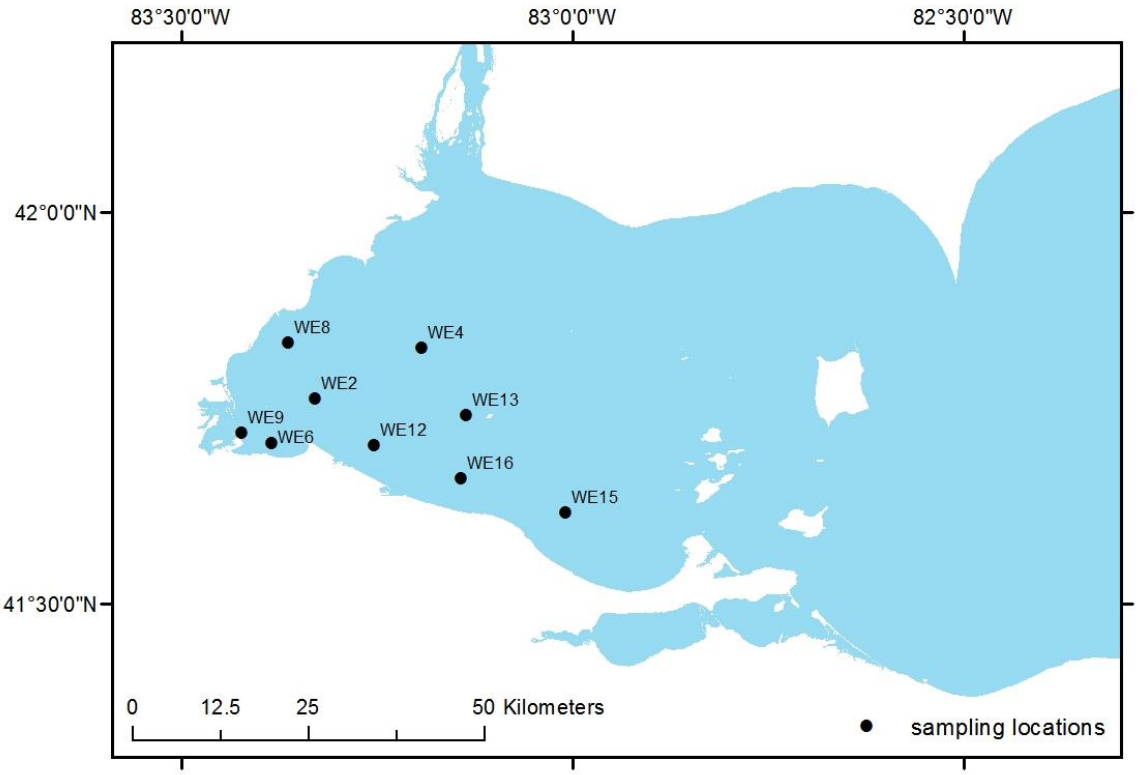

Figure B.1: Sampling station locations in Western Lake Erie, figure created by NOAA and provided through the National Centers for Environmental Information public online repository.

Appendix C

Commentary text published as

Basile, S., Lerner, M., & Rostamnezhad, K.: Boost university voices at COP24 UN climate meeting. Nature, 564(7734), 39, doi:10.1038/d41586-018-07610-8, 2018.

University voices in climate negotiations

Research institutions are appointed to act as official ‘observer’ delegates at international climate negotiations that are hosted by the United Nations and are otherwise closed to journalists and the outside world (see go.nature. com/2atycmq). As non-party stakeholders, they will provide a layer of transparency at this week’s 24th annual Conference of the Parties session, for example. Thanks to the University Climate Delegation Coalition (UCDC) that we launched last year, these delegates are no longer simply observers: they can now bring a wide range of research voices to the table.

As knowledge producers, climate delegates from research institutions are in a position to provide insight into and attention to climate policy. The UCDC aims to engage delegates across US institutions on common initiatives. Over several months, researchers talk to their delegate representatives about their priorities for climate-related policy topics — for example, for emissions inventories, technology transfer, ecosystem management and human rights. University delegations therefore provide an opportunity for the broader research community to connect with international climate negotiations and with climate advocacy.

Samantha Basile*, Michael Lerner* *University of Michigan, Ann Arbor, Michigan, USA.* Keyon Rostamnezhad *Northeastern University, Boston, Massachusetts, USA.*

**Competing interests declared (see go.nature.com/2rcnrdb for details).*

sjbasile@umich.edu